100. P. Eyerer, *Adv. Colloid Interface Sci.*, **3(3)**, 223 (1972).
101. E. A. Hauer and D. S. LeBeau, *J. Phys. Chem.*, **42**, 961 (1938).
102. R. O. Grisdale, in *The Art and Science of Growing Crystals*, Wiley, New York, 1963, Chapter 9.
103. M. Davies, *Nonlinear Behaviour of Molecules, Atoms and Ions in Electric, Magnetic or Electromagnetic Fields*, 1979, p. 301.
104. G. P. Jones, M. Gregson, and T. Krupkowski, *Chem. Phys. Lett.*, **13**, 266 (1972).
105. K. Hirano, *Nature*, **174**, 268 (1954).
106. A. R. Ubbelohde, *Trans. Faraday Soc.*, **36**, 863 (1940).
107. H. Dekameizer, *Helv. Chim. Acta*, **10**, 896 (1927).
108. G. E. Horonic and G. Yelonsky, *Proc. 1st Int. Atris Symp.*, **2**, 539 (1969).
109. M. Krole, J. Eichmeir, and R. W. Sciidn, in *Advances in Electronics and Electron Physics*, Academic, New York, 1964, p. 177.
110. A. P. Wiehner, *Am. J. Phys. Med.*, **48**, 3 (1961).
111. G. J. Evans and M. W. Evans, *J. Chem. Soc., Faraday II*, **76**, 667 (1980).
112. M. W. Evans, *Phys. Rev. Lett.*, in press, 1984.
113. D. Schmidt, M. Schadt, and W. Helfrich, *Nature*, **A27**, 277 (1972).
114. See A. G. Walton, in *Nucleation*, A. C. Zettlemayer, ed., Marcel Dekker, New York, 1969, Chapter 5.
115. N. B. Baranova and B. Y. Zeldovich, *Chem. Phys. Lett.*, **57**, 435 (1979).
116. M. W. Evans and G. J. Evans, *J. Mol. Liq.*, in press, 1984.
117. See, for example, SERC, *CCP5 Quarterly*, **Autumn** (1982).
118. P. C. M. van Woerkom, J. de Bleyser, M. de Zwart, and J. C. Leyte, *Chem. Phys.*, **4**, 236 (1974).
119. R. M. Lynden-Bell, *Mol. Phys.*, **33(4)**, 907 (1977).
120. R. L. Halfman, *Dynamics*, Addison-Wesley, Reading, Massachusetts, 1962.
121. H. Goldstein, *Classical Mechanics*, 1st ed., Addison-Wesley, Reading, Massachusetts, 1950.
122. M. Plank, *The Universe in the Light of Modern Physics*, George Allen & Unwin, 1931 (translated by W. H. Johnston from *Das Weltbeld der neuen Physik*, Joh. A. Borlk, Leipzig).
123. A. H. Piekara, *Optics and Laser Technology*, Butterworth and Co. Ltd., August, 1982, p. 207.
124. J. M. Stone, *Radiation and Optics*, New York, 1963.
125. G. J. Evans, *New Scientist*, submitted 1984.
126. B. Vonnegut, "Atmospheric Electrostatics," in *Electrostatics and its Applications*, Wiley, New York, 1977, Chapter 17.
127. B. Vonnegut, *J. Geophys. Res.*, **65(1)**, 203 (1960).
128. F. Heinmets, *Trans. Faraday Soc.*, **58(4)**, 788 (1962).
129. G. J. Evans, *Nature*, submitted (1984).
130. M. Calvin, *Les Prix Nobel*, 1961
131. D. Kashchiev, *Philos. Mag.*, **25**, 459 (1972).
132. M. Shablakh, L. A. Dissado, and R. M. Hill, *J. Chem. Soc., Faraday II*, **79**, 1443 (1983).
133. M. Volmer, *Kinetik der Phasenbildung*, Steinkopff, Dresden–Leipzig, 1939.

A REVIEW AND COMPUTER SIMULATION OF THE MOLECULAR DYNAMICS OF A SERIES OF SPECIFIC MOLECULAR LIQUIDS‡

M. W. EVANS

Adran Fathemateg Gymhwysol, Coleg Prifysgol Gogledd Cymru, Bangor, Cymru

and

GARETH J. EVANS

Department of Chemistry, University College of Wales, Aberystwyth, Dyfed, Wales

CONTENTS

‡Dedicated to the South Wales Area of the National Union of Mineworkers.

I. INTRODUCTION

In this review we will discuss the deficiencies and limitations of the traditional approach to the study of liquids by spectroscopy and stochastic analytical theory, and the extra depth of insight that may be obtained by means of computer simulation studies. We review the literature and compare results from different spectroscopies for a series of liquids ranging from liquids of C_{3v} symmetry, including two that form solid rotator phases, to molecules of lesser symmetry. (Optically active liquids are discussed in other articles of this volume.) We will see that results obtained for a particular liquid with different spectroscopies are sometimes contradictory. There are still obvious problems associated with the data-reduction processes. We will discuss the role of the various relaxation mechanisms that may contribute to a measured spectrum and show that experimental results are not always easily related to a purely orientational, single-particle mechanism. We will discuss the role of a distinct local structure, known to be present in some liquids, in distorting measured profiles, and we will see that in a liquid the various degrees of molecular freedom (rotation, translation, and vibration), rather than being decoupled, are more often coupled—and strongly so in some liquids.

In particular, computer simulation has shown the importance of rotation–translation interaction. The rotation and translation of the same molecule are normally coupled just as in a propeller, which, when it rotates, must simultaneously translate and move forward. We shall see that rotation–translation coupling, if strong, severely distorts spectral profiles. Consequently, our theories must be rototranslational in origin, and not purely rotational, as present theories are, if they are to be successful in reproducing experiments. In optically active liquids M. W. Evans has shown that rotation–translation interaction may be used to explain why the physical properties of enantiomers and of their racemic mixtures are different. (For example, at room temperature, a racemic mixture of lactic acid molecules is a liquid, whereas the individual enantiomers are solid.)

We have not had the foresight to envisage many of the subtleties of the liquid state. What follows will surprise some researchers, and, we hope, catalyze others into doing more precise and detailed experimentation using all of the dynamical probes in unison. Theoreticians should use the experimental and computer-simulated observations to develop more realistic analytical theories. Too often they have lost sight of the physical realities of liquid systems and, by increasing mathematical complexity, confused rather than clarified the situation. There is obviously still considerable progress to be made.

The set of operations that can be performed on a molecule constitutes a group in the mathematical sense. A set of operations is a group if the following are true:

1. The product of two or more operations is equivalent to a single operation that also belongs to the set.
2. The operations obey the associative law of multiplication.
3. The set includes the identity operator.
4. The inverse of every operation is also a member of the set.

In the first sections of this review we collate and compare the results from various spectroscopies for liquids composed of molecules of C_{3v} symmetry. We choose to classify our liquids in terms of the molecular symmetry because, as we shall see, the symmetry, and even the sizes of the atoms making up a molecule, determines the dynamics of a liquid system.

In later sections we extend our review and discussions to molecules of lower symmetry, and in other articles of the present volume we mention molecules with lower symmetry: the optically active liquids. The loss of symmetry affects the molecular dynamics. In particular, we shall see that it has a pronounced effect on at least one aspect of the dynamics, namely the way rotational and translational motions are mutually correlated.

The molecules of C_{3v} symmetry chosen for discussion have all been reported on extensively in the literature and are amenable to study by computer simulation using the new algorithms that have recently become available for polyatomic and "real" molecular liquids.

In reviewing the literature we look for insights into some of the following problems:

1. To what extent do collision-induced processes contribute to and distort measured spectral profiles? Depolarized-light-scattering and far-infrared absorption certainly exist for nondipolar spherical and tetrahedral molecules, in both the liquid and gaseous states. These spectra arise from a collision-induced mechanism: A fluctuating distortion of the symmetrical polarizability tensors of the isolated molecules is caused by the strong intermolecular interactions in the fluid. The interaction results in induced dipole moments (and consequently the far-infrared absorption) as well as asymmetry in the polarizability. It is probable that induced absorptions are present to some extent in all polar and nonpolar liquids and may give rise to measurable intensities in any of the spectroscopies. It has been postulated that for some liquids (e.g., the halogeno benzenes) the induced contributions make up as much as 50% of the total measured intensity.[1,2]
2. To what extent do rotational and translational motions contribute to the same profiles, and are they coupled? Evans and Evans[3] have shown through simulation and experiment how markedly the translation of a mole-

cule may affect *its own* rotation in the condensed state and have postulated that this effect explains the racemic modification in optically active liquids. The observation that a racemic mixture of lactic acid is a liquid at room temperature, yet its individual enantiomers are solid, may be explained in dynamical terms and, in particular, in terms of a rototranslational interaction that is modified in the racemic mixture relative to that in the individual enantiomers. These we term auto rotation–translation effects because they refer to the same molecule. But the rotation of a molecule may effect a simultaneous translation in neighboring molecules, so that rotation and translation may also be correlated in another sense; this we term cross rotation–translation. The significance of this effect has been clearly illustrated in a simple experiment by G. Ewing[4] on H_2 and HD in liquid argon. In H_2 in liquid argon, the rotational transitions observed in the far infrared do not differ from those calculated for the unperturbed gas. However, the spectrum of HD in liquid argon shows larger half-widths, erratic frequency shifts, and additional absorptions arising from the relaxation of the rotational selection rules, which is a consequence of rotation–translation coupling. The coupling perturbation is large in HD and small in H_2 because of the asymmetric mass distribution of the former—a small difference produces a pronounced effect. This cross rotation–translation coupling must also be significant in other liquids, but is not easily distinguished when the individual fine structure is not resolved, as is the situation in most liquids.

While discussing rotation–translation interaction we should also recall a hydrodynamic phenomenon in which local strains set up by transverse shear waves are assumed to be relieved by collective reorientations—a macroscopic translation–rotation interaction. This results in a shear-wave or "Rytov" dip observed in depolarized scattering. However, Berne and Pecora[5] point out the discrepancies that result from this hydrodynamical treatment. As molecular spectroscopists, we believe that all such phenomena have molecular origins, and indeed it is already more popular to treat this phenomenon with molecular models. Having said this, we emphasize that the phenomenon does not appear to be related to a specific microscopic structure and has been observed in a number of molecular liquids, including both polar and nonpolar liquids, both liquids composed of planar and those made of nonplanar molecules, and both liquids made of large and liquids made of small molecules. It would be interesting to characterize the phenomenon in terms of the molecular symmetry and of the atoms comprised by the molecule, following the procedure we shall adopt for the racemic modification in optically active liquids (discussed elsewhere in the present volume).

3. Are other modes of motion coupled [e.g., rotation–vibration, vibration–vibration (of two neighboring molecules), etc.]? If modes of motion are coupled, then spectral profiles may be severely distorted and not amenable

to conventional data reduction and theoretical analysis, there being no theories for these coupled motions. Infrared and Raman profiles are certainly obtained by the convolution of a rotational and a vibrational profile. Lynden-Bell[6] has emphasized that is a problem of some magnitude, because these components may be coupled to give complex, non-Lorentzian line shapes that are sometimes broader, sometimes narrower, than expected and that on occasions show central dips. It is a challenge to experimentalists to observe this central dip, which may occur when the solute motion is significantly faster than that of the solvent it is dissolved in. We suggest that it may be observed when a small dipolar molecule is dissolved in a glass or liquid crystalline system. It may also be shown that the linewidths and line shapes depend on the type of spectrum observed; that is, the modifications of the Raman ($\ell = 2$) and infrared ($\ell = 1$) profiles may not be the same.

4. How significant are cooperative phenomena (cross correlations) and the internal field in modifying the observed spectrum? That they *are* significant is established by dilution studies, which may, *but do not always*, reduce the problem. The problem may actually be increased when a probe solute is dissolved in a nonpolar solvent. These phenomena are poorly understood, but have their origin on the molecular scale; the cross rotation–translation interaction discussed above is an obvious example. These phenomena are unquestionably strong in some liquids; we consider one (acetonitrile) in Section IV. There, the existence of dimers and larger aggregates of molecules is postulated.[7] If this postulate is true, contributions to spectral profiles may arise from the rotation, translation, and vibration of single molecules and of dimers and larger aggregates of molecules, all of which may be coupled. Evans has postulated the existence of collective modes in acetonitrile, as have other workers considering different liquids and using different experiments (see Section II). These studies will be recalled in relevant sections.

Molecular liquids obviously pose significant problems for the deciphering of dynamic motions. The experimental situation is a complex one; no one technique yields a complete picture of the dynamic process because each emphasizes particular aspects of the motion, which are not easily resolved.

Computer simulation, when used in conjunction with experiments, may clarify certain aspects of dynamic motions. In fact, as we shall see, computer simulation does indeed clarify the role of rotation–translation coupling, particularly in the study of optically active liquids. This role is pronounced, except in the few instances of liquids forming rotator phases. The coupling increases in magnitude near the melting point, but decreases near the boiling point. Its magnitude in the enantiomers of an optically active system may differ from that in a 50:50 racemic mixture. All of this will be discussed at length in the following sections.

II. CHLOROFORM ($CHCl_3$)

We will start these review sections with a study of liquid chloroform [see M. W. Evans, *J. Mol. Liq.* **25**, 211 (1983)]. As in subsequent sections, we will review the literature and discuss the conclusions reached from such a survey. We will compare and evaluate these literature results with our own computer molecular-dynamics calculations, and will see that the situation is, in general, a confused one. The simulations at least clarify certain aspects of the discrepancies. A full treatment of cooperative phenomena lies outside the scope of analytical theories and present-day simulations, but a pattern does emerge indicating in which liquids such phenomena are significant and to what degree the various experimental probes are affected. We will discuss the role of rotation–translation coupling in all of the liquids considered.

Chloroform must be the most extensively studied molecular liquid. Evans[8] analyzed over 100 papers on its structure and dynamics in compiling his review and making comparisons with new simulation data. The structure of the liquid has been investigated with atom–atom pair distribution functions, which are obtainable from neutron- and X-ray-scattering experiments and the dynamics has been researched with most of the spectroscopies. Results of the structure investigations suggest that on the local level, a significant oriented structure exists in the pure liquid.

In a neutron-scattering experiment, a double-differential scattering cross section, $d^2\sigma/d\Omega\, dE$, is measured. It represents the number of neutrons scattered per unit solid angle and unit energy interval. In a diffraction experiment, the scattered neutrons are collected for each scattering angle, but no energy analysis is performed. The diffraction cross section may be split into coherent and incoherent terms, and the former into a self and a distinct term. The distinct term is related to the atomic pair correlation function $g_{\alpha\beta}(r)$, which gives the probability of finding a nucleus β at a separation r from a nucleus α. To obtain information about the pair correlation function, the maximum possible number of diffraction studies must be carried out. For chloroform, results of four diffraction experiments are available: X-ray data for $CH^{35}Cl_3$ and neutron data for $CH^{35}Cl_3$, $CD^{35}Cl_3$, and $CD^{37}Cl_3$.

In molecular liquids it is more appropriate to interpret the coherent differential cross section in terms of molecular pair correlations. The intermolecular terms contributing to the coherent distinct differential cross section for a molecule of C_{3v} symmetry may be written as[9]

$$\left(\frac{d\sigma}{d\Omega}\right)_{\text{inter}} = a_0^{(0)}a_0^{(0)*}h_{00}^{(000)} + 0.385a_0^{(1)}a_0^{(0)*}h_{00}^{(101)} + 0.179a_0^{(2)*}h_{00}^{(202)} - 0.064a_0^{(1)}a_0^{(1)}h_{00}^{(110)} \qquad (1)$$

where the $a_0^{(\ell)}$ are molecular scattering factors that can be calculated from the atomic scattering lengths and the atomic positions within the molecule and $h_{m_i m_j}^{(\ell_i\ell_j\ell_{ij})}$ is the Fourier–Bessel transform of the coefficients of the molecular pair correlation with the termination $\ell_i = \ell_j = 2$ being made. The coefficients $h_{00}^{(000)}$, $h_{00}^{(101)}$, $h_{00}^{(202)}$, and $h_{00}^{(110)}$ were determined by carrying out the four experiments above and solving the corresponding four simultaneous equations. These allowed us to calculate four coefficients of the molecular pair correlation function: $g_{00}^{(000)}$, $g_{00}^{(101)}$, $g_{00}^{(202)}$, and $g_{00}^{(110)}$.

The center–center correlation term, $g_{00}^{(000)}$ shows a peak at 4.8 Å with an area corresponding to six nearest neighbors.

The coefficients $g_{00}^{(101)}$ and $g_{00}^{(202)}$ are orientational correlation terms giving information concerning the orientation of a molecule relative to the center–center system irrespective of the orientation of the partner molecules. Above 4 Å $g_{00}^{(101)}$ is negative and $g_{00}^{(202)}$ is positive. Consequently, stronger parallel alignment of the molecular C_3 axis along the center–center line must be present ($0° \le \beta \le 54.7°$).

If the z-axis of the system is chosen to coincide with the C_3 axis of one chloroform molecule and β to the the angle between this axis and either the line joining the centers of the two molecules or the C_3 axis of a second molecule, then it is shown that: (1) for $\beta < 90°$ (parallel alignment of the C_3 axis), a negative $g_{00}^{(110)}$ results; and (2) for $\beta > 90°$ (antiparallel alignment), a positive $g_{00}^{(110)}$ results. Thus parallel and antiparallel alignment changes from one coordinate sphere to another.

In dielectric and light-scattering experiments, the correlation parameters $g_{00}^{(\ell)}$ (where $\ell = 1$ and $\ell = 2$, respectively) occur. These are related to the dipole–dipole coefficient $g_{00}^{(\ell\ell 0)}$ of the molecular point correlation function by the relation

$$g_{00}^{(\ell)} - 1 = (-1)^{\ell}(2\ell+1)^{-3/2} p \int_0^{\infty} g_{00}^{(\ell\ell 0)} 4\pi R^2\, dR$$

$$= (-1)^{\ell}(2\ell+1)^{-3/2} h_{00}^{(\ell\ell 0)} \qquad (\kappa = 0)$$

where for chloroform for $\ell = 1$, $g_{00}^{(1)} = 0.5 \pm 0.04$ from diffraction results. An estimation of $g_{00}^{(1)}$ from Kirkwood–Frohlich theory yields $g_{00}^{(1)} = 1.33 \pm 0.07$. It seems certain from neutron- and X-ray-scattering data that $g_{00}^{(1)}$ *must* be less than 1. The diffraction experimenters show that this discrepancy is a consequence of incorrect estimates of the dielectric constants or dipole moments in the fluid state. If we compare with the computer-simulated atom–atom pair distribution functions (pdfs) computed by M. W. Evans, we find that overall the pdfs are similar, although detailed agreement is not obtained (Figs. 1–3). The experimental results of Bertagnolli suggest that the

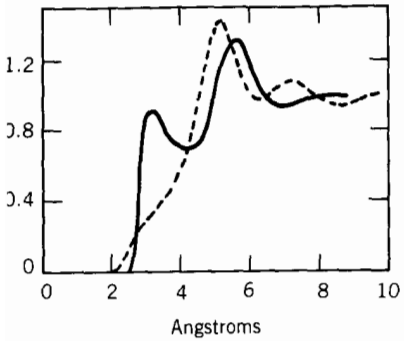

Figure 1. Atom–atom pair distribution functions: — , H—Cl; ---, H—H. [Reproduced by permission from M. W. Evans, *J. Mol. Liq.*, **25**, 211 (1983).]

chloroform structure is more tightly packed than the simulation parameters allow for (Fig. 1). However, this picture is not corroborated by Figs. 2 and 3, because the positions of the first peaks in the experimental and these numerical data agree closely. Thereafter the two data sources are less consistent. The position of the first peak in each pdf is satisfactorily established, but the noise level of the experimental pdfs is too great for detailed comment beyond this.

We should remember that there are considerable uncertainties associated with the diffraction study. Diffraction data represent a one-dimensional quantity that is the average of a number of quantities that vary with the three dimensions of the system, with the relative orientations within the system, and with time. A one-dimensional experiment cannot map a multidimensional function. There are also numerous sources of systematic error in the intricate process of reducing from the experimentally observed function to the distribution function describing the liquid structure. The overall experimental precision of ~1% currently obtainable is barely adequate, and for

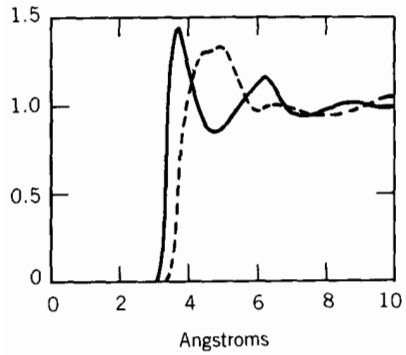

Figure 2. Atom–atom pair distribution functions: — , Cl—Cl; ---, Cl—C. [Reproduced by permission from M. W. Evans, *J. Mol. Liq.*, **25**, 211 (1983).]

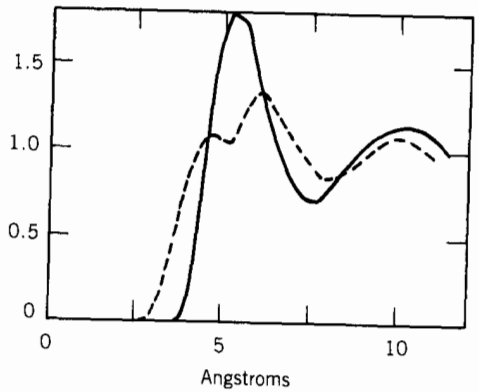

Figure 3. Atom–atom pair distribution functions: — , C—C; ---, C—H. [Reproduced by permission from M. W. Evans, *J. Mol. Liq.*, **25**, 211 (1983).]

data prior to 1960 systematic errors of 10% and more were the rule rather than the exception.

As we shall see in the following sections, problems of data reduction and systematic errors also plague the experiments used to probe the molecular dynamics. Consequently, disagreement among various experimental results is often present. We propose that computer simulation used in conjunction with the various spectroscopies may help clarify at least certain aspects of the dynamics. But first we should consider the contradictions that result when spectroscopic experiments are used in isolation to study chloroform.

All of the techniques use various assumptions and approximations in the data-reduction processes, which are used for transforming raw spectral data into correlation functions, correlation times, or some other function amenable to comparison with theory.

The early papers in the fields of infrared absorption, Raman, and Rayleigh scattering have been summarized by Brodbeck et al.[10] All calculated correlation times are compared with the simulation results of M. W. Evans in Table I. [The correlation time is defined here as the area under the correlation function (though the existence of many other definitions testifies to the confused state of the art). Correlation times allow the convenient comparison of various techniques.] Brodbeck et al. discuss the spread in the first- and second-rank orientational correlation times from various sources and comment further on the need for a universal definition of correlation time. First-rank orientational correlation times vary from 2.3 to 4.0 ps depending on definition. According to Brodbeck et al., a comparison of relaxation times from the ν_1, ν_2, and ν_3 (A_1 symmetry) fundamentals of chloroform reveals rotation–vibration coupling to be insignificant.

TABLE I
Experimental and Simulated Correlation Times for Chloroform[a]

Technique	Correlation times (at ambient T unless otherwise indicated)	Computer simulated correlation times (293 K).
Dielectric relaxation	Pure liquid: 5.4–6.4 ps Dilute *n*-hexane solution: 2.9 ps Dilute CCl_4 solution: 6.1 ps Pure liquid: 4.7–6.2 ps Dilute cyclohexane soln: 3.2 ps 10% v/v decalin soln: 4.3 ± 0.3 ps Dilute CCl_4 soln: 5.0 ps Pure liquid: 6.0 ps (294 K) 17.0 ps (223 K)	Pure chloroform at 293 K, 1 bar. First rank *autocorrelation* time of the dipole (C_{3v} axis) unit vector $\mathbf{e}_3$ $\tau_1(\mathbf{e}_3) = 3.6$ ps
Nuclear magnetic resonance relaxation	^{35}Cl transverse nuclear quadrupole relaxation times 2.0 ps (pure liquid); 1.8 ps (1.3 *n*-hexane); 3.4 ps (1.3 CH_2I_2)	A weighted mean of three second-rank correlation times of unit vectors $\mathbf{e}_1$, $\mathbf{e}_2$ and $\mathbf{e}_3$ in the principal moment of inertia axes $\tau_2(\mathbf{e}_1) = \tau_2(\mathbf{e}_2) = 1.5$ ps $\tau_2(\mathbf{e}_3) = 1.3$ ps
	^{13}C spin–lattice relaxation time: 1.60 ps	$\tau_2(\mathbf{e}_3) = 1.3$ ps
	D nuclear quadrupole relaxation: 1.84 ps	$\tau_2(\mathbf{e}_3) = 1.3$ ps
	Spin-spin relaxation: 1.5 ps, 1.74 ps	$\tau_2(\mathbf{e}_3) = 1.3$ ps
	Proton spin–lattice relaxation: 1.39 ps (298 K); 3.0 ps (219 K); 1.07 ps (363 K)	A mean of $\tau_2(\mathbf{e}_3) = 1.3$ ps $\tau_2(\mathbf{e}_1) = \tau_2(\mathbf{e}_2) = 1.5$ ps
	$\nu_3(A_1)$ (symm. CCl bend, $CDCl_3$): 5.3 ps, 6.8 ps, 6.6 ps. Variation of $\tau_2(\mathbf{e}_3)$ with def. 1.3–1.5 ps. Area defn. = 1.3 ps $\nu_1(A_1)$: 1.45 ± 0.15 ps (pure $CHCl_3$) $\nu_1(A_1)$: 1.20 ± 0.15 ps (20% mole fraction in CCl_4); 2.61 ± 0.15 ps (33% mole fraction in $(CD_3)_2CO$)	$\tau_2(\mathbf{e}_3) = 1.3$ ps (area defn.) $\tau_2(\mathbf{e}_3) = 1.3$ ps
Depolarized Rayleigh scattering	$\tau_r = 1.7$ ps $\tau_r(CDCl_3) = 2.9$ ps $\tau_r \pm 0.2$ ps (3.2) (1 bar) $\tau_r = 5.5(5) \pm 0.2$ ps (at 205 MPa $\tau_r = 2.95$ ps $\tau_r = 1.74$ ps (in 20% CCl_4 $\tau_g = 0.24$ ps (far wing Gaussian)	A weighted mean of $\tau_2(\mathbf{e}_1) = \tau_2(\mathbf{e}_2) = 1.5$ ps $\tau_2(\mathbf{e}_3) = 1.3$ ps (N.B. these are *autocorrelation* times)

TABLE I (*Continued*)

Technique	Correlation times (at ambient T unless otherwise indicated)	Computer simulated correlation times (293 K).
Far infrared absorption	Experimental peak frequencies (cm^{-1}) $\bar{\nu}_{max} = 36\ cm^{-1}$ a range of $= 45\ cm^{-1}$ 15 cm^{-1} $= 38\ cm^{-1}$ in the $\bar{\nu}_{max} = 30\ cm^{-1}$ literature (in 10% decalin v/v) $\bar{\nu}_{max} = 39\ cm^{-1}$ (in 10% decalin v/v) $\bar{\nu}_{max} = 25\ cm^{-1}$ (in 10% *n*-pentane v/v) $\bar{\nu}_{max} = 37\ cm^{-1}$ (in 10% diphenylmethane v/v) $\bar{\nu}_{max} = 50\ cm^{-1}$ (in 10% v/v decalin, supercooled to 110 K)	Simulated peak frequency, $\bar{\nu}_{max}(\text{sim.}) = 31\ cm^{-1}$ (N.B. from the rotational velocity *autocorrelation* function) Simulated peak frequency in pure $CHCl_3$ at 293 K, 1 bar = 31 cm^{-1} (Fig. 4)
	Intermolecular (translational) correlation times τ_c: 80.5 ps (298 K); 263 ps (219 K); 52.2 ps (363 K)	Calculated in the extreme narrowing limit from the center-of-mass velocity correlation time (τ_v) using $\tau_c = ma^2/12kT\tau_v = 2.1$ ps m = mass of mol. a = eff. radius
	A combination of D and ^{35}Cl nuclear quadrupole relaxation $\tau_{\parallel}$ (spinning) = 0.92 ps $\tau_{\perp}$ (tumbling) = 1.8 ps ^{13}C, nuclear Overhauser enhancement $^{13}C—^{1}H$: 1.26 ± 0.04 ps	$\tau_2(\mathbf{e}_1) = \tau_2(\mathbf{e}_2) = 1.5$ ps $\tau_2(\mathbf{e}_3) = 1.3$ ps $\tau_2(\mathbf{e}_3) = 1.3$ ps
Infrared bandshape analysis	N.B. These orientational times have been derived assuming that rotation–vibration coupling is negligible $\nu_1(A_1)$ (C—H stretch): 2.3–2.9 ps $\nu_1(A_1)$: variation with defn. of correlation time: 2.3–4.0 ps Area defn. = 2.6 ps	$\tau_1(\mathbf{e}_3) = 3.6$ ps $\tau_1(\mathbf{e}_3) = 3.6$ ps (area defn.)
Raman bandshape analysis	$\nu_1(A_1)$ (C—H stretch) 1.5 ps; 1.5 ps; literature 1.97 ps; 1.2 ps; variation 1.3 ps; 1.7 ps; 1.59 ps	$\tau_2(\mathbf{e}_3) = 1.3$ ps

TABLE I (*Continued*)

Technique	Correlation times (at ambient T unless otherwise indicated)	Computer simulated correlation times (293 K).
	$\nu_1(A_1)$ ($CDCl_3$): 1.7 ps literature 1.96 ps; 1.8 ps; variation 5.1 ps; 2.0 ps 3.1 ps	$\tau_2(\mathbf{e}_1) = \tau_2(\mathbf{e}_2) = 1.5$ ps $\tau_2(\mathbf{e}_3) = 1.3$ ps
	$\nu_2(A_1)$ (C—Cl stretch) literature 2.4 ps; 1.8 ps; variation 1.4 ps	
	$\nu_2(A_1)$ (C—Cl stretch literature $CDCl_3$): 2.4 ps [15]; variation 1.85 ps; 3.4 ps; 4.4 ps	
	Peak of Rayleigh second moment $= 45$ cm^{-1} Peak of $\nu_1(A_1)$ Raman second moment $= 50$ cm^{-1}	
Electric-field induced birefringence	Kirkwood factor $g_1 = 1.4$ Higher-order correlation factors: $g_2 = 1.7$, $g_3 = -0.4$ The factor g_1 compares with $g_1 = 1.32$ from far-infrared analysis and $g_1 = 1.25$ from dielectric permittivity	

[a] Compiled by M. W. Evans, *J. Mol. Liq.*, **25**, 211 (1983) and reproduced by permission. For references to original data sources, see this review in *J. Mol. Liq.*

The broadening of the ν_1 (C—H stretch) fundamental in liquid chloroform leads to an orientational autocorrelation function for the tumbling of this axis (the C_{3v}, or dipole, axis). Brodbeck et al. list first-rank P_1 (infrared) and second-rank P_2 (Raman) correlation times for this motion. For natural abundance $CHCl_3$ the former vary from 2.3 to 2.9 ps according to the depolarization ratio and the latter from 1.3 to 1.7 ps. The Raman orientational correlation times from the ν_2 (symmetric C—Cl stretch) range from 1.4 to 2.4 ps. These are affected by spinning and tumbling of the C_{3v} axis.

It is generally accepted that orientational correlation times from infrared and Raman bands are autocorrelation times, whereas the equivalent times from dielectric relaxation (first rank) and depolarized Rayleigh scattering (second rank) reflect the motions of many molecules, involving cross correlations. Soussen-Jacob et al.[11] have reported that the dielectric relaxation times varied from 5.4 to 6.4 ps in pure $CHCl_3$. They reported values of 2.9 and 6.1 ps for $HCCl_3$ diluted in *n*-hexane and CCl_4, respectively.

Systematic measurements have been reported in the dielectric/far-infrared region by Gerschel et al.[12] Gerschel and Brot[13] measured the static permittivity of chloroform along the gas–liquid coexistence curve to the critical point. The static Kirkwood g factor depends on the steric configuration, especially on the orientation of the dipole axis relative to the shape of the molecule. The value of g for the liquid phase of chloroform changes with temperature, and approaches unity at the critical point. Its value is the expected one of unity at all densities in the coexisting vapor, and about 1.25 in the liquid over a range of temperatures. The evolution of the dielectric relaxation time reported by Gerschel follows an Arrhenius law over a wide range of temperatures, but there is a definite temperature at which the liquid like rotational process evolves into a gaslike process in which the rotational motion is relatively freer. There is no particular critical phenomenon such as observable opalescence in the far infrared.

The study of a liquid in this way, over a range of state points, is more profitable than at one state point, as in the majority of the reported studies. Density has very rarely been used as a variable. An exception is the work of Jonas et al.,[14] who made a systematic study of liquid chloroform under hydrostatic pressure. They use second-moment analysis to reveal that "collision induced effects" play an important role in causing the second moment of the $\nu_1(A_1)$ band in liquid $CHCl_3$ and $CDCl_3$ to be density dependent. The collisional contribution to the second moment decreases with increasing density, and is revealed only by constructing the second-moment spectra using the far wings of the Raman line. These results, however, contradict those of Konynenberg et al.,[15] who suggest that there is no collisional contribution to the rotational second moment. Schroeder and Jonas[16] also measured the depolarized Rayleigh wing up to 4 kbar and out to about 200 cm^{-1}. Whereas the Raman bandshapes had dropped off fairly rapidly at 80 cm^{-1}, the Rayleigh bandshapes continue to about 180 cm^{-1} before decaying rapidly. They interpret this in terms of many-body collision effects at short times (in the range 0.03–0.5 ps).

The far infrared also produces the second moment, and Lund et al.[17] showed that Rayleigh and far-infrared second-moment spectra peak at the same frequency (45 cm^{-1}) and are similar in shape.

Claesson et al.[18] have also reported Rayleigh correlation times to 205 MPa. These vary linearly from 3.2 ± 0.3 ps at 0.1 MPa. The dependence of the rotational relaxation time on bulk viscosity at constant temperature is also linear, with a nonzero intercept. Claesson et al. compare their results with high-pressure nuclear magnetic resonance (NMR) and Raman data and discuss the effect of pressure on pair correlations. The NMR rotational relaxation times intersect the zero viscosity axis at different points from, and do not lie on the same straight line as, the Rayleigh correlation times. On

the basis of these measurements pair correlations would seem to be significant in chloroform. Claesson et al. point out that the Raman and NMR correlation times do not agree except at atmospheric pressure. A comparison of the Rayleigh and Raman times shows that pair correlations decrease as hydrostatic pressure is increased, which conflicts with the view of Schroeder and co-workers. In the absence of collision-induced effects, τ_ω should increase faster than τ_2, according to Claesson, if only because of the increase in the number of scatterers (N) in the scattering volume. However, that this is not observed might be explained if the collision induction hypothesis of Schroeder is correct.

The NMR and Rayleigh scattering times of Alms et al.[18] are also shown in Claesson's plot. On the basis of the reported measurements, pair correlations seem to be significant in chloroform. At high pressures the Rayleigh light-scattering and Raman times approach each other, suggesting that the magnitudes of the static and dynamic contributions to the pair correlations change with pressure, that the approximations used to obtain single-particle relaxation times from these scattering techniques are not valid, or a combination of both. Alms et al. show that the depolarized Rayleigh times they calculated are strongly concentration dependent for chloroform, perhaps supporting their view that strong pair correlations affect the data at high concentrations. Or it might support the different interpretation, in terms of collision-induced absorption, of the same set of results by Jonas and coworkers. Alms et al. report a dynamic correlation factor of 1 for pure liquid chloroform, which may be compared with Gerschel's static Kirkwood factor of 1.25.

The confusion and contradiction in the literature concerning the dynamics from Raman and Rayleigh scattering alone is already apparent, and it continues. Kamagawa,[20] for example, has reported a depolarized Rayleigh study of $CHCl_3$ in CCl_4 in which the relaxation times are independent of the concentration of solution, in direct contradiction to the findings of Alms et al. Kamagawa analyzes his spectra in terms of several different relaxation times (overcomplicating the problem), calculated from the half-widths of the central and far wing positions. He comes to a conclusion opposite to that of Schroder et al. concerning the collision-induced effects, suggesting, on the basis of his observed relaxation times, that the effects cannot be important. He asserts that if the spectrum is caused by a binary collision process, A should be proportional to N^2, whereas he observes A to be linear with N (where A is the integrated intensity and N the number density).

Analysis by M. W. Evans of far-infrared collision-induced processes (ref. 21, Chapter 11) shows that collision-induced effects are not pairwise additive in molecular terms in the *liquid state* (in the gas phase, an N^2 dependence may exist). The far-infrared evidence does agree in one respect with

Kamagawa's analysis, in that A is linear in N. However, the problem is not easily resolved with spectroscopic evidence alone. There are examples of liquids in which the collision-induced contribution is displaced from the permanent dipole absorption (an example is N_2O). But there is not always such a displacement to ease the interpretation, and Lund et al.,[17] who construct the second moment of the Rayleigh wing spectrum and compare it with the far infrared, establish that there is no distortion of the bandshapes in chloroform (the bandshapes from both spectral sources are similar, and peak at 45 cm^{-1}). This is typical of the problems associated with analyzing a broad, featureless band. All we can really say based on these results is that in chloroform either collision-induced effects are small or they have the *same frequency dependence* as the underlying reorientational process at ambient temperature and pressure. Any far-infrared conclusion, of course, must directly contradict one of these two extreme viewpoints arrived at in the literature from different probe experiments on the same sample.

The induced contributions to the Raman spectra are likewise uncertain. Schroeder et al.[14] construct the second moment of the far wing of the Raman ν_1 mode at pressures up to 4 kbar. At 30 bars this peaks at about 50 cm^{-1} (cf. the 45 cm^{-1} peak of Lund et al.[17] based on the Rayleigh wing), and the spectrum is noticeably similar in appearance to the zero-THz spectrum.[22] The area under this curve *decreases* rapidly with increasing number density as the hydrostatic pressure is increased to 5 kbar at 303 K. On this basis, Schroeder et al. conclude that multibody collision induction is responsible for the shape of the second-moment Raman spectrum of the chloroform ν_1 mode. The Rayleigh wings reported by Schroeder et al. behave similarly to the Raman ν_1 wing, and it is clear that the integrated intensity per molecule of the Rayleigh spectrum decreases in the wing portion as the pressure is increased to 4 kbar from 30 bars at 303 K. However, in neither the Raman nor the Rayleigh experiments does the behavior of the low-frequency part of the scattered intensity (close to the exciting line) as a function of pressure emerge. The *complete range* (0 THz dielectric, plus far infrared) should be the entity for analysis, as we have observed in our own spectroscopy. The low-frequency Raman and Rayleigh scattered intensities must dominate the overall integrated intensity. Conversely, if second moments are calculated (e.g., the far infrared), the low-frequency components are suppressed and the high-frequency components dominate. (We have discussed this at length elsewhere.[23]) Analyses should proceed through the zeroth, second, and higher moments if a satisfactory picture of the various contributory processes is to emerge.

It is possible, for example, to interpret the results of Schroeder in another way: in terms of dimer formation. If the population of dimers (which might even be weakly hydrogen bonded) were to increase with hydrostatic pres-

sure, which is plausible, then the effective moment of inertia of C—H scattering units would increase. This would show up as a decrease in the second moment of the Raman ν_1 band. Suzuki et al.[24] report that the infrared ν_1 band is markedly asymmetric, with a tailing on the high-frequency side at ambient temperature and pressure. They point out that the integrated intensity of the chloroform infrared ν_1 band increases from 11 to 198 $cm^2\ mol^{-1}$ on passage from the gas to the liquid phase, and interpret this in terms of hydrogen bonding. Rothschild et al.[25] reject this hypothesis on the basis of their infrared and Raman data, and several subsequent studies, including those of Schroeder et al., have been based on the assumption that the ν_1 band is homogeneous (i.e., unaffected by hydrogen bonding). Suzuki et al. point out that the infrared ν_1 fundamental is strongly asymmetric in bulk $CHCl_3$ and $CDCl_3$ and that its width in $CDCl_3$ is significantly narrower. Moradi-Araghi et al.[26] have postulated that vibration–rotation coupling is stronger for the ν_1 mode in $CHCl_3$ because of anharmonic terms in the vibrational Hamiltonian, but Suzuki et al. reinterpret this as the formation of dimers through hydrogen bonding. They suggest that the ν_1 infrared profile is composite, with contributions arising from a dimer species, the monomer, and a combination mode or pseudolattice vibration. The intensity of the dimer band is reported to decrease relative to that of the monomer band on dilution in CCl_4, but their positions remain constant. The peak frequency and absolute intensity of the monomer band are closer to the values for gaseous chloroform. It is precisely this high-frequency ν_1 profile that is reported by Schroeder et al. in their Raman studies. Suzuki et al. claim that *44% of the molecules in pure liquid $CHCl_3$* at ambient temperature and pressure *are bound into dimers*. They also comment on the uncritical use of the intensity of vibrational modes for the study of intermolecular interactions, asserting that a vibrational spectrum in the condensed phase is composed, in principle, of *different* band maxima and intensities, corresponding to different species of monomer and dimer.

There is little corroborative evidence from other sources for the existence of hydrogen bonding in liquid chloroform. In fact, Gerschel's dielectric–far-infrared studies suggest that the Kirkwood g factor remains near unity along the gas–liquid coexistence curve, although higher values for this factor have been proposed, as discussed earlier. The value of ΔU, the maximum energy of dipole–dipole interaction, for chloroform in the gas phase is, at ca. 900 cal mol^{-1}, one of the smallest calculated. For H_2O, CH_3OH, and CH_3CN, ΔU is 5–6 times larger.[27] Also, Tanabe et al.[28] have investigated the Raman ν_1 stretch of $CHCl_3$ in different solvents. The bandwidths of solutions of $CHCl_3$ in water are about twice as large as those of neat liquid, or of $CHCl_3$ in CCl_4 or C_6D_{12}. This contrasts with the behavior of solutes such as CH_3OH, CH_3CN, CH_3NO_2, and acetone, and provides unambiguous evidence that the hydrogen bonding between $CHCl_3$ and H_2O solvent

molecules is considerably weaker than in these other cases. On this evidence, the hydrogen bonding between $CHCl_3$ molecules in the pure liquid should be weak, amounting to no more than a slightly increased probability for certain configurations over others. There is no significant evidence for dimer formation in the X-ray- and neutron-diffraction atom–atom pdfs of Bertagnolli et al.[9]

It seems clear, however, that the infrared, and possibly the Raman, ν_1 fundamentals in $CHCl_3$ and $CDCl_3$ liquids are asymmetric, and consequently it is by no means unequivocal that the results of Schroeder et al. may be attributed to collision-induced absorption. Considering all of the evidence, it seems more plausible that the asymmetry of the ν_1 mode is caused by inhomogeneous broadening. This has recently been discussed by Laubereau et al.,[29] who find that rotational coupling with vibration, Fermi resonance, and resonance-energy transfer strongly affect the spontaneous Raman data. The second-moment behavior observed by Schroeder et al. may be explained in terms of decreased inhomogeneous broadening with increasing hydrostatic pressure. This assumes that the stimulated (Laubereau et al.) and spontaneous (Schroeder et al.) Raman processes behave similarly in this respect. In one sense, the inhomogeneous-broadening and hydrogen-bonding schools of thought can be reconciled as both being descriptions of the anisotropy of the local environment.

An interesting experiment is that of Moradi-Araghi et al.,[30] who have recently reported in detail a variety of reorientational correlation times obtained from the polarized and depolarized Raman spectra of the ν_1 band in neat $CHCl_3$, $CDCl_3$, and solutions of $CHCl_3$ in CCl_4, acetonitrile, and acetone. The second-rank orientational correlation functions decay more rapidly in CCl_4 than in the neat liquid, but more slowly in the two dipolar solvents. This is contrary to expectations based on classical rotational theory, according to Moradi-Araghi et al. The present authors feel that in saying this, Moradi-Araghi et al. are being overcritical of the diffusion models, which cannot be expected to follow the behavior of a polar solute in a more polar, strongly interacting solvent. Moradi-Araghi et al. proceed to interpret their results in terms of specific solute–solvent interactions causing a loss of reorientational correlation and vibrational dephasing in each solvent. They assume complete decoupling of rotation from vibration—a view shared by Brodbeck et al.[10] but not by van Woerkom et al.[31] If we accept this approximation, the second-rank correlation times vary from 1.45 ± 0.15 ps in pure $CHCl_3$ at room temperature and pressure to 1.20 ± 0.15 ps in 20% (mole fraction) $CHCl_3$ in CCl_4. These correlation times *are not* proportional to the bulk viscosity.

Van Woerkom et al. use isotope dilution methods to show that vibration is not statistically independent of rotation in the infrared spectra of liquid $CHCl_3$, $CDCl_3$, and $CHCl_3$–$CDCl_3$ mixtures. This point of view is shared

by Laubereau et al. for stimulated Raman scattering. The conclusion reached by Brodbeck et al. that rotation–vibration coupling is negligible conflicts with the conclusions of van Woerkom et al.

Wertheimer[32] has recently questioned the interpretation of isotropic Raman band contours in terms of vibrational autocorrelation functions. He considers other processes that may affect the broadening of a Raman band, including vibrational decoupling from excited quantum states, resonance transfer (vibrational exciton hopping), and pure dephasing (transition-frequency fluctuations). If he is right, the rotovibrational correlation function from a Raman band is collective and *not* a pure autocorrelation function. The complexity does not end there, because the homogeneous bandwidths are then only interpretable in terms of a sum of these processes, *together with cross terms from the interference mixing* of pure dephasing and resonance-transfer processes and of resonance-transfer transitions involving *different* pairs of molecules. Resonance-transfer contributions are reduced on dilution (for experimental purposes, isotopic dilution is convenient). Recall that Suzuki et al. produced evidence suggesting that the ν_1 mode of $CHCl_3$ is asymmetric and, in a sense, made up of weakly separated bands. For such circumstances Wertheimer provides a series of theoretical results tracing the origins of these weakly separated bands to the equivalent excitations in isotopic mixtures. The widths of the vibrational self-correlation functions are found to be essentially independent of concentration, because the nearly resonant transfer involving molecules of different types is almost as fast as the resonance transfer between molecules of the same species. The collective modes, involving two or more molecules, are dynamically coupled.

Wertheimer calls these processes "collision induced" processes. These differ from the collision-induced processes observed in the far-infrared or Rayleigh scattering experiments. The latter are multibody, non-pairwise-additive processes that involve the molecular polarizability anisotropy explicitly. Wertheimer assumes that the dynamic isotropic polarizability α of the liquid system is *a pairwise-additive* superposition of the polarizabilities of its individual molecules. This contradicts the Rayleigh–Schrödinger picture of basic quantum mechanics, in which polarizability is clearly not molecularly pair additive. Wertheimer's collision-induced processes are what we more normally call cross-correlations, that is, statistical influences of the motion of one molecule on that of another.

Wertheimer also summarizes the basic (and incorrect) assumptions about rotation–vibration coupling and cross-correlations made in the majority of papers in this field. Without these assumptions, the results of Schroeder et al. may be interpreted as indicative of the presence and significance of cross-correlations in the ν_1 mode because an increasing number density with hydrostatic pressure would not, in principle, cause the second moment to

decrease as observed. Döge et al.[33] have shown, in a careful study of chloroform dissolved in CH_3I solvent, how molecular-environment changes affect the ν_1 mode of $CHCl_3$: The band shape is "drastically" broadened.

Carlson et al.[24] have concluded that half of the scattering for a system of independent, noninteracting molecules is affected by cross-correlations (in the sense of Wertheimer) and by transient, collision-induced perturbations. They also argue that the Kerr effect and Cotton–Mouton effect (which we shall consider later) are unaffected by collision-induced phenomena. They proceed to develop an experimental technique, based on interference filters, for estimating the collision-induced intensity of the depolarized Rayleigh spectrum. This is based on the theory of Bucaro et al.,[35] who assume the collision-induced processes to arise from isolated binary collisions. However, the Kerr and Colton–Mouton effects are probably *not* free of induced effects, because collision processes affect also μ, the permanent dipole moment. The effect may be observed directly in the far infrared, where nondipolar molecules absorb over a broad range of frequencies because of induced temporary dipoles.

All in all, there is considerable uncertainty about the role of collision-induced absorption in the Rayleigh and Raman spectra of $CHCl_3$. Some authors do not discuss it or claim it to be unimportant. Others claim it accounts for as much as one-half of the relevant spectral intensity. More work is required on intensity measurements by Rayleigh scattering, on compressed vapors such as those of $CHCl_3$, and along the gas–liquid coexistence line, following the excellent work of Gerschel. Ho and Tabisz[36] emphasize the need for a theory of "close encounters" in the collision-induced Rayleigh scattering, assumed to be present in liquid chloroform.

Lastly, there is the question of the internal field to be solved. Burnham et al.[37] have made a detailed study of the internal-field corrections available in the literature, and point out that for Raman and Rayleigh scattering both the choice of the model and the local-field corrections are in question. To explain both the observed isotropic intensity and the depolarization ratio, it is necessary to use an ellipsoidal model of the internal field. If we wish to be able to comment on collision-induced depolarized Rayleigh intensities, we must first be concerned with solving the problem for any molecule whose polarizability tensor has anisotropic components.

The list of far-infrared and dielectric relaxation measurements available for chloroform is almost as lengthy as that of infrared, Raman, and Rayleigh scattering experiments. The dielectric and far-infrared spectra, considered *as an entity*, we call the 0 THz spectrum. The far infrared is the high-frequency adjunct of the low-frequency loss first considered in detail by Debye. It is unsatisfactory to consider one part of the frequency range without the other, because both together define the total molecular-dynamical evolution of an

ensemble of molecules in the condensed state. The two processes (the long- and short-time details) are separated by only a few decades of frequency in normal isotropic liquids, but may be separated by many decades of frequency (up to 14) in, for example, systems forming glassy or disordered states and liquid crystalline systems.

It is misleading to consider only a part of the total frequency span. Debye's model and extended rotational diffusion models, for example, work adequately at the lower frequencies, but may not even predict the existence of the high-frequency component. Debye's theory predicts that all liquids are more or less opaque at frequencies above 10^{12} Hz, including, of course, the visible-light frequencies. Yet it is still used frequently in the literature, either openly or in somewhat disguised form. Debye's model is a gross oversimplification the molecular dynamics that, particularly if used in data-reduction processes, confuses the interpretation of (and conclusions drawn from) experimental results. Experimentalists would not, in an ideal world, use these simplistic theories based on subjective ideas and incorporating so many *ad hoc* assumptions and often numerous adjustable parameters. As Gerschel has shown, it is far more profitable to expend one's energy in more detailed, precise, and extensive experimentation than to analyze a few room-temperature spectra with these models.

We have already reviewed Gerschel's studies of phenomena along the gas–liquid coexistence line. The rapid increase in interest in 0 THz spectrum is justified because of its ability to provide zeroth and second moments of the spectral system routinely and *without* the complication of mixing of intra- and intermolecular motions, which we have seen may severely distort Raman and infrared band profiles. Evans et al.[38] have indicated how one may obtain fourth and sixth moments from the high-frequency wing of the far-infrared band *providing* they are free of proper mode interference. Choosing the molecular liquid carefully is essential. An acceptable theory should be able to reproduce all of these spectral moments, not just the first one or two (the usual literature procedure).

In addition to the substantial shifts in the frequency of maximum absorption ($\bar{\nu}_{max}$) observed by Gerschel, $\bar{\nu}_{max}$ shifts occur on dilution in nonpolar solvents. According to Leroy et al.,[39] the pure-liquid spectrum peaks at 36 cm^{-1}, but the location of the peak varies from 25 to 33 cm^{-1} in various solvents (e.g., it is at 30 cm^{-1} in decalin). These shifts reflect directly the importance of the environment in determining the molecular dynamics, but there is *no straightforward and predictable dependence*. When chloroform is dissolved in decalin and *n*-pentane, $\bar{\nu}_{max}$ shifts from 36 cm^{-1} to lower frequencies, as anticipated and in accord with the predictions of molecular-dynamics theories. But in CCl_4, $\bar{\nu}_{max}$ actually shifts to *higher* frequencies. So too in diphenylmethane a smaller but discernible shift to higher frequencies occurs. The data show the extreme importance of the local molecular environment in determining the measured spectra. No current simple diffusional theory would predict these shifts to higher frequencies on dilution. The solvent is generally assumed to reduce dipolar cross-correlations, but apparently such cross-correlations may actually be increased in some solvents. (We will see further examples of this in the later sections on CH_3I and, in particular, CH_3CN dissolved in CCl_4.) In such solvent shifts, the reduction of cross-correlations and solvent rotational hindrance and interaction are contributory and competing factors that affect the overall dynamics of the solute probe. Nuclear magnetic resonance spectroscopists, who use dilution methods extensively to obtain correlation times, in particular should bear these factors in mind. Evans[22] compared far-infrared data with low-frequency results and the far-infrared results of other groups. His data are corrected for the contribution of an intermolecular mode at higher frequencies (Fig. 4).

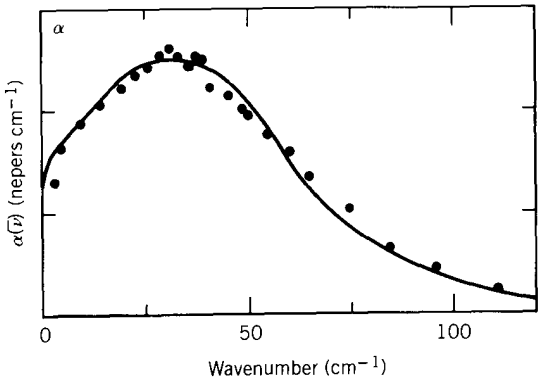

Figure 4. The far-infrared spectrum of chloroform at 293 K, 1 bar: computed (●) and measured (—). [Reproduced by permission from M. W. Evans, *J. Mol. Liq.*, **25**, 211 (1983).]

The effect of hydrostatic pressure on this spectrum is to shift the peak to higher frequencies, as Gerschel showed by heating the liquid in a closed vessel. The effect of supercooling in decalin solvent is again to shift $\bar{\nu}_{max}$ to considerably higher frequencies and to sharpen the band profile.

The integrated intensity of the far-infrared band has been compared with the theoretical predictions based on the Gordon sum rule for the pure liquid by Hindle et al.[40] and for a 10% solution in decalin by Reid and Evans.[4] Both groups use a simple frequency-independent correction for the internal field—an oversimplification. However, Hindle et al. find that 88% of the observed intensity is produced by the sum rule, whereas Reid and Evans find that 73% of the intensity is produced by the sum rule in a 10% solution in

decalin. This suggests that there is at least a 25% contribution to the measured intensities, even in a 10% solution, that *may not* be attributed to a purely rotational origin—assuming the validity of the Gordon sum rule.

Bossis[42] has discussed the application of this sum rule to highly dipolar molecules, in which in principle a mechanism of dipole-induced dipole induction should cause the theoretical intensity to be supplemented considerably. He elaborates on the original work of Gordon and concludes that induced effects are unlikely to be important in liquid chloroform and that, consistent with the results of Gerschel et al., they disappear at the critical point. We point out that the contour of any dipole-induced dipole absorption would be the same as that of the permanent dipole absorption—note the similarity of the bandshapes for polar liquids and nonpolar liquids in the far infrared.[21] Quadrupole-induced dipole absorption, on the other hand, would peak at a higher frequency.

Further evidence against a simple mechanism of collision-induced absorption contributing significantly to the chloroform spectrum is the apparent linearity of the integrated absorption intensity with dilution. However, such studies should be extended to concentrations well below 1%. In CH_3CN, for example, a distinct nonlinearity exists that is not observed until the concentration is approximately 10%. Dilution studies should cover the widest range possible.

However, to proceed it is necessary to assume that the far-infrared band of liquid chloroform is due to reorientation of the permanent dipole moment. Several groups have attempted to reproduce this unreduced band shape accurately, including Quentrec and Bezot,[43] Evans,[22] Reid and Evans,[41] and Evans et al.[38] A recent development in the field of theoretical modeling is the constrained librator model of Gaiduk and Kalmykov,[44] which was fitted to liquid-chloroform data over the 0 THz range using a minimum of adjustable variables. Hermans and Kestemont[45] have also considered theoretically the 0 THz chloroform absorption.

Nuclear magnetic resonance results are also extensive. We have reviewed some of these data already in the section on Rayleigh and Raman scattering. A disadvantage of NMR measurements is that they can produce only correlation times and not complete correlation functions (see ref. 21, Chapter 6). Forsen et al.[46] have discovered pronounced solvent effects on the chlorine magnetic-resonance relaxation of liquid chloroform (^{35}Cl and ^{37}Cl nuclei) at 303 K. They give ^{35}Cl transverse relaxation times for the neat liquid and for solutions. For the neat liquid this time is 2 ps, in a 1 : 3 solution in *n*-hexane it is 1.8 ps, and in a 1 : 3 solution in CH_2I_2 it is 3.4 ps. Shoup and Farrar[47] have measured the ^{13}C spin–lattice (R_1) and spin–spin (R_2) relaxation rates for 60% enriched chloroform. R_1 is dominated by the intramolecular dipole–dipole interaction with the proton, and R_2 by scalar coupling to the

chlorine nuclei. The activation energies associated with the anisotropic molecular motion, and the rotation diffusion constant, were obtained from the ^{13}C relaxation data and found to agree well with those obtained from D and Cl studies by Huntress.[48] Spin-rotation contributions were assumed to be small, and intermolecular contributions to the total R_1 were not considered. R_1 is determined, therefore, by a correlation time τ_c characteristic of the tumbling motion of $CHCl_3$ (i.e., motion of the C_{3v} symmetry axis). The $^{13}C—H$ vector is on the axis, and spinning *around* C_{3v} does not contribute to R_1. R_1 is related to τ_c using the expression involving the dipole–dipole relaxation of two unlike spins, assuming the model of rotational diffusion for the molecular dynamics. This gives a correlation time of 1.6 ps, compared with a value of 1.74 ps from nuclear D quadrupole relaxation. These values are smaller than the transverse relaxation time (2 ps) reported by Forsen et al.[46] Two more values of τ_c are listed by Brodbeck et al.,[10] namely 1.5 and 1.73 ps at ambient temperature and pressure.

A rotating-frame spin–lattice relaxation time of 44 μs has recently been reported by Ohuchi et al.[49]; this compares with the ^{35}Cl nuclear quadrupole relaxation time of 21 μs in pure $CHCl_3$ reported by Forsen et al.[46] The spin-rotation mechanism is neglected by Shoup and Farrar.[47] The NMR relaxation time reported by Alms et al.[19] agrees with the Rayleigh-scattering correlation time at infinite dilution. Dinesh and Rogers[50] have also measured the proton spin–lattice relaxation in liquid chloroform from 219 to 363 K at 1 bar. According to these authors, the spin-rotational relaxation rate is *larger* than the intramolecular dipolar term over the entire temperature range, which finding conflicts with the view of Shoup and Farrar. Dinesh and Rogers point out the considerable disagreement in the NMR literature on chloroform, which extends to the actual value of the proton spin–lattice relaxation time and to the various contributory factors involved. They write the experimental spin–lattice relaxation rate as a sum of contributions from at least five different sources: intra- and intermolecular dipolar mechanisms, spin rotation, scalar coupling, and the anisotropy of the chemical shift tensor. The first three depend on temperature, the scalar-coupling term on temperature and frequency, and the chemical shift tensor on the strength of the magnetic field used. Dinesh and Rogers neglect the last two contributions and from the first three extract a rotational correlation time *using rotational diffusion theory*. They also derive a translational correlation time, but point out that they make many assumptions in data reduction before arriving at this parameter. The rotational correlation time varies from 3 ps at 219 K to 1.39 ps at 298 K to 1.07 ps at 363 K, and the translational correlation time from 263 ps at 219 K to 80.6 ps at 298 K to 52.2 ps at 363 K. The rotational correlation times are taken from Huntress,[48] and also quoted are diffusion coefficients for tumbling and spinning in $CDCl_3$. The anisotropy of the

molecular diffusion is much greater at 219 K, and at 293 K and 1 bar the motion about the symmetry axis is faster than the motion about a perpendicular axis by a factor of about 2. In contrast, in the gas phase, $CDCl_3$ rotates about twice as fast about a perpendicular axis as it rotates about the C_{3v} axis. This conflicts with the data of Forsen et al. on ^{35} Cl transverse relaxation times. Huntress attributes the liquid-phase behavior to weak hydrogen bonding or self-association.

Farrar et al.[51] report the temperature dependence of ^{13}C relaxation studies in $CHCl_3$. Duplan et al.[52] report the Overhauser effect on the $^{13}C—^{1}H$ nuclei in chloroform, and give a relaxation time of 1.26 ± 0.04 ps for the motion of the axis perpendicular to the C—H axis. This compares with an equivalent value of 1.8 ps from Huntress and values of 1.6, 1.5, and 1.7 ps from other sources in the literature.

Nonlinear techniques have been used to study chloroform. Ho and Alfano[53] and Ratzch et al.[54] pioneered use of the "electrooptical Kerr effect," in which liquid-phase anisotropy is induced by electromagnetic radiation, enabling experimentation on a picosecond time scale using trains of laser pulses. Beevers and Khanarian[55] have used the electric-field-induced Kerr effect to study a number of liquids, including chloroform, over the temperature range 175–343 K. The Kerr effect is related to the polarization $\langle P_1(\cos\theta)\rangle_E$ and alignment $\langle P_2(\cos\theta)\rangle_E$, where P_1 and P_2 are the first and second Legendre polynomials, respectively, and θ is the angle between the dipole axis of the reference molecule and the applied field. Beevers and Khanarian combine Kerr-effect, dielectric, and light-scattering data to analyze the temperature dependence of $\langle P_2(\cos\theta)\rangle_E$. They compare their results with those obtained from studying the effect of an applied electric field on the NMR relaxation, and conclude that there is no hydrogen bonding of significance in chloroform and that orientational order is determined primarily by shape and electrodynamic effects. They estimate a value for the Kirkwood g factor of 1.4, which is larger than the estimate of Gerschel and deviates even further from the diffraction results, which demand that this should be less than 1. They estimate g_2 and g_3 to be 1.7 and -0.4, where

$$g_2 = 1 + \sum_{i \neq 1} \langle \tfrac{3}{2}\cos^2\theta_{1i} - \tfrac{1}{2} \rangle$$

$$g_3 = 1 + \sum_{i \neq 1} \sum_{i \neq 1 \neq j} \langle \tfrac{3}{2}\cos\theta_{1i}\cos\theta_{1j} - \tfrac{1}{2}\cos\theta_{ij} \rangle$$

The value of g_1 remains constant with temperature, but g_2 and g_3 show a weak temperature dependence. It is not clear why this temperature dependence should exist.

Beevers and Khanarian discuss some of the theoretical difficulties associated with the reduction of Kerr-effect data. We have already referred to the possible contribution from induced effects, but the main problem, as with so many of these experimental techniques, revolves around the contribution of the internal field. There is no easy or available solution to this problem. Proutière and Baudet[56] point out that in the Kerr-effect experiment the applied field is so strong that it is necessary to take into account nonlinear polarization phenomena and Buckingham et al.[57] have shown that hyperpolarizability effects are discernible in the Kerr effect when applied to gases. Proutière and Baudet compare their Kerr-effect results with those obtained from other sources, and show that the theoretical expression of Langevin and Born is not valid in the condensed state of matter. They derive an improved theoretical expression for the Kerr constant that still contains some of the uncertainties referred to above, and discuss the influence of electrostriction. Few seem to have discussed the bulk turbulence that is induced in the presence of these strong fields, as reported recently for nondipolar liquids by Evans.[58]

The nonlinear refractive index of liquid chloroform has been derived for the first time by Ho and Alfano[53] using the optical Kerr effect induced by picosecond laser pulses. This factor contains all the nonlinear contributions from electronic, librational, and reorientational motions, and the technique used to derive it is potentially of interest.

Brillouin scattering and sound dispersion can be used in combination to provide information on density fluctuations and vibration–translation coupling. Takagi et al.[59] have made ultrasonic measurements in liquid chloroform over the frequency range 3 MHz to 5 GHz using pulse–echo overlap, high-resolution Bragg reflection, and Brillouin scattering. The observed velocity dispersion revealed two relaxation processes, one at 650 MHz and the other at 5.1 GHz, both at 293 K. The lowest (261 cm^{-1}) and the second-lowest (366 cm^{-1}) fundamental vibrational modes have a common relaxation time of 50 ps. Every mode above the third has a relaxation time of 290 ps. These compare with the relaxation time of 104 ps measured by Samios et al.[60]

Yoshihara et al.[61] have measured the refractive indices and Brillouin frequencies for chloroform, which show significant deviations from values predicted based on the law of corresponding states. Altenberg[62] has discovered that the velocities of sound in a number of organic compounds, including chloroform, are smaller than in the deuterated analogues. Samios et al.[60] measured the temperature dependence of the relaxation strength, which is an indication of the nature of the observed relaxation process. They observed translation–vibration energy transfer involving the lowest and second-lowest energy level. The temperature dependence of the relaxation time provides information on the inelastic collision cross section and on the nature of the

intermolecular potential. Vallauri and Zoppi[63] have analyzed the temperature variation of the relaxation time in liquid chloroform, which is described by these authors as "non-associated."

This then has been a short synopsis of a substantial literature search by M. W. Evans on one of the most studied of molecular liquids. It is difficult, as the reader may now appreciate, to explain this mass of experimental data consistently. We cannot even conclude that the liquid is nonassociated without having to explain some observations that strongly suggest otherwise. If there is association, then further analysis relating to single-molecule behavior is severely complicated, and perhaps even meaningless. Confusion exists concerning the role of collision-induced scattering, rotation–vibration coupling, vibration cross correlation, rotation–translation coupling, and even the anisotropy of diffusion in liquid chloroform. The NMR relaxation data, for example, support two irreconcilable conclusions about whether chloroform spins faster than it tumbles.

Let us see if the computer simulation by M. W. Evans helps reconcile any of these apparent discrepancies. In the simulation, the equations of translational motion are solved with a third-order predictor routine, and those of rotational motion are solved using as coordinates the angular momentum and the three unit vectors along the principle axes of the moment-of-inertia tensor. The Lennard-Jones parameters are as follows:

$$\sigma(\text{H—H}) = 2.75\ \text{Å}$$
$$\sigma(\text{Cl—Cl}) = 3.50\ \text{Å}$$
$$\sigma(\text{C—C}) = 3.20\ \text{Å}$$
$$\varepsilon/k(\text{H—H}) = 13.4\ \text{K}$$
$$\varepsilon/k(\text{Cl—Cl}) = 175.0\ \text{K}$$
$$\varepsilon/k(\text{C—C}) = 51.0\ \text{K}$$

Partial charges were added to each atomic site of

$$q_{\text{H}} = 0.131|e|$$
$$q_{\text{C}} = 0.056|e|$$
$$q_{\text{Cl}} = -0.063|e|$$

Correlation times (experimental and simulated) are compared in Table I. By comparison of the reorientational autocorrelation functions of $\mathbf{e}_3$ (a unit vector in the C_{3v} axis) and $\mathbf{e}_1$ (a unit vector in a perpendicular axis through the center of mass), the simulation yields the conclusion that the anisotropy of the rotational diffusion is smaller than that of Huntress and *opposite in sense*. That is, the spinning motion, characterized by $\langle \mathbf{e}_1(t)\cdot\mathbf{e}_1(0)\rangle$, has a longer correlation time than the tumbling, characterized by $\langle \mathbf{e}_3(t)\cdot\mathbf{e}_3(0)\rangle$. This is the "gas phase" result, and is the result suggested by Forsen et al.[46] based on ^{35}Cl measurements. It is also interesting to note that the Raman correlation times for the totally symmetric C—Cl band ($\nu_3(A_1)$) listed by Brodbeck et al.[10] are longer than those from the $\nu_1(A_1)$ and $\nu_2(A_2)$ modes, which again means that spinning is *slower* than tumbling, not faster as suggested by Huntress.

The first- (τ_1) and second- (τ_2) rank simulated autocorrelation times are as follows:

$$\tau_1(\mathbf{e}_1) = 3.9\ \text{ps}$$
$$\tau_2(\mathbf{e}_1) = 1.5\ \text{ps}$$
$$\tau_1(\mathbf{e}_3) = 3.6\ \text{ps}$$
$$\tau_2(\mathbf{e}_3) = 1.3\ \text{ps}$$

Dielectric results *do not* give single-particle correlation times, so the simulated times compare with those estimated from dielectric relaxation of 4.7–6.2 ps in neat solution and 3.2–5 ps (depending on the solvent) in solution. There is a large degree of uncertainty to the experimental correlation times, and they all tend to be longer than the simulated times.

As we have said, the far infrared is the high-frequency adjunct of the dielectric loss, and may be related via a Fourier transform to the rotational velocity autocorrelation function $\langle \dot{\mathbf{e}}_3(t)\cdot\dot{\mathbf{e}}_3(0)\rangle$. This is similar in shape to the orthogonal autocorrelation function $\langle \dot{\mathbf{e}}_1(t)\cdot\dot{\mathbf{e}}_1(0)\rangle$, indicating that at short times the computer predicts little diffusional anisotropy. The Fourier transform of $\langle \dot{\mathbf{e}}_3(t)\cdot\dot{\mathbf{e}}_3(0)\rangle$ peaks at 31 cm^{-1}, which compares with experimental values of 36 cm^{-1} in the pure liquid and 30 cm^{-1} in cyclohexane. The *shapes* of the simulated and experimental curves are similar (Fig. 4), so if the result is not simply fortuitous, collision-induced absorption, hydrogen bonding, and internal-field effects are all small. However, we must recall that the experimental spectrum is the result of the interaction of electromagnetic radiation with an ensemble of molecules, so that cross terms are certainly important. We would not have anticipated such good agreement between the experiment and simulation, because the two techniques are not strictly comparable—the simulation can produce *only* autocorrelation functions. A frequency-dependent correction has to be applied to the experimental spectral intensity to account for this dynamic internal field effect. After this correction has been applied, the resulting bandshape may be related to a correlation function, assuming the validity of the fluctuation–dissipation theorem in the adiabatic approximation. Chatzidimitriou-Dreismann and

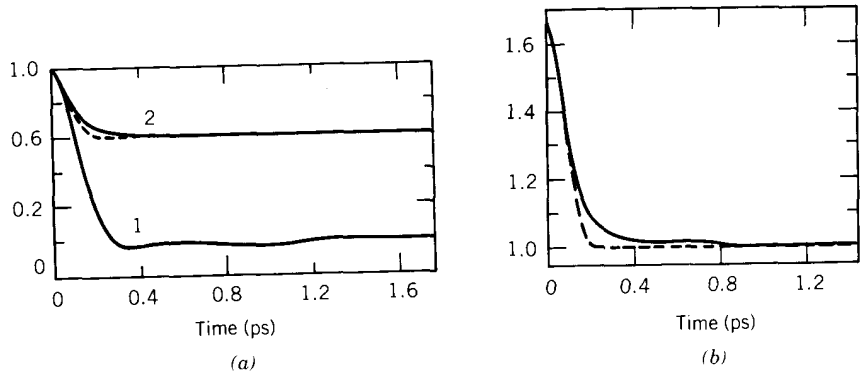

Figure 5. The non-Gaussian behavior of the pdfs governing the approach to equilibrium. (*a*) Linear velocity autocorrelation function: 1, $\langle \mathbf{v}(t)\cdot\mathbf{v}(0)\rangle/\langle \mathbf{v}(0)\cdot\mathbf{v}(0)\rangle$; 2, $\langle \mathbf{v}(t)\cdot\mathbf{v}(t)\mathbf{v}(0)\cdot\mathbf{v}(0)\rangle/\langle \mathbf{v}^4(0)\rangle$; ---, Eq. (4), the Gaussian result based on line 1. (*b*) Close-up of the non-Gaussian effect. —— , $\langle \mathbf{v}(t)\cdot\mathbf{v}(t)\mathbf{v}(0)\cdot\mathbf{v}(0)\rangle/(\langle v^2(0)\rangle\langle v^2(0)\rangle)$; ---, the Gaussian result: $1 + \frac{2}{3}(\langle \mathbf{v}(t)\cdot\mathbf{v}(0)\rangle/\langle v^2(0)\rangle)^2$. [Reproduced by permission from M. W. Evans, *J. Mol. Liq.*, **25**, 211 (1983).]

Lippert[64] have questioned the validity of this approximation. The use of a nonadiabatic fluctuation–dissipation theory opens up a range of possibilities, because several of the "symmetry theorems" on the fundamental properties of autocorrelation functions and spectral moments are valid only in the adiabatic approximation.

The computer simulation by M. W. Evans was not used to provide an accurate assessment of the intensity of the far infrared but rather to determine the shape and position of the spectrum. However the exercise of comparison needs to be repeated at state points under hydrostatic pressure and to the critical point.

The computer simulation suggests the following:

1. The pdfs governing the approach to equilibrium are not Gaussian (Fig. 5).
2. Rotation–translation coupling is significant (Fig. 6).

These observations cannot be accounted for with classical (purely rotational) theories for molecular diffusion based on the Langevin or Fokker–Planck equations. We shall see in the following sections concerned with other liquids that this conclusion is a valid and general one. Currently popular analytical theories are gross oversimplifications of the molecular dynamics.

III. IODOMETHANE (CH_3I)

Taking moments of inertia as a criterion, iodomethane [M. W. Evans and G. J. Evans, *J. Mol. Liq.*, **25**, 177 (1983)] is almost a linear molecule and is

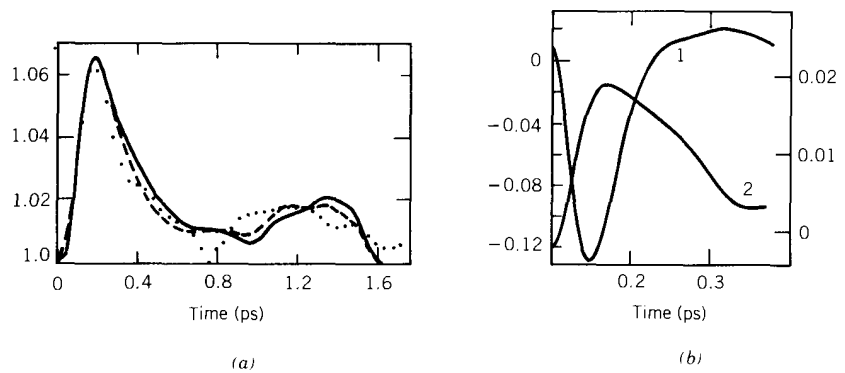

Figure 6. Rotation–translation coupling in chloroform. (*a*) —— , $\langle \dot{v}^2(0)J^2(t)\rangle/(\langle v^2(0)\rangle\langle J^2(0)\rangle)$; ●, $\langle v^2(t)J^2(0)\rangle/(\langle v^2(0)\rangle\langle J^2(0)\rangle)$; ---, as for ——, but with 4560 time steps as opposed to 3600 time steps in the running time average $\langle\bullet\rangle$. (*b*) The rototranslational first-rank mixed autocorrelation functions $\langle \mathbf{v}(0)\mathbf{J}^T(t)\rangle$ in the molecule fixed frame: 1, $\langle \mathbf{v}_1(0)\mathbf{J}_2(t)\rangle/(\langle \mathbf{v}_1^2\rangle^{1/2}\langle \mathbf{J}_2^2\rangle^{1/2})$; 2, $\langle \mathbf{v}_2(0)\mathbf{J}_1(t)\rangle/(\langle \mathbf{v}_2^2\rangle^{1/2}\langle \mathbf{J}_1^2\rangle^{1/2})$. [Reproduced by permission from M. W. Evans, *J. Mol. Liq.* **25**, 211 (1983).]

therefore one of the simplest systems available for study. Good agreement between theory and experiment and among the various experiments is therefore expected, but, as we shall see, problems that are not easily resolved do exist in the reduction of the data. For example, Fig. 7 shows the infrared correlation function with various corrections applied. The decay and overall shape of the function may be changed considerably by such corrections. Also, the problem is not necessarily eased if we study the liquid in solution. For example, in CCl_4 the correlation function, as anticipated, decays somewhat faster, reflecting the more isotropic environment and the decrease in angular correlation between neighboring molecules. However, the viscosity of a mixture of CH_3I and CCl_4 may actually be greater than that of the neat liquid by a factor of as much as 1.7. The implications of this are significant, because the rotational diffusion models (of Debye and others) predict that the rotational diffusion constant is inversely proportional to the viscosity of the fluid. The models fail in this instance because they demand a larger value for the relaxation time of the mixture and thus a slower exponential decay of the correlation function.

Iodomethane has, in fact, nine vibrational modes, each of which may be used to obtain information on rotovibrational diffusion. There are three totally symmetric modes of symmetry species A_1 and three doubly degenerate E modes. All are both infrared and Raman active. A correct analysis of rotation–vibration coupling is necessary before accurate information can be obtained on rotational diffusion and its anisotropy. If we are to use classical dynamics these bands must be symmetrical. This must also be true of the

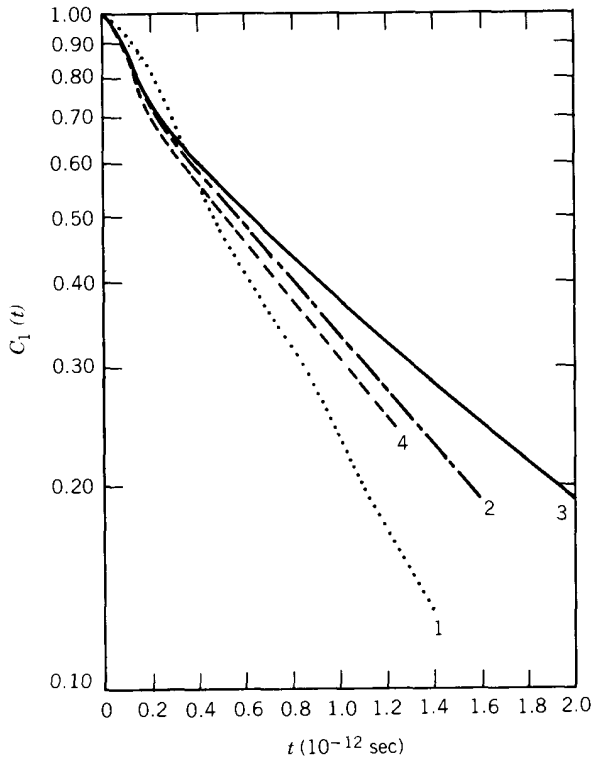

Figure 7. Infrared correlation functions of CH_3I calculated from the ν_3 band. The curves show changes of the angular correlation function as various corrections are applied. Curve 1, Rothschild (1970) (see ref. 15); curve 2, Fulton (1970) (see ref. 15); curve 3, Fulton's results further corrected for hot bands and the presence of isotopes; curve 4, Favelukes et al. (1968) (see ref. 15). [Reproduced by permission from P. Van Konynenberg and W. A. Steele, *J. Chem. Phys.*, **56**, 5776 (1972).]

infrared E bands, which contain information about both spinning and tumbling (motions around and of the C_{3v} symmetry axis). The A_1 bands are symmetric, but the half-width of the ν_1 band is greater than those of the ν_2 and ν_3 bands, which are roughly the same. Rotovibrational effects are therefore present in the A_1 modes. Coriolis forces introduce strong vibration–rotation effects into the E-type modes because of the double degeneracy. The Coriolis force may also be transferred from an E mode to an A_1 type. The E bands are asymmetric, so that quantum effects are important because of spinning about the C_{3v} axis. The moment of inertia of the symmetry axis is approximately 20 times smaller than that about any perpendicular axis through the center of mass, and the free-rotational velocity is nearly 5 times

that for motion of the C_{3v} axis (the dipole axis). The $\nu_4(E)$ band is the least affected by the force.

The results of several early investigations have been summarized by Goldberg and Persham[65] and are displayed in Table II. They conclude that not all of the bands are equally amenable to a simple analysis, and only by studying as many as possible can one expect to obtain a reasonable result from infrared and Raman spectroscopy. This viewpoint is extended by Hyde-Campbell et al.,[66] who investigated a combination of $\nu_3(A_1)$ and ^2D relaxation times. These authors report a large effect of density on the molecular motion of methyl iodide; their orientational (P_2) and angular-momentum relaxation times are listed in the table. Using ^2D and spin–lattice NMR relaxation times, they obtained diffusion coefficients for spinning and tumbling. As the density changes, however, the rotation of the methyl group about the C_{3v} axis remains largely unaffected, and it is pointed out that any "serious" attempt to characterize the molecular dynamics in a liquid must involve data taken under hydrostatic pressure. They suggest that the true effects of temperature show up only at constant density.

Döge and Schaeffer[67] calculate a Raman correlation time for spinning at 293 K using a relatively simple model for the bandshape. Arndt and Yarwood[68] extend the analysis to the overtones involved with $0 \rightarrow 1$ and $0 \rightarrow 2$ transitions. The effect of the intermolecular potential, and therefore the observed rate of vibrational relaxation, depends on the normal coordinates of the mode concerned. Several other groups have studied liquid methyl iodide by infrared, Raman, or Rayleigh spectroscopy. Their results are shown as correlation times in Table II. Cheung et al.[69] calculate the infinite-dilution intercept of the Rayleigh correlation time to be 1.8 ± 0.2 ps, which is roughly comparable to the Raman correlation times obtained from totally symmetric stretching. They compare their results with the Raman correlation times of 1.6 ps given by Wright et al.[70] and 2.2 ps given by Patterson and Griffiths.[71] Dill et al.[72] have derived angular-position and angular-velocity autocorrelation functions, and point out that the major axis of the rotational diffusion tensor coincides with that of the polarizability tensor, and that in this liquid depolarized Rayleigh scattering will measure an average reorientational time only.

An interesting result is that of Constant and Fauquembergue.[73] They list correlation times for solutions of CH_3I. The solvent used has a pronounced effect on the dynamics of the solute molecules. For example, the first-rank correlation time (infrared) for a 20% (mole fraction) solution of CH_3I in CCl_4 is 3.2 ± 0.1 ps, whereas in hexane it is 2 ± 0.1 ps. We saw for chloroform in the last section that the effect of a solvent is not always to reduce cross correlations. Our own far-infrared results for CH_3I (Fig. 8) show that the plot of $\bar{\nu}_{max}$ (the wavenumber of maximum absorption) versus concentration of

TABLE II
Experimental and Simulated Correlation Times for CH_3I[a]

Some Relaxation Times for Liquid Methyl Iodide			
Technique		Measured relaxation time (ps)	Computed autocorrelation time (ps) at 293 K
Dielectric	(i)	3.6_5 (pure liquid)	$\tau_1(\mathbf{e}_3) = 1.5$
	(ii)	2.5 (infinite dilution in Cl_4	$\tau_1(\mathbf{e}_3) = 1.5$
NMR relaxation	(i)	0.27 ± 0.07 (weighted mean second-rank, pure)	$\tau_2(\mathbf{e}_3) = 0.5$
	(ii)	0.50, as above	$\tau_2(\mathbf{e}_1) = 0.05$
	(iii)	1.42 (of C_{3v} axis at 1 bar, 303 K)	$\tau_2(\mathbf{e}_3) = 0.5$
		3.30 (of C_{3v} axis at 3 kbar, 303 K)	
		0.10 ($\perp$ to C_{3v} axis at 303 K, at both 1 and 2 kbar)	$\tau_2(\mathbf{e}_1) = 0.05$
	(iv)	Angular momentum correlation time, lab. frame	
		$\tau_J = 0.03_2$ at 1 bar, 303 K	$\tau_J = 0.01$
		$\tau_J = 0.01_3$ at 2 kbar, 303 K	
	(v)	1.4 (NMR dipole relaxation	$\tau_2(\mathbf{e}_3) = 0.5$
	(vi)	1.4 (Debye–Stokes theory)	$\tau_2(\mathbf{e}_3) = 0.5$
	(vii)	1.6 (of C_{3v} axis at 1 bar)	$\tau_2(\mathbf{e}_3) = 0.5$
		0.07 to 0.08 ($\perp$ C_{3v} axis at 1 bar)	$\tau_2(\mathbf{e}_1) = 0.05$
Infra-red Bandshape Analysis	(i)	3.6 (pure liquid)	$\tau_1(\mathbf{e}_3) = 1.5$
	(ii)	3.1 (pure liquid)	$\tau_1(\mathbf{e}_3) = 1.5$
	(iii)	3.2 ± 0.1 (20% mole fraction in CCl_4)	$\tau_1(\mathbf{e}_3) = 1.5$
		2.0 ± 0.1 (20% mole fraction in hexane)	$\tau_1(\mathbf{e}_3) = 1.5$
Raman bandshape analysis	(i)	0.8 (ν_1)	
		1.1 (ν_2)	$\tau_2(\mathbf{e}_3) = 0.5$
		1.4 (ν_3)	
		1.4 (ν_2)	
		1.5 (ν_3)	$\tau_2(\mathbf{e}_3) = 0.5$
		1.7 (ν_3)	
	(ii)	1.3 ± 0.1 (20% mole fraction in CCl_4)	
		0.8 ± 0.1 (20% mole fraction in hexane)	$\tau_2(\mathbf{e}_3) = 0.5$
	(iii)	1.6 (ν_3 Raman and ^{2}D NMR spin-relaxation)	$\tau_2(\mathbf{e}_3) = 0.5$
		0.07 to 0.08 ($\perp$ to C_{3v} axis, $\nu_3 + {}^2$D NMR)	$\tau_2(\mathbf{e}_1) = 0.05$

TABLE II (*Continued*)

Some Relaxation Times for Liquid Methyl Iodide			
Technique		Measured relaxation time (ps)	Computed autocorrelation time (ps) at 293 K
	(iv)	0.05 (ν_4, $\perp$ to C_{3v} axis)	$\tau_2(\mathbf{e}_1) = 0.05$
		1.6 ± 0.2 (mean value)	$\tau_2(\mathbf{e}_3) = 0.5$
		In the range: 1.18 to 1.36 (ν_3, depending on wing cut-off frequency)	$\tau_2(\mathbf{e}_3) = 0.5$
Depolarized Rayleigh scattering		0.94 (pure liquid)	$\tau_2(\mathbf{e}_1) = 0.05$
			$\tau_2(\mathbf{e}_3) = 0.5$
		3.1 (pure liquid)	$\tau_2(\mathbf{e}_1) = 0.05$
		1.8 ± 0.2 (infinite dilution in 46 : 54 isopentane : CCl_4)	$\tau_2(\mathbf{e}_3) = 0.5$
		2.2 (pure liquid)	A mean of three times as above
		1.0 (pure liquid)	A mean of three times as above
Far-infrared and second		$\bar{\nu}_{max} = 60 \pm 2$ cm^{-1} (100% v/v CH_3I in decalin)	
Rayleigh moment		$T_q = 1980$ g $\bar{\nu}_{max} = 100$ cm^{-1} (pure liquid, this work)	
Rayleigh second moment analysis		$R(\bar{\nu}) = \bar{\nu}^2 I(\bar{\nu})$ $= 64$ cm^{-1} (pure CH_3I) $= 58$ cm^{-1} (pure CD_3I)	Compares with a far-infrared peak frequency of 100 cm^{-1} in the pure liquid (this work)
Incoherent neutron scattering		Studied in the gaseous, liquid, and solid states. Qualitative result: there is "freedom of translational motions" in the pure liquid.	Computer simulation (this work) provides quantitative evidence for rotation–translation coupling. Raman and infrared work provides evidence for rotation–vibration coupling
Coherent anti-Stokes Raman scattering (CARS)		Correlation time from all sources of 0.85 ± 0.2	
Vibrational relaxation		2.73 (ν_1, isotropic at 287 K)	
		2.81 (ν_2)	
		2.77 (ν_3)	

[a] Compiled by M. W. Evans *J. Mol. Liq.*, **25**, 177 (1983). Reproduced by permission. For references to original data sources, see this review in *J. Mol. Liq.*

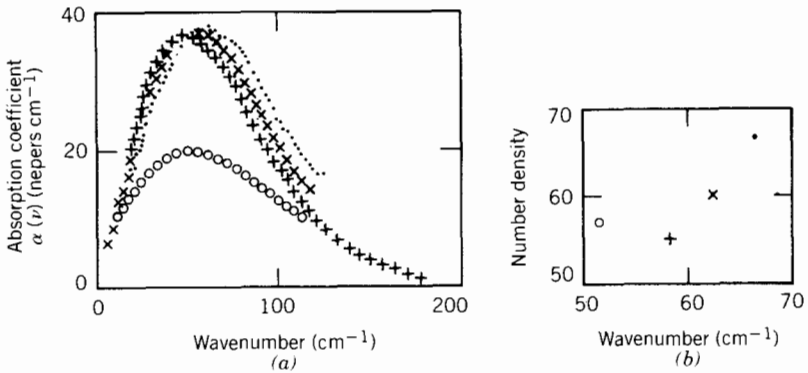

Figure 8. The plot of $\bar{\nu}_{max}$ (the frequency of maximum absorption) against concentration for solution of CH_3I in CCl_4. ●, Heat solution; ×, 75% solution; +, 50% solution; ○, 25% solution (all percentages volume/volume). [Reproduced by permission from M. W. Evans and G. J. Evans, *J. Mol. Liq.*, **25**, 177 (1983).]

CH_3I dissolved in CCl_4 is *not* linear, as would be anticipated if the effect of the dilution was only to remove cross correlations. The same nonlinearity is observed in other solvents.

It is already emerging that CH_3I is not such a simple and representative molecular liquid. There are large contributions to its measured properties from collision-induced absorption. Shermatov and Atakhodzhaev[74] have studied the ν_3 mode of methyl iodide to 150 cm^{-1}. At high values of $\Delta\nu$ a weak absorption maximum due to collision induction dominating the second-moment spectrum is observed. In addition, rotation–vibration coupling affects some, if not all, of the spectra to an unknown extent.

Laubereau and Kaiser[75] have postulated a new and useful way for studying this interaction directly. They have examined the vibrational modes of methyl iodide in the electronic ground state with picosecond laser-pulse spectroscopy. The vibrations are excited with an intense laser pulse via stimulated Raman scattering or by resonant infrared absorption. After the passage of the first pulse, the excitation process rapidly terminates and free precessional decay of the vibrational system occurs. The instantaneous state of the excited system is monitored by a second "interrogating" pulse after a variable delay. However, this method, which allows one to look directly at the vibration–rotation coupling of methyl iodide at short and intermediate times, awaits theoretical development for its proper interpretation.

Gburski and Szczepanski[76] have concluded that it is *impossible* to separate the different vibrational contributions to picosecond laser-pulse experiments using classical infrared and Raman spectroscopy. The isotropic part of a Raman line *cannot* be related to a single relaxation process. They

provide a clear account of the problems involved in the interpretation of vibrational relaxation in picosecond laser-pulse experiments. A number of physical processes contribute to line shapes in picosecond dephasing. These include phase relaxation, rotational motion, isotope splitting, and inhomogeneous broadening due to a distribution of molecules with different resonance frequencies depending on the environment. Other problems include the coupling of vibrational and rotational motion due to transition-dipole to transition-dipole coupling and dephasing via vibrational anharmonicities not contained in the Laubereau–Fischer model (see ref. 77).

Gburski and Szczepanski also have considered the problems of interpreting the *vibrational* part of the overall motion and conclude that dephasing processes involving no energy transfer between the ensemble of molecular oscillation and the lattice usually dominate in the line-broadening process. This conflicts diametrically with a prediction of Gillen et al.[78] Their correlation times showed a large temperature dependence, larger than that observed experimentally, which implies that dipolar coupling is a minor effect and that resonant-energy exchange is the dominant factor. The true temperature dependence is not clear from the literature. The modulation times of Doege et al.[79] show a moderate temperature dependence, but this is not observed at all by Trisdale and Schwartz.[80] The difference between the two results is attributable to the methods of calculation. Trisdale and Schwartz used polarized and depolarized Raman spectra of the ν_1 (2950 cm^{-1}), ν_2 (1150 cm^{-1}), and ν_3 (525 cm^{-1}) modes, calculating correlation functions only on the high-frequency side of the bands to get at the vibrational components. Kubo's line-shape theory was applied to describe the spectra in terms of relaxation through vibrational dephasing. This provides a bandshape of the form

$$G_{iso}(t) = \exp\{-M_{2v}[\tau_m^2(e^{-t/\tau_m}-1)+\tau_m]\}$$

where M_{2v} is the vibrational second moment and τ_m is a measure of the decay time of the stochastic perturbation. $M_{2v}^{1/2}\tau_m$ determines the nature of the vibrational relaxation (i.e., either motionally narrowed or inhomogeneous). Following evaluation of M_{2v} by numerical integration, Trisdale and Schwartz varied τ_m to obtain the best least-squares fit to the experimental and theoretical isotropic functions. M_{2v} is almost temperature independent for ν_1 and ν_3, but decreases markedly with increasing temperature for C—H bonding (ν_2). The area beneath $G_{iso}(t)$ gives the isotropic relaxation times, which increase with temperature for all three vibrations, but much more sharply for ν_2 than for the other two modes. The effect of dilution is to slow significantly the relaxation of the ν_2 mode; the ν_1 band is affected similarly

by solution. This is attributed to intermolecular dipole or resonant-energy-transfer effects.

Döge[81] and van Woerkom et al.[82] have shown that for a long-range dipole–dipole potential, τ_m should be one-half of the dipole reorientational correlation time obtained from "either dielectric or infrared" spectroscopy. The predicted times of Gillen et al. are 5 to 10 times longer.

Trisdale and Schwartz[80] discuss the Laubereau–Fischer model.[83] This model assumes that vibrational dephasing results directly from binary hard-sphere collisions. The hard-sphere collision times (τ_c) are compared with those derived by Hyde-Campbell et al. from the Enskog model. Though qualitative agreement is obtained, recent studies of ν_1 in liquid CH_3I suggest that the principle decay mechanism of this mode is via population relaxation and not via resonance-energy transfer, and that intermolecular energy exchange dominates the relaxation of the ν_3 mode. Furthermore, if the primary mechanism of relaxation is by dephasing from short-range repulsive forces, it is expected that both τ_c and τ_m will represent the time between collisions in the liquid, yet the temperature trends for these two are not in agreement, particularly for ν_3.

Considerable confusion exists in the literature even if we consider vibrational relaxation alone for CH_3I. The situation is complicated further when rotovibrational experiments are analyzed. The experiments themselves produce composite results owing to a combination of relaxation processes that may be coupled and thereby distort each other considerably. Theoretical treatments are too simple; ideas are subjective and do not stand up to incisive analysis. Conclusions based on the "force fitting" of these models to Raman and infrared bandshapes are at best approximate and at worst misleading, causing greater confusion. Quoting Hildebrand:[84]

> A model should be regarded as suspect if it yields inferences in serious conflict with any of the pertinent properties of a system, regardless of how closely it can be made to agree with some, *especially if there are adjustable parameters*. A model that is inconsistent with all properties, even if only approximately, can probably be made more precise, but if it is in irreconcilable conflict with any part of the evidence it is destined to be discarded, and in the meantime predictions and extrapolations based on it should be regarded as unreliable.

To test these models we need as much data over as wide a range of conditions as possible. Careful attention should be paid to the reduction of the data into forms suitable for comparison with theory and to the measurement of the data itself. Bansal et al.[85] emphasize the importance of looking well out into the wings of spectra. They find a marked disagreement between their own results on the $\nu_3(A_1)$ band profile (measured out to 175 cm^{-1}) of CH_3I and those of other workers. Their second-rank orientational relaxation times vary from 1.36 to 1.18 ps *according to where the band is truncated*. Their results are all markedly shorter than that of 1.6 ± 0.2 ps quoted by Steele.[86] Also, in infrared and Raman experiments the contribution from hot bands should be allowed for. Roland and Steele,[87] using coherent anti-Stokes Raman scattering to investigate polarized and depolarized bands for the symmetric stretch of liquid CH_3I at 526 cm^{-1}, found an appreciable hot-band intensity overlapping the fundamental. Their experimental correlation time is 0.85 ± 0.2 ps. They also quote the value of 1.6 ± 0.2 ps estimated by Steele from an analysis of the spontaneous Raman bands.

There have already been attempts to use computer simulation to unravel these complex experimental infrared and Raman results. Maple et al.[88] showed that the transient statistics of reorientation are non-Gaussian, that is, that nonequilibrium fluctuations approach equilibrium faster than the average correlation function does (this is referred to as "Gordon's equilibrium conjecture"). Riehl and Diestler[89] find that the vibrational correlation functions for their model of methyl iodide were highly oscillatory in the range up to 5 ps, whereas the normalized center-of-mass velocity autocorrelation functions were not exponential in their decay characteristics. The first-rank orientational autocorrelation functions obtained by Maple et al. were not oscillatory in the range up to 3 ps.

Once again there is contradiction and confusion. Spectroscopists should heed the advice of Goldberg and Persham[65] to study all nine vibrational modes available and the advice of Hyde-Campbell et al.[66] to look at the liquid under hydrostatic pressure over a temperature range. The mechanisms governing vibrational relaxation are not established with any degree of certainty, and no attempt has been made to produce the more revealing and appropriate higher spectral moments. Far-infrared spectra provide automatically the second spectral moment of the dielectric loss spectrum.

As an example of moment analysis, we recall the work of Nielsen et al.[90] on the depolarized Rayleigh wing spectrum of liquid methyl iodide. The higher moment $R(\bar{\nu}) = \bar{\nu}^2 I(\bar{\nu})$ was calculated from the experimental data. $R(\bar{\nu})$ peaks at about 64 cm^{-1} for CH_3I and 58 cm^{-1} for CD_3I. This shift in frequency was compared with a corresponding far-infrared frequency shift of ~ 6 cm^{-1}. Kubo's theory, as used by Trisdale, would leave these higher moments undefined, that is, produce a plateau in $R(\bar{\nu})$. The popular extended diffusion models of Gordon (M and J) are not able to shift the peak frequency of $R(\bar{\nu})$, as observed experimentally, when temperature is varied, when external pressure is applied, or when a solute is dissolved in a nonpolar and noninteracting solvent.

What of NMR relaxation for CH_3I? Discrepancies are again apparent when we consider NMR results. Nuclear quadrupolar relaxation times (of CD_3I), ^{13}C relaxation times, and the intramolecular part of the proton relaxation times have all been measured. Measurements of the nuclear Overhauser effect show that the last two are affected by a nondipolar relaxation mechanism that is spin rotational in origin. Schwartz[91] points out that the effective reorientational correlation time from ^{13}C NMR is a consequence of spin-rotation and dipolar coupling, the dominant mechanisms. At 301 K, this time is 0.27 ± 0.07 ps, a weighted mean of second-rank orientational correlation times (Table II) about all three principal moment-of-inertia axes. Schwartz obtained this value using Overhauser enhancement on natural-abundance $^{13}CH_3I$ with a $180°-\tau-90°$ pulse sequence. He finds that extended diffusion models cannot characterize the reorientational dynamics. Steele,[86] summarizing the early work in this field, points out that temperature studies suggest that reorientation of the symmetry axis is governed by small-step diffusion. However, this result was arrived at despite the fact that the estimated ratio of P_2 to P_1 correlation times from Raman and infrared differs greatly from the value of $\frac{1}{3}$ necessary for rotational diffusion. The temperature dependence of the relaxation times for rotation about the symmetry axis, on the other hand, is quite minimal, so that Griffiths[92] suggests that motion about this axis is governed by inertial effects and almost free.

Heatley[93] produces a mean second-rank orientational correlation time τ_2 of 0.5 ps, which compares with the value of 0.27 ± 0.07 ps from Schwartz's work. Hyde-Campbell et al.[66] have produced ^2D relaxation times over a range of density and temperature, and derive resultant molecular angular-momentum correlation times of $\tau_J = 0.03$ ps at 1 bar, 303 K; and 0.01 ps at 2 kbar, 303 K. τ_J increases with temperature at constant density. Griffiths[92] combines ^2D NMR and diffusion coefficients parallel and perpendicular to the C_{2v} symmetry axis. The reorientational dynamics are highly anisotropic. These diffusion coefficients have been converted to relaxation times, which are tabulated in Table II. *Unequivocal NMR relaxation times cannot be calculated because of the uncertainties in the Raman times discussed at length above.*

Neutron-scattering studies on CH_3I have been reported for the gaseous, liquid, and crystalline solid states. Fischer[94] has measured the neutron-scattering cross section (in barn proton) for methyl iodide. This increases with increases in the neutron wavelength in the range 4–17 Å. The cross section for CH_3I at 17 Å is 254 barn proton and the slope (in barn Å) of σ versus neutron wavelength is 13.9. The latter is related to rotational "barriers" and decreases smoothly with increases in the NMR rotational relaxation time. The neutron method has some advantages, according to Fischer, for the separation of internal molecular rotations from reorientations of the whole molecule.

Janik et al.[95] have also studied CH_3I by neutron inelastic scattering. They studied the lattice molecular dynamics of solid and liquid CH_3I. The spectrum for the solid arose from lattice vibrations (below 120 cm^{-1}) and from intramolecular vibrations of the CH_3I molecules (above ~ 500 cm^{-1}). Peaks obtained in the intermediate region were higher harmonics of the torsional vibrations. The spectrum for the liquid was regarded as proof of the "freedom of translational motions" in the liquid state.

Apart from such semiqualitative results, it is not anticipated that significant insight into the molecular dynamics of CH_3I can be obtained by means of neutron scattering. The experimental information is a complex conglomerate, rich in information perhaps, but indecipherable with present techniques and knowledge.

Let us see what our computer-simulation results tells us about the dynamics of this molecular liquid. The interaction between two methyl iodide molecules was modeled with a 5×5 Lennard-Jones atom–atom "core" with point charges localized at each site. Multipole–multipole terms are therefore represented by means of charge–charge interactions.

The parameters used in the simulation were as follows:

$$\varepsilon/k(\text{H—H}) = 13.4 \text{ K}$$
$$\sigma(\text{H—H}) = 2.60 \text{ Å}$$
$$\varepsilon/k(\text{C—C}) = 51.0 \text{ K}$$
$$\sigma(\text{C—C}) = 3.20 \text{ Å}$$
$$\varepsilon/k(\text{I—I}) = 314.0 \text{ K}$$
$$\sigma(\text{I—I}) = 4.10 \text{ Å}$$

The cross terms were evaluated with Lorentz–Berthelot combining rules. The carbon and hydrogen parameters were the same as those used for $CHCl_3$. The I—I parameters were obtained using the molecular crystal data of Eliel et al.[96] The electrostatic interactions were represented by point charges, which were calculated using bond moments and bond distances. This provided the following values:

$$q_H = 0.055|e|$$
$$q_C = -0.043|e|$$
$$q_I = -0.122|e|$$

Charge–charge interactions are long ranged, but their relatively small magnitude in this instance allowed us to use periodic boundary conditions with 108 molecules.

The simulation run was initiated at 293 K, with a molar volume of 62.2 cm^3 at 1 bar. The 108 methyl iodide potentials were arranged initially on a face-centered cubic lattice in a cube with a half-side of 11.17 Å, the potential cut off distance. This is over twice the longest Lennard-Jones σ used. According to Bossis et al.,[97] medium-range correlations disappear at about 10 Å from a given molecule, even in intensely dipolar molecules.

All computed and experimental correlation times are collected in Table II. The computed times are generally shorter than their experimental counterparts. The computer-simulation method is, of course, pair additive. This may be an oversimplification in the case of CH_3I, because far-infrared results (Fig. 8), for example, show that the absorption cross sections of spectra for CH_3I dissolved in "noninteracting" solvents are clearly nonlinear. The CH_3I molecules are easily polarized, and induced effects, which are not pair additive, must be large. We have therefore also compared the simulated results with spectral results for CH_3I in dilute solutions, obtaining better experimental–simulated agreement, although the measured correlation times remain longer. For example, the dielectric relaxation time at infinite dilution is 2.5 ps, compared with a simulated time of 1.5 ps, and the infrared relaxation time of a 20% (mole fraction) solution in hexane is 2 ± 0.1 ps, compared with the computed time of 1.5 ps. Raman experimental times range from 0.8 to 1.7 ps, compared with a simulated time of 0.5 ps. Rayleigh correlation times range from 0.9 to 3.1 ps.

These are weighted averages of correlation times about each of the three principal axes in CH_3I. By using a combination of Raman and NMR relaxation, some authors have obtained estimates of second-rank correlation times for motion about the C_{3v} axis—the "spinning" of CH_3I, as opposed to the "tumbling" observed with dielectric spectroscopy. These times range from 0.05 to 0.08 ps and compare well with the simulated time of 0.05 ps. Seventy to ninety percent of the decay of these spinning autocorrelation functions is completed before they become exponential, so the CH_3I potential used in the computer simulation allows the molecule to rotate quite freely. We can conclude that the spinning motion of CH_3I is relatively unaffected by polarizability and induction effects, which are not accounted for in the simulation, and that the tumbling motion is severly affected by collision induction and other processes.

Dill et al.[72] have used Raman and Rayleigh scattering to obtain an angular-velocity correlation function, which is compared with the simulated function in Fig. 9. The latter is distinctly nonexponential. The influence of the spinning motion on the tumbling manifests itself through the oscillations superimposed on the basic structure of the autocorrelation function. This supports Steele's conclusion that rotational diffusion theory cannot describe the molecular motion in liquid CH_3I. The simulated autocorrelation function decays much more rapidly than the function derived by Dill. Kluk[98] shows that the angular-velocity autocorrelation function, obtained from the 525 cm^{-1} Raman (ν_2) band, has an even deeper negative overshoot than Dill's and intersects the time axis at about 0.2 ps.

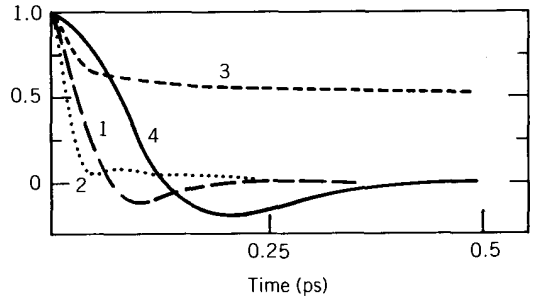

Figure 9. Comparison of Raman and Rayleigh scattering angular-velocity correlation functions with simulated functions. 1, $\langle \mathbf{J}(t)\cdot\mathbf{J}(0)\rangle / \langle J^2(0)\rangle$; $\mathbf{J}$ = molecular angular momentum, laboratory frame. 2, $\langle \boldsymbol{\omega}(t)\cdot\boldsymbol{\omega}(0)\rangle / \langle \omega^2(0)\rangle$; $\boldsymbol{\omega}$ = molecular angular velocity, laboratory frame. 3, $\langle \mathbf{J}(t)\cdot\mathbf{J}(t)\mathbf{J}(0)\cdot\mathbf{J}(0)\rangle / \langle J^4(0)\rangle$. 4, Normalized angular-velocity autocorrelation function from the work of Dill et al.[72] [Reproduced by permission from M. W. Evans and G. J. Evans, *J. Mol. Liq.*, **25**, 177 (1983).]

Zero-terahertz spectroscopy unquestionably produces some of the most discriminating data for the evaluation of molecular models. In CH_3I it demonstrates quite clearly the deficiencies of the computer simulation. The rotational velocity autocorrelation function of $\mathbf{e}_3$, where $\mathbf{e}_3$ is a unit vector on the C_{3v} axis, may be related via a Fourier transform to the power absorption coefficient, $\alpha(\bar{\nu})$ (in neper cm^{-1}), of the far infrared. Straight Fourier transforms of our far-infrared data are compared with the rotational-velocity autocorrelation functions for spinning and tumbling in Fig. 10. These are, respectively, $\langle \dot{\mathbf{e}}_1(t)\cdot\dot{\mathbf{e}}_1(0)\rangle / \langle \dot{e}_1^2(0)\rangle$ and $\langle \dot{\mathbf{e}}_3(t)\cdot\dot{\mathbf{e}}_3(0)\rangle . \langle \dot{e}_3^2(0)\rangle$. In CH_3I the C_{3v} axis is, of course, the dipole axis. There is a mismatch between the experimental and simulated functions. The experimental functions contain contributions from induced absorptions and multibody correlations that complicate their analyses. Some of these effects are lessened by dilution, but there is still a significant discrepancy between the computed and measured functions for 10% (volume/volume) CH_3I in decalin.

Figure 11 illustrates the center-of-mass linear-velocity autocorrelation functions for CH_3I computed in the laboratory and moving-axis frames of reference. The components of the velocity autocorrelation function are not isotropic in the frame of reference that moves with the molecule.[99] The laboratory-frame autocorrelation function has the characteristic long negative tail, and its second moment is transiently non-Gaussian, but attains the Gaussian equilibrium level of $\frac{3}{5}$. This is also the case with the computed sec-

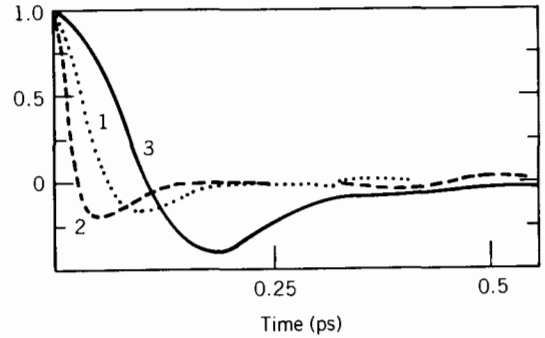

Figure 10. Comparison of far-infrared and simulated rotational velocity autocorrelation functions for CH_3I. 1, $\langle \dot{\mathbf{e}}_3(t)\cdot\dot{\mathbf{e}}_3(0)\rangle/\langle \dot{e}_3^2\rangle$; 2, $\langle \dot{\mathbf{e}}_1(t)\cdot\dot{\mathbf{e}}_1(0)\rangle/\langle \dot{e}_1^2\rangle$; 3, straight Fourier transform of the far-infrared power absorption of 10% CH_3I in decalin. [Reproduced by permission from M. W. Evans and G. J. Evans, *J. Mol. Liq.*, **25**, 177 (1983).]

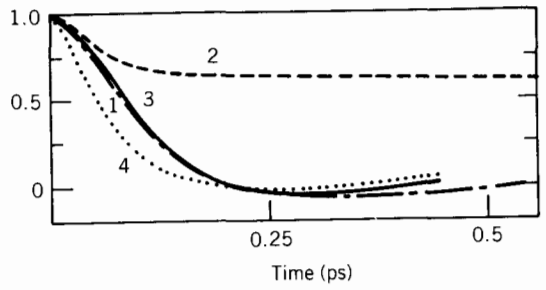

Figure 11. The simulated center-of-mass linear-velocity autocorrelation functions for CH_3I in laboratory and moving-axis frames of reference. 1, $\langle \mathbf{v}(t)\cdot\mathbf{v}(0)\rangle/\langle v^2(0)\rangle$, laboratory frame; 2, $\langle \mathbf{v}(t)\cdot\mathbf{v}(t)\mathbf{v}(0)\cdot\mathbf{v}(0)\rangle/\langle v^4(0)\rangle$, laboratory frame; 3, $\langle \mathbf{v}_C(t)\mathbf{v}_C(0)\rangle/\langle v_C^2(0)\rangle$, moving frame; 4, $\langle \mathbf{v}_A(t)\mathbf{v}_A(0)\rangle/\langle v_A^2(0)\rangle$, moving frame. [Reproduced by permission from M. W. Evans and G. J. Evans, *J. Mol. Liq.*, **25**, 177 (1983).]

ond-moment autocorrelation function $\langle \mathbf{J}(t)\cdot\mathbf{J}(t)\mathbf{J}(0)\cdot\mathbf{J}(0)\rangle/\langle J^4(0)\rangle$, which is initially non-Gaussian but finally reaches the equilibrium Gaussian level of about 0.5 for the C_{3v} symmetry of CH_3I. The angular-velocity second-moment autocorrelation function attains a final level of about 0.4, again the Gaussian result.

The (2,1) and (1,2) elements of the autocorrelation matrix $\langle \mathbf{v}(0)\mathbf{J}^T(t)\rangle$ show that the coupling of rotation with translation in this liquid is unexpectedly strong. This coupling will indirectly affect, to an unknown degree, the laboratory-frame autocorrelation functions measured in the spectroscopies. The calculated correlation times are disparate and must be regarded as subject to revision until methods enable us to estimate the non-rotational spectral intensities.

IV. ACETONITRILE (CH_3CN)

Acetonitrile [M. W. Evans, *J. Mol. Liq.*, **25**, 149 (1983).] is an interesting molecule of C_{3v} symmetry because there is evidence from a number of spectroscopic sources that a strong local order exists in it that persists in solution down to concentrations of less than 10%. Acetonitrile has a large dipole moment (3.9D).‡ When $g_{00}^{(2)}$, the second-rank structure factor, and $g_{00}^{(1)}$, the first-rank structure factor (or the Kirkwood g factor), are estimated using ^{14}N relaxation and dielectric spectroscopy, respectively, the value of $g_{00}^{(2)}$ is 1.4, indicative of parallel or antiparallel alignment on the local level, and $g_{00}^{(1)}$ is 0.78; the negative deviation from unity of the latter indicates that this pair ordering extends to neighbors *that do not belong* to the first shell of reference particles. The same is observed in a diffraction (combined X-ray and neutron) experiment. A first-nearest-neighbor peak is predicted at 4.7 Å and a second at 8.5 Å. Further, it is concluded that below 4.4 Å preferred orientations of the dipole axis relative to the center–center line are found in the range 90–125°, whereas from ca. 5.2 Å on up preferred orientations are in the range 0–54.7°. At 6.8 Å a second reversal occurs that restores the initial situation.[100]

The existence of this local structure should affect some if not all of the spectroscopies, and should certainly complicate attempts to obtain single-particle properties (e.g., single-particle correlation times) from the experiments.[101] Depolarized-light scattering and far-infrared spectroscopy results certainly reflect contributions from correlated mutual dipoles. With such a distinct local order, contributions to spectral profiles that may be rotational, translational, or vibrational in origin may arise from pairs or clusters of molecules, and, of course, these modes could be coupled, severely distorting band shapes.

It is not surprising, therefore, that M. W. Evans[102] finds, in reviewing the literature, that only the NMR results are even fairly consistent with his computer-simulated (6×6 site–site model) results. He attributes the discrepancies to (1) long-range orientational cross correlations due to association and (2) polarizability effects. The simulation clarifies certain aspects of the reported discrepancies that seem to be more numerous for CH_3CN than for CH_3I and $CHCl_3$, the two liquids already considered.

Bien et al.[103] used the techniques of NMR spin–lattice relaxation, Raman, and infrared spectroscopy to obtain orientational correlation functions from the degenerate (F) bands of acetonitrile. The shapes of the parallel bands [ν_1 (C—H) = 2944 cm^{-1}, ν_2 (C≡N) = 2253 cm^{-1}, ν_3 (C—H stretch) = 1376 cm^{-1}, and ν_4 (C—C) = 917.5 cm^{-1}] are distorted by hot bands. For perpendicular bands ν_5 (as $C—H_{stretch}$) = 3002 cm^{-1}, ν_6 (as $C—H_{bend}$) = 1444

‡1 D ≈ 3.3356×10^{-3} cm.

cm^{-1}, ν_7 ($C—C_{bend}$) = 1039 cm^{-1}, and ν_8 ($C\equiv N_{bend}$) = 378.5 cm^{-1}. The perpendicular bands provide a correlation time for motion about the C_{3v} symmetry axis. Bien et al. provide an angular-momentum correlation time for motion about the mutually perpendicular axes (of I_B or I_C) that differs from that obtained using NMR relaxation by Bull.[104] Their result is in better agreement with that of Schwartz[105] who gives an "effective" second-order orientational correlation time of 0.38 ps. Schwartz also obtained an effective laboratory-frame angular-momentum correlation time of 0.093 ps using NMR spin–lattice (^{13}C) relaxation.

Breulliard-Alliot and Soussen-Jacob[106] reported infrared correlation times for motion parallel and perpendicular to the C_{3v} symmetry axis. Fourier transforms of the raw data from all eight fundamentals produce eight different correlation functions. Vibrational relaxation causes the correlation function from ν_1 to decay much more rapidly than those from ν_2 or ν_4, which are similar. The ν_5, ν_7, and ν_8 correlation functions are different because of Coriolis coupling. They calculate P_1 infrared correlation times of 0.09 ps for motion around the C_{3v} symmetry axis and 5.7 ps for motion of the C_{3v} axis itself, and P_2 correlation times of 0.38 ps and 1.5 ps, respectively, for the equivalent motions.

Numerous papers have been devoted to the comparison of NMR, Rayleigh, and Raman correlation times. The attempts have been summarized by Tiffon et al.,[107] who plot single-particle ^{14}C NMR relaxation times versus η/T for CH_3CN in CCl_4 solutions. Here η is the bulk viscosity and T the absolute temperature. For neat CH_3CN, and for 0.0182 and 0.0037 mole fraction solutions in CCl_4, these plots are linear, having nearly the same intercept as $\eta/T \to 0$ of $\tau_0 = 0.29$ or 0.23 ps, depending on the value taken for the nuclear quadrupole coupling constant. This is in complete contradiction to the work of Whittenberg and Wang,[108] who find a zero intercept when assuming that $\tau_s = \tau_{Raman}$, the effective Raman-derived correlation time. The τ_0 value of Tiffon et al. is almost the same as the free rotor correlation time of the major axis of CH_3CN (0.33 ps at 295 K). The existence of the positive intercept has been discussed by Hynes et al.[109]

Tiffon et al. quote the single-particle Raman (ν_1) relaxation time of Patterson and Griffiths[110], $\tau_s = 0.9$ ps. These authors also report a Rayleigh correlation time τ_{LS} of 1.8 ps. Whittenberg and Wang also report $\tau_{LS} = 1.8$ ps, but, using the Raman ν_2 band, deduce that $\tau_s = 1.5$ ps. They find that both τ_{LS} and τ_s are independent of concentration in CCl_4, and that $\tau_s = \tau_{LS}$ at infinite dilution. They ascribe any discrepancy between τ_{LS} and τ_s to isotropic relaxation mechanisms affecting the Raman band. This conclusion is contested by Versmold,[111] who reports τ_{LS} for CH_3CN and CH_3CN in CCl_4 and τ_s from ^{13}C NMR. He relates a monotonic increase of τ_s with dilution directly to the shear viscosity. He concludes that the increase in τ_{LS}, however, is *not* related to the shear viscosity, and discusses the τ_{LS}/τ_s ratio in terms of a decrease in orientational correlations.

From ^{14}N NMR relaxation, Tiffon et al.[107] report $\tau_s = 1.29$ ps (solid-state NQC) and $\tau_s = 1.01$ ps (gas-state NQC) as limits between which the effective second-rank single-particle orientational correlation time may be defined at 295 K. They point out that the results of Whittenberg and Wang and of Versmold are contradictory. They show that the linear dependence of τ_s on viscosity is true only at high CH_3CN concentrations because association between CH_3CN molecules disappears at roughly a 0.2 mole fraction of CH_3CN, the concentration at which the single-particle correlation times dramatically decrease. This is consistent with the far-infrared results of Knozinger et al.[112] and G. J. Evans,[101] who find that CH_3CN clusters remain in CCl_4 down to concentrations of less than 0.2 of a mole fraction. Fini and Mirone[113] arrive at the same conclusion by studying weak, high-frequency anisotropic components in the totally symmetric Raman vibrational bands of CH_3CN. They identified cluster vibration using isotropic and anisotropic Raman scattering on the shoulders on the ν_2 and ν_4 fundamentals. G. J. Evans[101] has also postulated the existence of cluster vibrations (collective modes) in his far-infrared spectrum.

Amorim da Costa et al.[114] conclude that energy transfer from excited vibrational states to rotational motion affects the Raman bandwidths so severely in liquid acetonitrile as to make impossible any interpretation of the differences between Raman and Rayleigh bandwidths. Yarwood et al.[115] also emphasize the difficulty of effectively separating out vibrational effects in the ν_1 and ν_3 infrared and Raman bands of CH_3CN in dilute CCl_4 solution. In another paper,[116] they conclude from a study of the ν_1, ν_3, and $2\nu_3$ bands that the second-rank (Raman) reorientational correlation times (ν_3 band) do not agree with the literature values from other bands, even though the ν_2 and ν_3 times are self-consistent.

NMR relaxation shows that the rotational motion is anisotropic. A molecule diffuses about its C_{3v} axis about 10 times more easily than about the mutually perpendicular axes of the principal moment-of-inertia frame. Rayleigh and dielectric correlation times are necessarily weighted averages of the three diffusion coefficients corresponding to these three axes of the frame. The anisotropy may be established by using a combination, for example, of ^{14}N and ^{2}D relaxation times obtained by means of nuclear quadrupole relaxation. ^{13}C and ^{1}H NMR relaxation can also be employed for this purpose, as demonstrated by Heatley[117] and Lyerla et al.[118] Heatley produces an effective (averaged) second-rank correlation time of 0.32 ± 0.06 ps with a ratio of 9.6 between the diffusion constant for spinning of the C_{2v} axis and those governing tumbling around perpendicular axes. Leipert et al.,[117] using ^{13}C spin–lattice relaxation times and nuclear Overhauser en-

hancement in the range 239–314 K, conclude that dipole–dipole and spin–rotation effects are important.

It should be noted that almost all of the NMR papers use the theory of rotational diffusion of Debye or, at best, M and J diffusion theory in their data-reduction processes. These models are oversimplified[21] and can only produce approximately correct correlation times.

The parameters used in M. W. Evans's 6×6 atom–atom representation[102] are those available in the literature, namely

$$\sigma(\text{H—H}) = 2.75\ \text{Å}$$
$$\sigma(\text{C—C}) = 3.20\ \text{Å}$$
$$\sigma(\text{N—N}) = 3.31\ \text{Å}$$
$$\varepsilon/k(\text{H—H}) = 13.4\ \text{K}$$
$$\varepsilon/k(\text{C—C}) = 51.0\ \text{K}$$
$$\varepsilon/k(\text{N—N}) = 37.3\ \text{K}$$

The point charges were estimated by M. W. Evans in two ways. First, the dipole and quadrupole moments were calculated directly following Stucky et al.[120] using experimental results from X-ray and neutron diffraction on the electron-density distribution of acetonitrile. He thus obtained values of

$$q_{C_1} = 0.01|e|$$
$$q_{C_2} = 0.16|e|$$
$$q_N = -0.20|e|$$
$$q_H = 0.01|e|$$

where C_1 is the methyl and C_2 the nitrile carbon atom. Second, he used the CNDO/2 calculation of Pople and Beveridge,[121] which produces values of

$$q_{C_1} = -2.02|e|$$
$$q_{C_2} = 0.09|e|$$
$$q_N = -0.16|e|$$
$$q_H = 0.03|e|$$

The values used in the simulation were averages from both sources.

The moment of inertia of CH_3CN about the unique (C_{3v}) axis is about 18 times smaller than the other two (equal) principal moments of inertia. It is anticipated, therefore, that the anisotropy of the rotational motion must

be large and must involve translation of the molecular center of mass—the coupling of rotation with translation should be pronounced. The interpretation with analytical theories of the spectroscopic results discussed above ignores this interaction.

Some of the simulated correlation times are compared with available experimentally derived correlation times in Table III. Our main conclusions are as follows:

1. The NMR times are similar to those of Bien et al.[103] Yarwood et al.,[122] and Schwartz.[105] The correlation times from spin–lattice relaxation are shorter than the simulated counterparts (in both static and moving frames). Tiffon's[107] results are significantly in error. It is worth recalling, however, that Tiffon finds that his correlation times decrease "dramatically" at a concentration of less than a 20% mole fraction of CH_3CN in CCl_4, suggesting that strong cross correlations affected his results for the pure liquid.
2. The simulated correlation times for the infrared and Raman spectra are nearly always shorter than the experimental times. The only exception, in fact, is the P_1 correlation time of Breulliard-Alliot and Soussen-Jacob.[106] The overall discrepancy is much greater than those for the liquids $CHCl_3$ and CH_3I, discussed earlier (Sections II and III). The discrepancies are so large and so inconsistent from experimentalist to experimentalist that we must conclude that severe errors arise in the data-reduction processes. For example, Amorim da Costa[114] believes that energy transfer from excited vibrational states to rotational motion affects the Raman bandwidths severely. The table shows a considerable spread in the experimental times themselves (3.2–5.7 ps) and that the experimental range straddles the computed range (0.09–5.7 ps, as compared with 0.3–0.7 ps).
3. In both Rayleigh and dielectric cases the discrepancy between the experimental and simulated correlation times is very large. It might be more meaningful to extrapolate the available Rayleigh and dielectric relaxation times to infinite dilution but care must be taken. There is evidence that some "non-interacting" solvents actually encourage association. The dielectric relaxation times of acetonitrile actually increase in both CCl_4 and benzene.

We have carefully reexamined the far-infrared spectrum of CH_3CN with the aim of isolating the effects, if any, of a well-defined local structure on the spectra of the liquid.[101] Some dielectric work has been reported, so that the complete 0 THz profiles are available. The dielectric relaxation time of acetonitrile in CCl_4 (25% volume/volume) has been measured as 3.3 ps at 303 K by Eloranta and Kadaba,[123] who also measure the far-infrared part of the frequency-dependent loss. Their values compares with the relaxation time of 3.8 ps measured by Krishnaji and Mansingh.[124] These relaxation times happen to agree with the reorientational P_1 correlation time of 3.2 ps

TABLE III
Experimental and Simulated Correlation Times for CH_3CN[a]

Technique	Correlation times	Computer simulation (293 K, 1 bar)
Infrared absorption	Reorientation of C_{3v} axis, $\tau_1 = 3.2$ ps $\tau_1 = 5.7$ ps	τ_1 (e_3) = 0.7 ps
	Reorientation about C_{3v} axis, $\tau_1 = 0.09$ ps	τ_1 (e_1) = 0.3 ps
Dielectric relaxation	Pure acetonitrile at 303 K, $\tau_1 = 3.3$ ps	τ_1 (e_3) = 0.7 ps
	Pure acetonitrile, $\tau_1 = 3.8$ ps 25% v/v in benzene, $\tau_1 = 6.7$ ps 25% v/v in CCl_4, $\tau_1 = 7.6$ ps	
Raman scattering	Reorientation of C_{3v} axis, $\tau_2 = 1.5$ ps Reorientation about C_{3v} axis $\tau_2 = 0.38$ ps (symmetric A_1 vibration–rotation), Reorientation of C_{3v} axis $\tau_2 = 0.9$ ps (symmetric ν_1 stretch), Reorientation of C_{3v} axis $\tau_2 = 1.5$ ps (symmetric ν_2 stretch),	τ_2 (e_3) = 0.4 ps τ_2 (e_1) = 0.2 ps τ_2 (e_3) = 0.4 ps τ_2 (e_3) = 0.4 ps
Rayleigh scattering	Reorientational correlation time, $\tau_2 = 1.8$ ps Reorientational correlation time (second-rank many-particle orientational correlation times), $\tau_2 = 1.8$ ps	A weighted mean of: τ_2 (e_2) = 0.4 ps; τ_2 (e_2) = τ_2 (e_1) = 0.2 ps
NMR relaxation	Spin lattice relaxation, angular momentum correlation times in the principal moment of inertia frame (297 K): $\tau_w = 0.063$ ps (NQC = 172.5 kHz) $\tau_w = 0.044$ ps (NQC = 160.0 kHz) $\tau_w = 0.025$ ps	0.19 ps Both acfs 0.12 ps nonexponential
	Spin-lattice relaxation (^{13}C), effective lab. frame angular momentum correlation time, $\tau_J = 0.093$ ps	0.15 ps (nonexponential acf)
	^{14}N nuclear-quadrupole relaxation, mean second rank orientational correlation time, $\tau_2 = 1.29$ ps (NQC = solid state) $\tau_2 = 1.01$ ps (NQC = gas)	Mean of τ_2 (e_3) = 0.4 ps; τ_2 (e_2) = τ_2 (e_1) = 0.2 ps
	^{13}C to ^1H spin–spin relaxation, mean (i.e., isotropic) second-rank orientational correlation time, $\tau_2 = 0.43 \pm 0.06$ ps $\tau_2 = 0.38$ ps The molecule spins about 10 times faster than it tumbles	Mean of τ_2 (e_3) = 0.4 ps; τ_2 (e_2) = τ_2 (e_1) = 0.2 ps

[a] Compiled by M. W. Evans *J. Mol. Liq.*, **25**, 149 (1983). Reproduced by permission. For reference to original data sources, see this review in *J. Mol. Liq.*

measured by Rothschild[125] from the ν_4 band, but the infrared correlation time of Breulliard-Alliot and Soussen-Jacob[106] is 5.7 ps.

That not all solvents are "noninteracting" is established by the fact that the relaxation time in benzene (25% volume/volume) decreases from 6.7 ps at 297 K to 3.1 ps at 333 K. In carbon tetrachloride under the same conditions, the relaxation times are 7.6 ps and 4.5 ps, respectively.

Burnham and Gierke[126] have observed a strong local order using the Kerr-effect experiment, the Cotton–Mouton effect, and light scattering to obtain orientational pair correlation functions that suggest a strong antiparallel alignment. Beevers[127] has also used the optical Kerr effect, and points out that acetonitrile is strongly dipolar and optically anisotropic, so that the Kerr effect can be traced back to the orientation of the dipoles.

Some papers have been devoted to the equilibrium structure of liquid acetonitrile. Kratochwill[128] determined the ^{13}C relaxation rate of the nitrile carbon and the self-diffusion coefficient of acetonitrile over a wide temperature range. The $^{13}C—H$ intermolecular part of the total relaxation rate was determined by isotope substitution and dilution, and combined with the known intermolecular proton relaxation rate to yield the orientation-dependent molecular pair distribution function. In the first coordination sphere, the molecules are arranged antiparallel. Kratochwill provides atom–atom pair correlations derived from X-ray and NMR measurements for the methyl-to-nitrile and the methyl-to-methyl carbon pairs of an acetonitrile molecule described by the rod I—S—T, where I is the methyl group, S is carbon, and T is nitrogen.

Hsu and Chandler[129] have used the X-ray-scattering data of Kratochwill in a RISM calculation of molecular distribution functions. They conclude that although the molecule has a large electric dipole moment, dipole–dipole interactions are unimportant in determining the microscopic structure. In Fig. 12 we compare the simulated atom—atom pdfs for nitrogen–nitrogen, carbon–carbon, and hydrogen–hydrogen. Though the overall shapes are similar, it is clear that the RISM theory tends to overestimate the intensity of the first peak and underestimate its position. The best agreement is found for the carbon–carbon pdfs. The worst mismatch is for the hydrogen–hydrogen pdfs: The pronounced first peak of RISM theory is reduced to a flat shoulder in the computer simulation. This mismatch is *not* caused by electrostatic interactions, because the essential shape of the computed pdfs is retained when we remove the point charges and work with the Lennard–Jones atom–atom cores.

Hsu and Chandler point out that scattering experiments can probe linear combinations of the Fourier transforms of these pair distribution functions and can be used to determine the structure factor. Their simple RISM theory does describe the experimental results of Kratochwill[128] and Bertagnolli

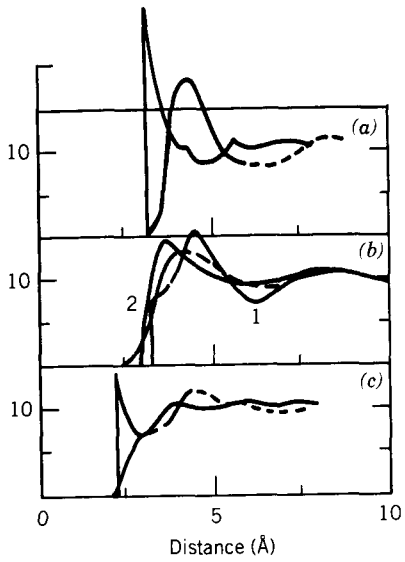

Figure 12. Comparison of simulated atom–atom pdfs for nitrogen–nitrogen, carbon–carbon, and hydrogen–hydrogen with those calculated using RISM theory: — , RISM theory; ---, computer simulation. (*a*) Nitrogen–nitrogen. (*b*) Carbon–carbon: (1, nitrile carbon; 2, methyl carbon. (*c*) Hydrogen–hydrogen. [Reproduced by permission from M. W. Evans, *J. Mol. Liq.*, **25**, 149 (1983).]

et al.[100] to within the uncertainty of the data. They point out the interesting fact that when two CH_3 groups come together, the hydrogen atoms must interlock, and there are two well-resolved intermolecular H—H lengths associated with the same pair of neighboring molecules. So even though they consider dipolar interactions to be of "little importance," there are strong pair correlations between neighboring molecules. The most probable location of a neighboring CH_3CN molecule is at right angles at a distance of 3.5–4.5 Å. There is, they conclude, a "mild tendency" for the angle between the principal (C_{3v}) axes to be between 60° and 120°. The most preferred orientation is near $\theta = 0°$ or $\theta = 180°$ (i.e., parallel alignment), but relatively few pairs of molecules are close enough to be so oriented. There are slightly more than 12 RISM neighbors in the first coordination shell. The coupling of orientational and translational coordinates is negligible outside the first coordination shell, but inside it is fairly strong. This, at least, is in accord with the simulation by M. W. Evans.[102] As we have said, we observe in CH_3CN some of the strongest R–T coupling in the series of polyatomic molecular liquids we have so far simulated (Fig. 13), and certainly the strongest interaction for a molecule of C_{3v} symmetry.

We have seen postulates of parallel alignment and antiparallel alignment, postulates of insignificant pair correlations inside the first coordination shell, and postulates of the existence of clusters of molecules—cluster vibrations have even been assigned. Lippert et al.[130] have reported strong effects of

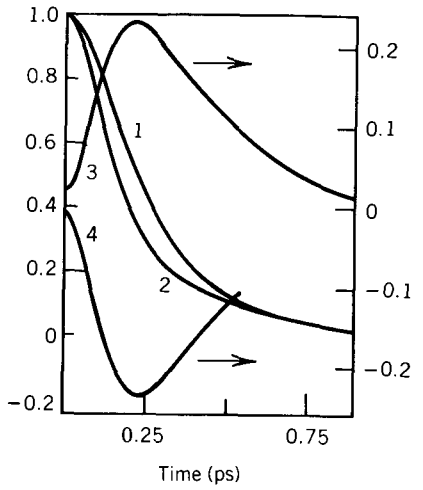

Figure 13. Rotation–translation coupling in CH_3CN. (1) Center-of-mass velocity autocorrelation function component $\langle v_3(t)v_3(0)\rangle / \langle v_3^2(0)\rangle$ in the moving frame of reference. (2) $\langle v_2(t)v_2(0)\rangle / \langle v_2^2(0)\rangle$, which is not isotropic with (1) in the moving frame. (3) $\langle v_2(t)J_1(0)\rangle / [\langle v_2^2\rangle^{1/2}\langle J_1^2\rangle^{1/2}]$, the (2,1) component of the mixed linear velocity–angular momentum (**J**) correlation function in the moving frame of reference. (4) $\langle v_1(t)J_2(0)\rangle / [\langle v_1^2\rangle^{1/2}\langle J_2^2\rangle^{1/2}]$. [Reproduced by permission from M. W. Evans, *J. Mol. Liq.*, **25**, 149 (1983).]

external electric fields on the infrared spectra of CH_3CN, which seems to indicate that the *electrodynamic interactions can be transmitted and enhanced over a macroscopic distance.*

Let us look at the far-infrared spectrum of acetonitrile again. Figure 14 shows typical spectra of CH_3CN.[131] The neat liquid is extremely absorbing, so that only small path lengths (0.03 mm) of the liquid can be studied by

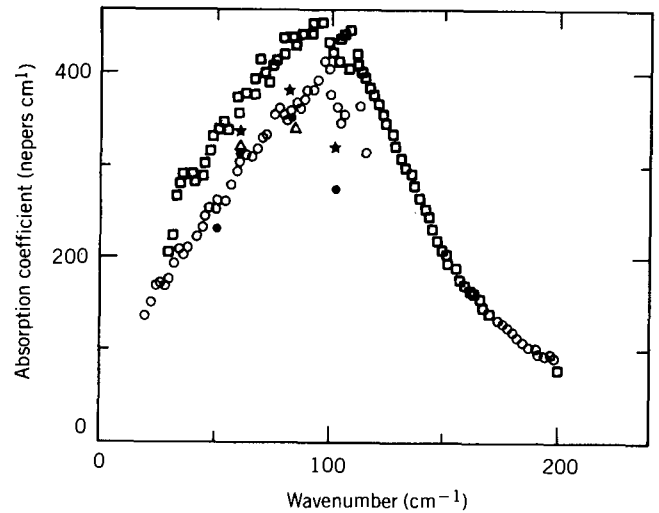

Figure 14. The far-infrared spectrum of CH_3CN.[131] [Reproduced by permission from M. W. Evans, *J. Mol. Liq.*, **25**, 149 (1983).]

normal transmission methods. We therefore estimate an uncertainty of at least 10% for measurement with the interferometric technique. Two runs, obtained using beam dividers that cover the spectral ranges 10–100 and 60–240 cm^{-1}, are shown. The spectra are deliberately not superimposed in order that the reader may judge the typical uncertainties involved. We note the appearance of structure on the low-frequency sides of the spectra. It is encouraging that the high-frequency sides decay smoothly and that spectra of solutions of CH_3CN in CCl_4 (10% and less) all produce smooth profiles. This detail cannot be attributed to channel spectra (internal reflections), which for acetonitrile would be separated by much larger frequencies and would anyway span the whole frequency range.

One feature in the spectrum, in particular, appears to be substantiated: a laser point at 103 cm^{-1}, chosen to coincide with the apparent minimum of the strongest line near the frequency of maximum absorption. Four laser points in all are shown. These are considered to define more precisely the absolute intensity. Three at lower frequencies agree well with the result obtained using a 100-gauge beam divider (interferometric spectroscopy). The fourth laser point seems to be at a lower intensity than that measured with the interferometric spectrometer, suggesting perhaps that at 4-cm^{-1} resolution the spectral detail is incompletely resolved.

One study in the literature may give some support to this result. Knozinger et al.[112] have reported spectra for the neat liquid and for the liquid in solution. Their spectrum for the former also shows signs of a "dip" at the frequency of peak intensity. Their frequency of maximum absorption is, at ca. 80 cm^{-1}, lower than our own (ca. 95 cm^{-1}), although ours agrees well with the measurement of ca. 93 cm^{-1} by Yarwood et al.[122] In their study Yarwood et al. do not appear to resolve the same detail. This could be a consequence of the averaging procedure used in obtaining the spectrum as well as of any subsequent data reduction.

The far-infrared spectrum for CH_3CN is certainly composite in nature. This is conclusively established in dilution studies. We have made our own measurements at concentrations of between 0.5 and 10% volume/volume (or, as number densities of CH_3CN in CCl_4, between 0.5 and 7.5×10^{20} molecules cm^{-3}). This concentration range was chosen because NMR results, discussed above, have suggested an association of CH_3CN molecules at higher concentrations (> 20%) that *gradually* disappears at roughly 20%, the concentration at which the single-particle correlation times dramatically decrease. This observation has now been shown to be consistent with our own[131] and those of Yarwood et al. and Knozinger et al. in the far infrared. We observe an apparent linear dependence of $\bar{\nu}_{max}$ (the frequency of maximum absorption) with number density up to a concentration of ca. 25%, at which distinct nonlinearity occurs; our and Yarwood's data agree well. This nonlinearity tells us that the absorptions are not solely single particle in nature, and that other contributions to the profiles exist.

We have postulated, as did Knozinger et al., that the band is composite in nature, with contributions arising from:

1. Single particle motions (the "Poley absorption," which is characteristic of all molecular liquids in the far infrared and has been measured in a computer-simulation experiment).
2. Absorption by dimers of molecules.
3. Absorption by larger aggregates of molecules.

Contributions (2) and (3) may be rotational, translational, or vibrational in origin.

The existence of the Poley absorption is established in the dilution studies. The frequency of maximum absorption shifts gradually to lower frequencies at higher dilution, so that a 0.5% solution has a maximum absorption at 70 cm^{-1} compared with (95 cm^{-1} in the neat liquid). There is also a lack of any temperature dependence of the spectra at the lowest concentration, although a distinct temperature dependence exists at higher concentrations. Also, this absorption at 70 cm^{-1} is much closer to that predicted in our 6×6 site–site model molecular-dynamics simulation.

The existence of a contribution from dimers of molecules (item 2 above) is more difficult to establish. It was first proposed by Jakobsen and Brasch.[132] To test the hypothesis, Bulkin[133] measured the spectra of five aliphatic nitriles. He measured the spectra of dilute solutions of CH_3CN in nonpolar solvents (CCl_4, benzene, and cyclohexane), and varied concentrations such that the product of multiplying concentration by pathlength was kept constant. It was not then possible to measure a decrease in the intensity of the absorption band. To explain this, he considered a monomer–dimer equilibrium, which revealed that if the association constant is ca. 10^3, the pure liquids are almost completely associated and there will be a decrease in dimer concentration of only ca. 5% on 500-fold dilution. This seems to be the case in CH_3CN. The equilibrium also reveals that if a system is only partially associated, dilution will eventually effect complete dissociation into monomers. Saum[134] had already proposed that butyronitrile (C_3H_7N) represented a case of only 75% association, so that if the dimer hypothesis held, any dimer absorption should disappear in a sufficiently dilute solution of this liquid. This was indeed found to be the case in a 0.25% solution of butyronitrile in cyclohexane: At this concentration the intermolecular dimer vibration band disappeared, leaving only an intramolecular vibration band that Saum assumed was a fundamental mode of the isolated molecule. But perhaps the strongest evidence of all is that dimers of molecules of CH_3CN

have long been postulated to exist even in the vapor phase.[27] Rowlinson's[27] second-virial-coefficient calculations for ΔU, the maximum value of the dipole–dipole energy of interaction, gave a value for CH_3CN of 4640 cal mol^{-1}, which is larger than that for water, 4440 cal mol^{-1}.

The contribution from larger aggregates of molecules (item 3 above) has been considered carefully by Knozinger et al.[112] They observed the temperature dependence of the spectra at higher concentrations, at which larger aggregates of molecules might be expected to exist. Both total band intensity and frequency of maximum absorption decrease when the temperature is raised between 263 and 313 K. In addition, there is an increase in the band intensity at 263 K and a decrease in the total band intensity at 313 K when the concentration is increased; an increase of concentration also shifts the band maximum to higher wavenumbers independently of the temperature applied. All of this is explained only if at least two different types of aggregates are present. A whole *set* of intermolecular vibrational transitions or rotations and translations of aggregates of molecules may then exist and strongly, though perhaps not completely, overlap. It may be this incomplete overlap of contributory absorptions that we now observe at low frequencies in the far infrared.

There is other evidence supporting the existence of these collective, intermolecular modes, in an isotropic liquid, and G. J. Evans[101] has postulated the existence of such in liquid crystalline systems. Lobo et al.[135] propose that collective modes arising from oscillations of the long-range interactions between electric dipoles could exist in certain liquids. Ascarelli[136] studied nitromethane as a characteristic dipolar liquid with a large dipole moment (3.4 D) and observed the existence of these collective modes with a power reflection technique. When a mylar electret was inserted into his sample, the frequency of maximum absorption of the collective mode shifted by some 30 cm^{-1}. The mylar electret, he supposed, produced a further aggregation of dipoles. A model calculation showed that an externally applied field stabilizes aggregates of molecules the radii of which are above a certain value—aggregates that would normally be unstable. The electric field favors the growth of regions where the concentration of dipoles is increased. This may be observed with a simple experiment in which the gap between a pair of square brass electrodes is sealed with two transparent (polymeric) windows. The complete cell is immersed into the pure (conducting impurities removed), neat liquid and a field is applied. The liquid is drawn into the enclosed gap. Aniline, for example, could be suspended to a height of 11 cm in this way. Some of the most striking effects are to be observed on nondipolar solvent liquids such as CCl_4. The effect is so strong in this instance that fine droplets of liquid are sprayed rapidly through the top of two parallel electrodes 13 cm long.[101] Lippert et al.[130] and Evans and Evans[137] have both reported spectroscopic effects of electric fields on isotropic molecular liquids. One of us (M.W.E.) reports on electric-field effects in computer simulation experiments elsewhere in this volume.

In concluding we emphasize that it is not possible to analyze these complex bandshapes with present dynamic theories for the liquid state. The best models for the rotary motions and currently available computer simulations can be expected to reproduce only the "Poley absorption"—that arising from single-particle orientation motions. Translational effects are normally ignored, and rototranslational theories are either intractable or involve unacceptably large numbers of adjustable parameters. Cooperative behavior cannot yet be simulated because of the number of molecules involved and because of the limitations imposed by the speeds of present-day computers.

This situation discussed in this section applies *to all* the spectroscopies. The association is a natural property of the liquid that persists to concentrations of less than 10% and may even be enhanced in some solvents at higher dilution. It is not a trivial problem, therefore, to obtain single-particle properties for CH_3CN, as the discrepancies and contradictions in the literature show. It is questionable if it is meaningful and desirable even to attempt to do so in such an associated system.

V. BROMOFORM ($CHBr_3$)[‡]

Bromoform is an interesting example of a molecule with C_{3v} symmetry because it possesses a solid rotator-phase state, the liquid freezing at 281 K. We define such a state as one in which rotational motion is comparatively free and translational freedom is restricted—the molecules are constrained to sites in the solid lattice. Consequently, in this state of matter we anticipate a small coupling of rotation with translation that may persist even in the liquid state.

Brodbeck et al.,[138] in reviewing the literature on bromoform, notice again the difficulty of comparing results obtained with different techniques by way of measured or calculated correlation times because of the variety of definitions of correlation time: "The literature results may double according to definition." Boldeskal et al.[139] define the correlation time as the time taken by the normalized autocorrelation function in question to fall to $1/e$. Other authors[138] use the bandwidth $\Delta\omega$ to calculate the relaxation time τ as proportional to $\Delta\omega^{-1}$ of the zeroth moment of the particular autocorrelation function under question. As we shall see, no overall viewpoint is attained from the comparison of these correlation times for bromoform.

[‡]This section is based on a computer simulation and literature search by M. W. Evans, reported as ref. 147 (editor's note).

We will use our proposed methodology to see if computer simulation of the various correlation functions can help bring some consistency to the results and, in particular, to prove our hypothesis that the interaction of rotation with translation must be small. We use again the atom—atom Lennard-Jones positive-charges framework and the available intermolecular-potential parameters to construct spectra of various kinds.

The interaction between $CHBr_3$ molecules is modeled by a 5×5 atom–atom Lennard-Jones "core" with point charges localized at each atomic site. The Lennard-Jones parameters are as follows:

$$\sigma(\text{H—H}) = 2.75\ \text{Å}$$
$$\sigma(\text{Cl—Cl}) = 3.50\ \text{Å}$$
$$\sigma(\text{C—C}) = 3.20\ \text{Å}$$
$$\varepsilon/k(\text{H—H}) = 13.4\ \text{K}$$
$$\varepsilon/k(\text{Br—Br}) = 263.0\ \text{K}$$
$$\sigma(\text{Br—Br}) = 3.7\ \text{Å}$$

The H and C parameters are as for chloroform (Section II). The parameters for Br were taken from the values of Eliel et al.,[140] which successfully reproduce crystal-phase properties such as heat of sublimation. The calculation of partial charges is based on the very simple lcao technique of del Re.[141] Taking into account the slightly smaller dipole moment of $CHBr_3$ in comparison with $CHCl_3$, the increase in bond length from C—Cl to C—Br, and the slightly smaller electronegativity of Br in comparison with Cl, M. W. Evans arrives at the following estimate of partial charges for $CHBr_3$:

$$q_{\text{H}} = 0.021|e|$$
$$q_{\text{C}} = 0.055|e|$$
$$q_{\text{Br}} = -0.059|e|$$

To compare results from the simulation with those available from experiments, we adopt once more the definition of a correlation time used throughout this article.

The moments of inertia of bromoform calculated by M. W. Evans with Hirschfelder's[142] dyadic minimization technique are

$$I_A = 6.87\times10^{-38}\text{g cm}^2$$
$$I_B = I_C = 1.352\times10^{-37}\text{g cm}^2$$

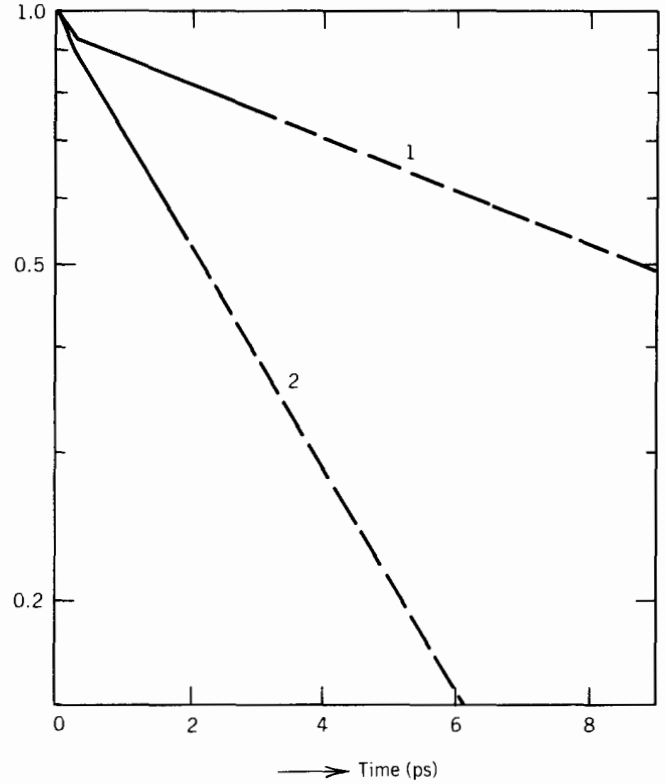

Figure 15. Computer-simulated orientational autocorrelation functions for bromoform: 1, $P_1(\mathbf{e}_A)$; 2, $P_2(\mathbf{e}_A)$. (Reproduced by permission from ref. 147.)

The dipole unit vector is $\mathbf{e}_A$. We define the first-rank, P_1, orientational correlation time as the area beneath the autocorrelation function $\langle \mathbf{e}_A(t)\cdot\mathbf{e}_A(0)\rangle$, and the second-rank, P_2, orientational correlation time as the area beneath the autocorrelation function $\frac{1}{2}\langle 3[\mathbf{e}_A(t)\cdot\mathbf{e}_A(0)]^2 - 1\rangle$. The simulated autocorrelation functions are shown in Fig. 15. The latter correlation time can also be obtained from NMR dipole–dipole relaxation because the dipole–dipole ^{13}C NMR relaxation time refers to the ^1H-to-^{13}C vector of $CHBr_3$, which is directionally the same as $\mathbf{e}_A$.

We will use only spectroscopic data that we consider to have been correctly reduced, and make allowances for the various factors that contribute to spectral profiles discussed at length in Section I. For example, Sandhu[143] finds that spin rotation and inter- and intra-molecular dipole–dipole relaxation contribute to the observable nuclear spin relaxation. He calculates a

TABLE IV
Experimental and Simulated Correlation Times for Bromoform[a]

Technique	Experimental correlation time (ps)[b]	Simulated autocorrelation time (ps)[c]
Dielectric relaxation		
	19.0	11.0 ($\mathbf{e}_A$)
Infrared		
ν_1 stretch (C—H)	8.2 ± 3.3	11.0 ($\mathbf{e}_A$)
Raman		
ν_1 stretch (C—H)	5.1 ± 1.0, 2.0 ($1/e$), 3.1, 4.4,	2.8 ($\mathbf{e}_A$)
ν_2 (CBr_3 symmetric stretch)	3.4, 4.4	Weighted mean of 2.8 ($\mathbf{e}_A$), 4.5 ($\mathbf{e}_B$,$\mathbf{e}_C$)
ν_3 (CBr_3 symmetric bend)	5.3, 6.6, 6.8	4.5 ($\mathbf{e}_B$,$\mathbf{e}_C$)
Rayleigh scattering	10.1	Weighted mean of 2.8 ($\mathbf{e}_A$), 4.5 ($\mathbf{e}_B$,$\mathbf{e}_C$)
NMR		
intramolecular $\mu-\mu$	4.1 (average)	Weighted mean of 2.8 ($\mathbf{e}_A$), 4.5 ($\mathbf{e}_B$,$\mathbf{e}_C$)
Intermolecular $\mu-\mu$	$\tau_c = 10.4$	$\tau_v < 0.1$[d]
translational correlation time		$\tau_r \approx 11.3$

[a] Compiled by M. W. Evans, and reported in *J. Chem. Soc., Faraday II*, **79**, 137 (1983). Reproduced by permission. See this paper for original data sources.
[b] Multiple values represent literature variation.
[c] In the rotator phase at 273 K, $\tau_1(\mathbf{e}_A)$ (first rank) is 18.0 ps and $\tau_2(\mathbf{e}_A)$ (second rank) is 5.7 ps from the computer simulation.
[d] Center-of-mass velocity.

translational correlation time of 10.4 ps at 298 K, making the assumption that the diffusion tensor is related to the effective molecular radius by Stokes's law. He calculates a rotational (P_2) correlation time of 4.1 ps, which is much less than one-third of the dielectric (P_1) relaxation times of 19 ps measured by Soussen-Jacob et al.[144] and of 24.4 ps at 293 K decreasing to 13.3 ps at 323 K measured more recently by Sharma and Agarwal.[145] This is therefore inconsistent with the theory of rotational diffusion, which nevertheless was used by all three sources in deriving their correlation times.

In Table IV we compare the simulated correlation times with these experimental results. The agreement is satisfactory for the "single particle" infrared and Raman correlation times. The infrared (C—H stretch) rotational correlation time, for example, is 8.2 ± 3.3 ps, compared with a computer-simulated time of 11.0 ps. There is satisfactory agreement between the NMR rotational mean correlation time of Sandhu and the three computed times (one for each axis, i.e., $P_2(\mathbf{e}_A)$, $P_2(\mathbf{e}_B)$, and $P_2(\mathbf{e}_C)$). However, there is at first sight a serious difference between the intermolecular NMR translational correlation time of 10.4 ps and the computer-simulated time of < 0.1 ps.

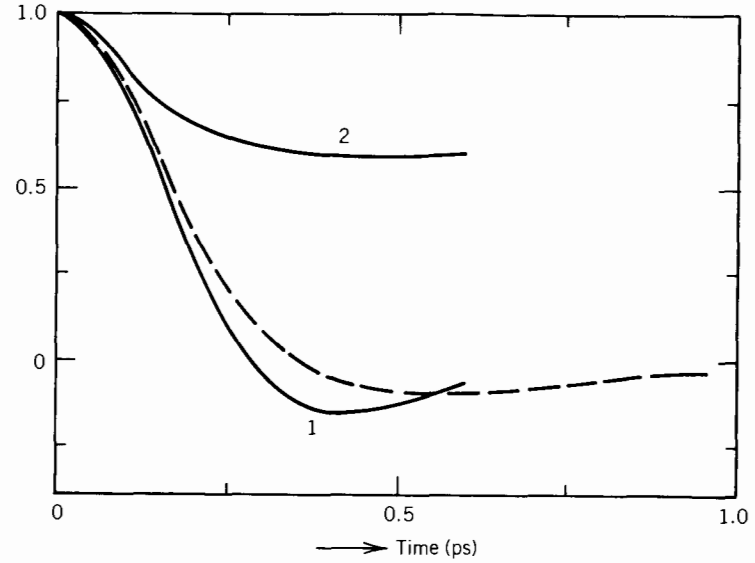

Figure 16. Computer-simulated center-of-mass velocity autocorrelation functions for $CHBr_3$, 293 K, 1 bar: 1, $\langle \mathbf{v}(t)\cdot\mathbf{v}(0)\rangle / \langle v^2(0)\rangle$; 2, $\langle \mathbf{v}(t)\cdot\mathbf{v}(t)\mathbf{v}(0)\cdot\mathbf{v}(0)\rangle / \langle v^4(0)\rangle$; ---, $\langle \mathbf{v}_3(t)\mathbf{v}_3(0)\rangle / \langle v_3^2(0)\rangle$, molecule fixed frame. (Reproduced by permission from ref. 147.)

However, Sandhu assumes that the motion is describable by the diffusion equation and an exponentially decaying $\langle \mathbf{v}(t)\cdot\mathbf{v}(0)\rangle$; thus τ_c as measured by Sandhu is given by

$$\tau_c = \frac{a^2}{12D} = \frac{Ma^2}{12kT\tau_v}$$

where a is the molecular radius, M the molecular mass, and τ_v the velocity correlation time. We must adjust τ_v of the molecular dynamics accordingly and relate it to τ_c as above. Assuming a molecular radius of 3.6 Å and using the molecular mass, we obtain a "simulated" τ_c of 11.3 ps. However, this point is academic, because the computer-simulated center-of-mass velocity autocorrelation function is not exponential, as assumed by Sandhu in his derivation, and has a characteristic long time tail (Fig. 16).

Agreement between simulation and experimental data is not satisfactory for dielectric relaxation, far-infrared absorption, and depolarized Rayleigh scattering techniques (Table IV). This is again anticipated, because the multimolecular counterparts of $\langle \mathbf{e}_A(t)\cdot\mathbf{e}_A(0)\rangle$ and $\frac{1}{2}\langle 3[\mathbf{e}_A(t)\cdot\mathbf{e}_A(0)]^2 - 1\rangle$ are obtained from these techniques. These data give information on groups or

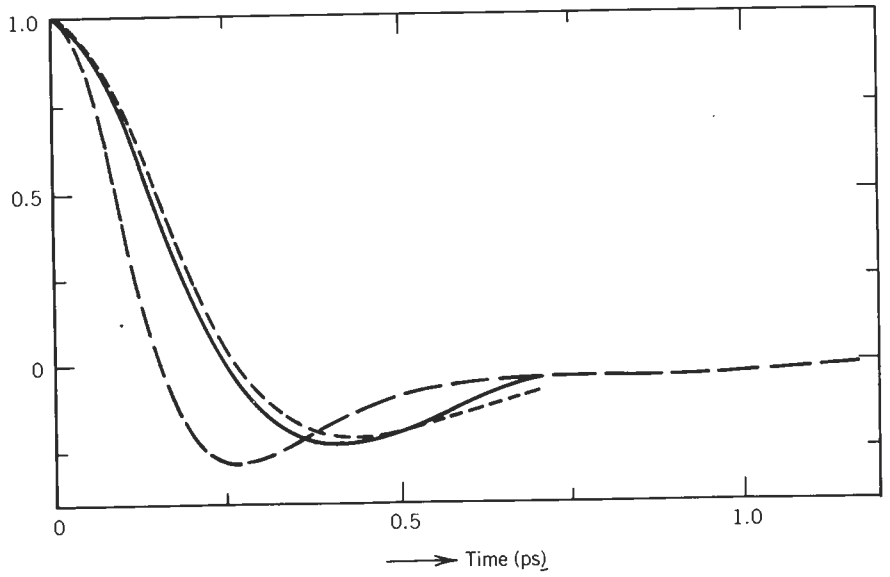

Figure 17. Rotational velocity correlation functions: – – –, experimental; —, simulation $\langle \dot{\mathbf{e}}_A(t)\cdot\dot{\mathbf{e}}_A(0)\rangle/\langle\dot{\mathbf{e}}_A^2(0)\rangle$; ------, $\langle \dot{\mathbf{e}}_C(t)\cdot\dot{\mathbf{e}}_C(0)\rangle/\langle\dot{\mathbf{e}}_C^2(0)\rangle$. $\mathbf{e}_A$ is the dipole vector. [Reproduced by permission from ref. 147.]

ensembles of molecules, and the cross correlation functions involved are much more difficult to simulate. The evidence provided by Brodbeck et al. seems to indicate that the correlation times involved in cross correlation are longer than those of the autocorrelation functions. For example, the dielectric relaxation time measured by Soussen-Jacob is 19 ps, and the infrared rotational correlation time measured by Brodbeck is 4.1 or 8.2 ps (depending on definition). Similarly, the ν_1 stretch Raman correlation times from various sources lie in the range 2–5.1 ps, and the depolarized Rayleigh correlation time of Patterson and Griffiths[146] is 10.1 ps.

The discrepancy is clearly displayed in Fig. 17, which shows the simulated rotational velocity autocorrelation function and the Fourier transform of the $\alpha(\omega)$ far-infrared power absorption of liquid bromoform.[147] We have therefore also simulated a "multimolecular rotational velocity correlation function" for bromoform using subspheres built up of three or four $CHBr_3$ molecules. However, this does not produce results significantly different from the computed correlation function of Fig. 16.

The far-infrared spectra (Fig. 18) firmly substantiate the existence of the solid rotator phase. The rotator-phase spectrum is shifted slightly to higher

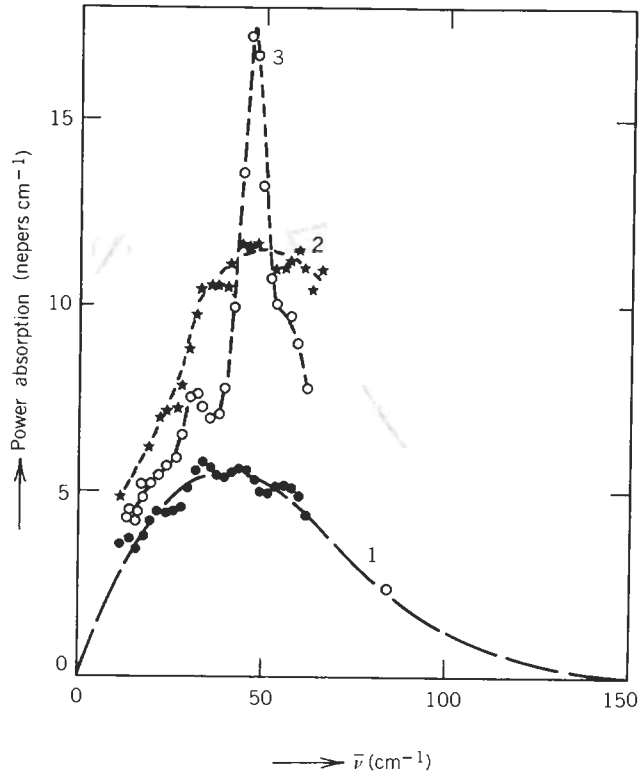

Figure 18. Far-infrared absorption of bromoform in liquid and rotator-phase states: 1, liquid state at 295 K, O laser point (84 cm^{-1}); 2, rotator phase at 273 K (as for the liquid, a broad, featureless band); 3, crystalline solid (note that the lattice modes are resolved). (Reproduced by permission from ref. 147.)

frequencies, but remains a broad and featureless band. No lattice modes, characteristic of the crystalline solid, are resolved until the sample is cooled to below −2°C. The solid rotator phase exists between −2 and +8°C. Depending on the rates of heating and cooling, a marked hysteresis may be observed as the sample is cooled and reheated through this phase.

In a moving frame of reference, discussed at length in this volume, M. W. Evans observes directly the coupling of rotation with translation by constructing the matrix $\langle \mathbf{v}(t)\mathbf{J}^T(0)\rangle$. By symmetry, in this molecule the only nonvanishing elements of this matrix are (1, 2) and (2, 1). These are illustrated in Fig. 19 and are very small in the liquid state (the same is true, as anticipated, in the rotator-phase solid).

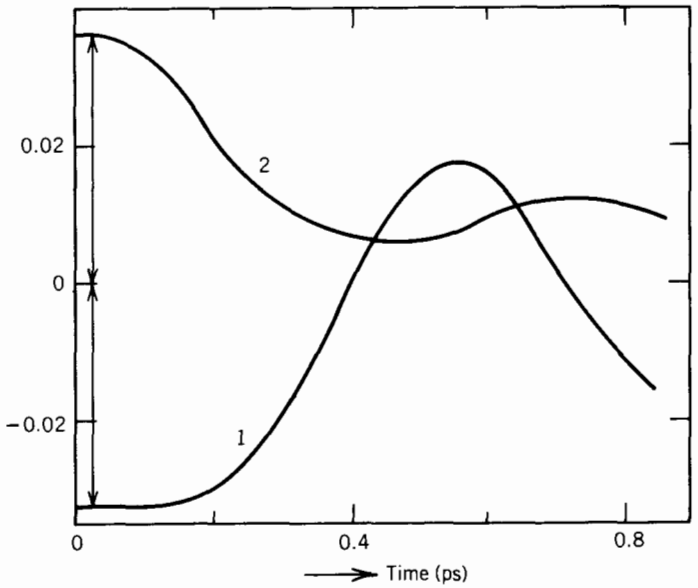

Figure 19. Rotation–translation autocorrelation function $\langle \mathbf{v}(t)\mathbf{J}^T(0)\rangle$ in the moving frame: 1, the (1,2) component; 2, the (2,1) component. The noise level is indicated on the ordinate axis by arrows, showing that the extent of coupling is small and within the noise level of the simulation. (Reproduced by permission from ref. 147.)

VI. TERTIARY BUTYL CHLORIDE

Tertiary butyl chloride [M. W. Evans et al., *J. Chem. Soc., Faraday II*, **79**, 767 (1983)] is an example of a molecule of C_{3v} symmetry for which two solid rotator phases are known to exist between the isotropic liquid and crystalline solid states. The transition temperatures are

$$T_c \rightarrow \text{II} = 182.9 \text{ K}$$
$$T_{\text{II}} \rightarrow \text{I} = 219.25 \text{ K}$$
$$T_{\text{I}} \rightarrow \text{liq} = 247.53 \text{ K}$$

where "c" signifies the crystalline state, liq. the isotropic liquid, and II and I are the two rotator-phase states.

Lassier and Brot[148] have studied *t*-butyl chloride in its crystalline and rotator-phase states using models of molecular rotational diffusion to interpret their dielectric and far-infrared results. They calculated lattice energies for phases II and I. The difference between the computed energies of phases I and II was found to be equal to the observed enthalpy of transition, which is configurational rather than purely electrostatic in origin. Lassier and Brot calculated the configurational energy and energy of transition using:

1. The energy of repulsion.
2. The London attraction energy.
3. The electrostatic energy between permanent charges.
4. The energy of formation of the induced polarization.
5. The charge-induced dipole energy.
6. The energy between induced dipoles.

The first two terms were found to be some 10 times as large as the electrostatic energy, which in turn was an order of magnitude greater than the polarization and induction energies.

Larson and Mansson[149] have studied the rotational motions that dominate the elastic and quasielastic scattering of the liquid. None of the models used satisfactorily reproduced the measured data, even though models ranging from free rotation to "undamped libration" were considered. Goyal et al.,[150] reporting on neutron-scattering studies in the rotator-phase state, attribute its origin to molecular orientation about the C—C axis. According to Goyal, the dipole axis is frozen and reorientation between individual sites occurs at 12-ps intervals. The different depths of the energy well cause Davydov splitting of the infrared spectrum.

Both these groups consider rotation in *t*-butyl chloride to be wholly decoupled from translation. The agreement of their results with those from other techniques is not good; for example, the P_1 correlation time from neutron scattering is 3 ps at 325 K, compared with the dielectric relaxation time at 233 K of 7.7 ps. The P_2 orientational correlation time from neutron scattering is 1.2 ps.

Heatley[117] provides a proton–^{13}C magnetic resonance relaxation time for (assumed) isotropic rotational diffusion of 1.05 ± 0.10 ps in the liquid state at 308 K. Boguslavskii et al.[151] have measured the temperature dependence of the solid-state NMR relaxation, and find an effect of large-amplitude reorientational and translational motions in the electric field gradient of the resonant nucleus that persists over the temperature range of the phase transition. Koeksal,[152] using ^{3}H spin–lattice relaxation at 60 MHz between 100 and 330 K, discerned three types of motion: center-of-mass translation, molecular tumbling, and methyl-group torsion.

Constant and Fauquembergue[153] have studied the Raman C—Cl stretch over a wide temperature range for liquid *t*-butyl chloride neat and in CCl_4 and *n*-hexane solution. They compare their results with Heatley's, assuming in the data-reduction process that there is (1) no rotation–vibration cou-

pling, (2) no vibrational cross correlations between molecules, and (3) no collision-induced scattering. Their correlation time of 1.2 ± 0.1 ps is only in fair agreement with Heatley's value. They also made a direct comparison of the Raman and Rayleigh correlation functions in pure liquid *t*-butyl chloride at room temperature (298 K). The P_2 correlation time is, at 1.3 ± 0.05 ps, slightly longer than the C–Cl Raman correlation time. They attribute this to cross-correlation effects, concluding that collision-induced effects are too weak to be detected. Carlson and Flory[154] contest this conclusion, reporting that induced scattering is very significant over a range of frequencies. They assert that no less than 50% of the absolute intensity of the depolarized Rayleigh spectrum is collision induced. Czarniecka et al.[155] have also compared their Raman correlation times with those of Constant and Fauquembergue, and find better agreement.

As we compared P_2 correlation times above, so we may compare the P_1 correlation times from infrared bands and 0 THz absorption or with the Rayleigh "power spectrum" (obtained by multiplying the Rayleigh band by $\bar{\nu}^2$, where $\bar{\nu}^2$ is the wavenumber).

Constant and Fauquembergue report a C–Cl stretch correlation time of 4.2 ps at 288 K decreasing to 2.8 ps in 20% (mole fraction) *n*-hexane solution. The dielectric time of Czarniecka et al. is 4.9 ps. Reid and Evans[156] find that in a 10% solution in decalin the dielectric relaxation time is reduced to 3.6 ps. There is a better agreement between the "P_1 experiments" for this particular liquid. The agreement suggests that cross correlations must be small, a suggestion supported by the similarity of the Raman and Rayleigh correlation times. Reid and Evans analyze their data using a model of itinerant oscillation that predicts a correlation time of 3 ps for *t*-butyl chloride in decalin, in fair agreement with the experimental value. They also observe that in the glassy state this is increased to microsecond magnitude, and proceed to discuss the validity of the Gordon sum rule in this instance (the integrated intensity of the experimental band is 325 cm^{-2}, whereas the Gordon sum rule gives 266 cm^{-2}).

All in all, the conclusions to be reached from the large number of studies on this system, particularly those conclusions relating to the extent of collision-induced absorption, are again inconsistent. *t*-butyl chloride is therefore another liquid that we hope to gain further insight into using computer simulation. It is also ideal for simulation work because, as Lassier and Brot have shown, the electrostatic energy is so much smaller than the effective Lennard-Jones energy that periodic boundary conditions are not likely to be a problem. The experiments above also suggest that it is safe to ignore polarization and induction effects.

M. W. Evans[137] has reproduced a range of spectral data in a computer simulation using the atom–atom Lennard-Jones and partial-charge parameters of Lassier and Brot and ignoring polarizability and induction effects. The Lennard-Jones parameters are as follows:

$$\sigma(\text{C—C}) = 3.4 \text{ Å}$$
$$\sigma(\text{CH}_3\text{—CH}_3) = 4.0 \text{ Å}$$
$$\sigma(\text{Cl—Cl}) = 3.6 \text{ Å}$$
$$\varepsilon/k(\text{C—C}) = 35.8 \text{ K}$$
$$\varepsilon/k(\text{CH}_3\text{—CH}_3) = 158.6 \text{ K}$$
$$\varepsilon/k(\text{Cl—Cl}) = 127.9 \text{ K}$$

The Lorentz–Berthelot combining rules used by Lassier and Brot provide the cross terms. The partial-charge parameters of Lassier and Brot are:

$$q_{\text{CH}_3} = 0.054|e|$$
$$q_{\text{C}} = 0.038|e|$$
$$q_{\text{Cl}} = -0.201|e|$$

The simulations were carried out at 293 K, 1 bar, in the liquid and at 228 K, 1 bar, in rotator phase I. Haffmans and Larkin[157] obtained a density of 0.96 g cm^{-3} for rotator phase I at 228 K (fcc, $a = 8.62$ Å, four molecules per unit cell) and this was used by M. W. Evans to calculate the input molar volume for the computer simulation.

Table V compares some of the correlation times from the simulation with experimental results at 293 K, 1 bar; and 228 K, 1 bar. Figure 20 shows the results of computer simulation[137] compared with the infrared, Raman, and Rayleigh orientational correlation functions of Constant and Fauquembergue. The agreement of the correlation functions is fair and within experimental error in some cases. It is probable that (1) reorientational effects have been factored out correctly from vibrational dephasing effects in the liquid, and (2) the same is true of the Raman second-rank orientational autocorrelation function.

Carlson and Flory[34] have suggested that a large amount of collision-induced scattering occurs in *t*-butyl chloride, which conflicts with the view of Constant and Fauquembergue. The results of the computer simulation indicate that the theoretical, $P_2(\mathbf{e}_A)$ autocorrelation function has a similar time dependence similar to that of the multimolecule correlation function from the Rayleigh wing of Constant and Fauquembergue. So, we can at least say that the time dependence of the collision-induced effects, if they are significant, is the same as that of the scattering due to the permanent molecular polarizability anisotropy.

TABLE V
Experimental and Simulated Correlation Times for *t*-Butyl Chloride[a]

Technique	Experimental correlation times	Simulated autocorrelation times (293 and 228 K) ps
Infrared	C—Cl stretch, 288 K	τ_1 (e_C) = 4.0
	Pure liquid TBC: 4.2 ps	A weighted mean of:
	20% mole fraction TBC in *n*-hexane: 2.0 ps	τ_1 (e_C) = 4.0; τ_1 (e_A) = τ_1 (e_B) = 3.2
	Totally symmetric C—CH_3 stretch: 1.49 ps	
Raman	C—Cl stretch: 1.2 ps	τ_2 (e_C) = 1.5; τ_2 (e_A) = τ_2 (e_B) = 1.2
	20% mole fraction in *n*-hexane: 0.8 ps	
Rayleigh	Pure liquid at 298 K: 1.3 ps	A weighted mean of:
		τ_2 (e_C) = 1.5; τ_2 (e_A) = τ_2 (e_B) = 1.2
Dielectric Relaxation	Pure liquid: 4.9 ps	τ_1 (e_C) = 4.0; τ_1 (e_A) = τ_1 (e_B) = 3.2
	10% decalin solution: 3.6 ps	
	Rotator phase I: 274 K: 5.6 ps	
	Rotator phase I: 238 K: 7.4 ps	
	Rotator phase I: 233 K: 7.7 ps	τ_1 (e_C) = 9.5; τ_1 (e_A) = τ_1 (e_B) = 5.2
NMR relaxation	$^1H—^{13}C$ spin–spin: 1.05 ± 0.1 ps	τ_2 (e_C) = 1.5; τ_2 (e_A) = 1.2
Neutron scattering	Mean time between successive reorientations:	
	10 ps at 208 K	
	(Rotator II): 14 ps at 193 K	
	P_1 (dipole vector): 235 K: 3.0 ps	τ_1 = 9.5
	P_2 (dipole vector): 235 K: 1.2 ps	τ_2 = 5.2 at 228 K

[a] Compiled by M. W. Evans, and reported in *J. Chem. Soc. Faraday Trans. II*, **79**, 767 (1983). Reproduced by permission. See this paper for original data sources.

We can investigate further the role of orientational cross correlations using far-infrared data. Larkin,[158] Reid,[159] and Evans and Evans[137] have reported far-infrared studies. In Fig. 21 we compare simulated and measured rotational velocity correlation functions. Initially, the decays of the two functions are the same, but then the experimental function decays more quickly and has a slightly deeper overshoot, indicating that cross-correlation functions are significant but not markedly so. The effect of dilution corroborates this. The effect is small and the integrated intensity is linear in the molecular number density [at least in the range studied, but again there is a need to extend these dilution studies to concentrations of 1% and less (see Section IV)]. We can attribute the discrepancy between the measured integrated intensity and that obtained using Gordon's sum rule, referred to earlier, only to some limitation of the sum rule. Reid and Evans[156] have discussed the validity of the Gordon sum rule in this context, and Bossis[161] has extended the analysis to include anisotropic cavities and the internal-field effect.

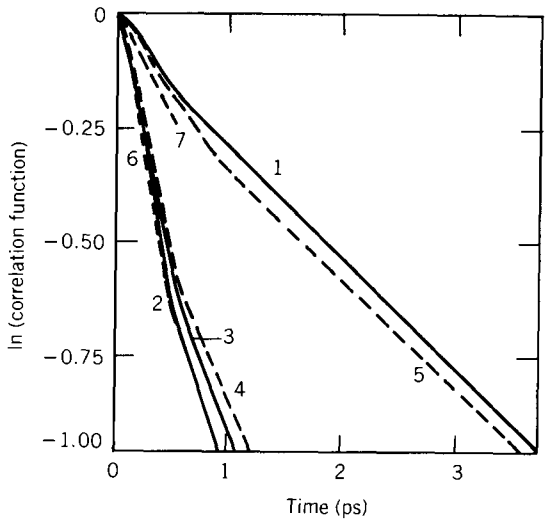

Figure 20. Comparison of computer-simulation results with the experimental data for liquid *t*-butyl chloride at 293 K. 1, P_1 orientational autocorrelation function from the infrared bandshape; 2, P_2 orientational autocorrelation function from Raman scattering; 3, P_2 orientational autocorrelation function from Rayleigh scattering; 4, Simulated orientational autocorrelation function of the dipole vector (C_{3v} symmetry axis), P_2 autocorrelation function; 5, as for 4, P_1 autocorrelation function; 6, as for 4, vector $\perp C_{3v}$ axis; 7, as for 5, vector $\perp C_{3v}$ axis. [Reproduced by permission from M. W. Evans et al., *J. Chem. Soc., Faraday II*, **79**, 767 (1983).]

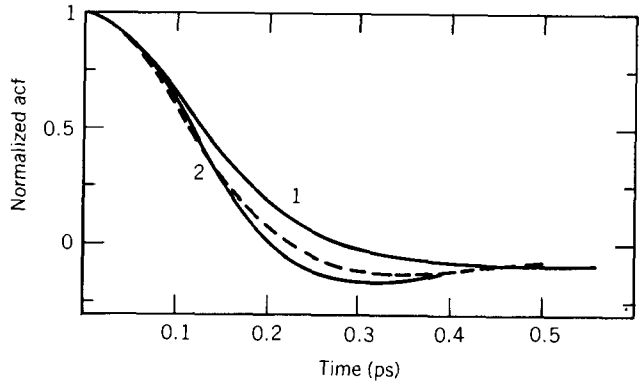

Figure 21. Comparison of simulated and measured rotational velocity correlation functions for *t*-butyl chloride: 1, computer-simulated $\langle \dot{e}_C(t) \cdot \dot{e}_C(0) \rangle / \langle \dot{e}_C^2 \rangle$; 2, Fourier transform of far-infrared spectrum; ---, $\langle \dot{e}_A(t) \cdot \dot{e}_A(0) \rangle / \langle \dot{e}_A^2 \rangle$, illustrating the anisotropy of the rotational motion. [Reproduced by permission from M. W. Evans et al., *J. Chem. Soc., Faraday II*, **79**, 767 (1983).]

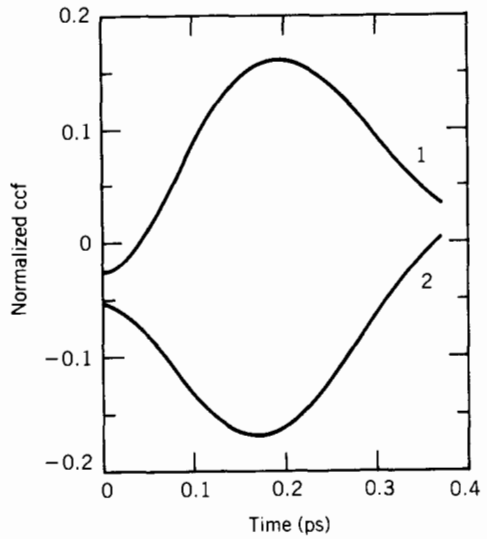

Figure 22. Elements of $\langle \mathbf{v}(t)\mathbf{J}^T(0)\rangle$ in the moving frame of reference. 1, $\langle v_2(t)J_1(0)\rangle / [\langle v_2^2\rangle^{1/2}\langle J_1^2\rangle^{1/2}]$, the (2,1) element; 2, the (1,2) element. The noise level is demonstrated by the $t = 0$ intercept, which is zero by symmetry in the absence of noise. [Reproduced by permission from M. W. Evans et al., *J. Chem. Soc., Faraday II*, **79**, 767 (1983).]

M. W. Evans[137] uses the numerical method to investigate dynamical properties that are not directly observable by experiment. First he considers rotation–translation interaction, which we recall, was insignificant in bromoform. Again, it must be investigated in a moving frame of reference. For *t*-butyl chloride the (1,2) and (2,1) elements of the rototranslation matrix $\langle \mathbf{v}(t)\mathbf{J}^T(0)\rangle$ do not vanish by symmetry for $t > 0$. The result is shown, suitably normalized, in Fig. 22. Despite the statistical noise, it is clear that there is a real, but small, statistical correlation between the two modes of motion.

It is again interesting to examine what differences exist between the solid rotator phases and the liquid phase. In particular, we may compare the liquid and rotator phases over a short (molecular) range (less than 10 Å, within which distance correlations persist) by constructing atom–atom pdfs. The functions are illustrated in Fig. 23. The functions measure the probability of finding an atom of molecule B at a distance r from an atom of molecule A given the position of the latter atom relative to the origin in the laboratory frame of reference. The correlations disappear at 10 Å, the range of the first coordinate shell, in both instances (rotator and liquid). The lack of long-range order in the rotator phase suggests why this phase is incapable of supporting phonon modes such as may be observed in the crystalline phase below 182.9 K.

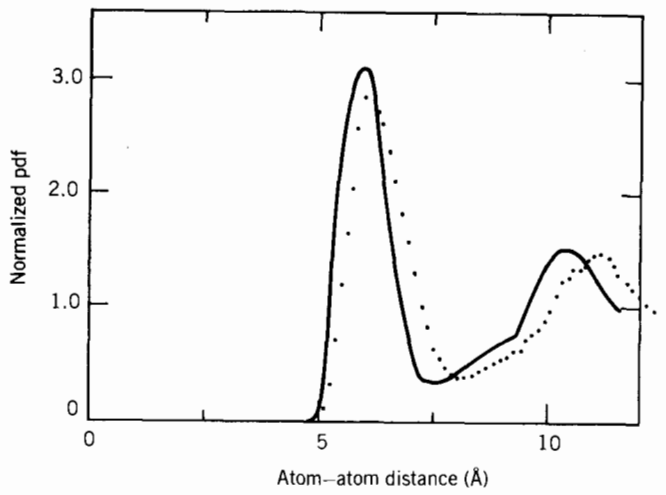

(*a*)

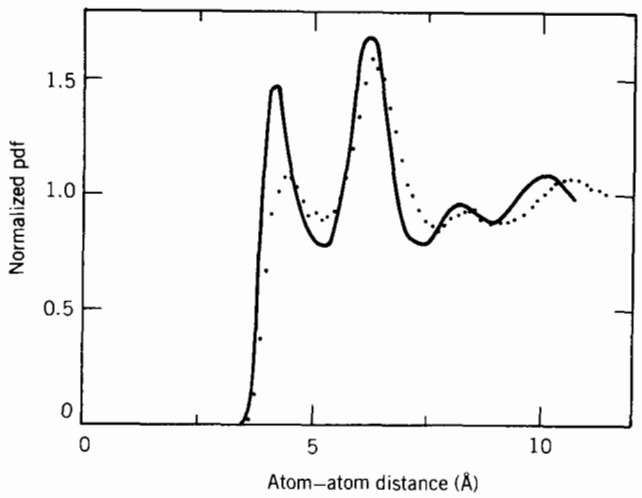

(*b*)

Figure 23. Atom–atom pdfs of *t*-butyl chloride: — , liquid at 293 K; ●, rotator phase I at 228 K. (*a*) Carbon–carbon function. (*b*) Methyl–methyl function. [Reproduced by permission from M. W. Evans et al., *J. Chem. Soc., Faraday II*, **79**, 767 (1983).]

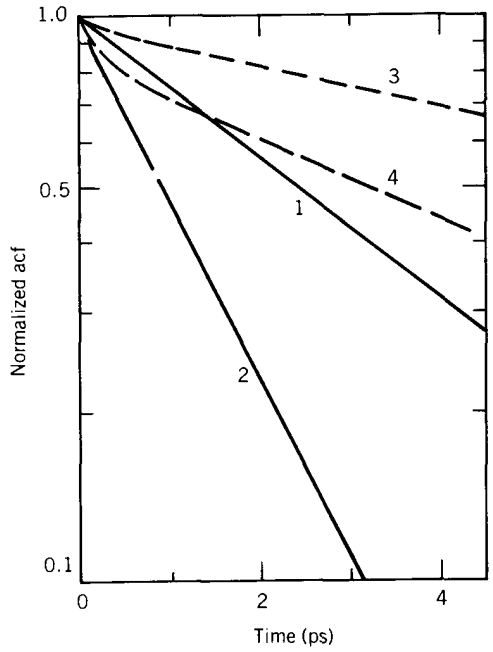

Figure 24. Comparison of neutron-scattering and simulation results. 1, P_1 autocorrelation function from neutron inelastic scattering in rotator phase I at 235 K; 2, as for 1, but P_2 autocorrelation function; 3, $P_1(\mathbf{e}_C)$, computer simulation; 4, $P_2(\mathbf{e}_C)$, computer simulation. [Reproduced by permission from M. W. Evans et al., *J. Chem. Soc., Faraday II*, **79**, 767 (1983).]

The rotator phases I and II of *t*-butyl chloride have been studied in depth with thermal neutron scattering.[149] In Fig. 24 we compare their first- and second-rank orientational correlation functions with those from the computer simulation by M. W. Evans.[137] The functions derived by neutron scattering decay far more quickly than the computer-simulated autocorrelation functions. The dielectric relaxation time of 7 ps at 283 K measured by Lassier and Brot is also longer than time derived from the area beneath the P_1 function obtained with neutron scattering. The discrepancy may partly be attributed to the slight persistence of rotation–translation interaction even into the rotator phases. The area beneath the P_1 function at 228 K agrees better (Table V) with the measured dielectric relaxation time (8.5 ps).

Finally, in Fig. 25 we compare the rotational velocity autocorrelation function computed at 228 K with the straight Fourier transform of the far-infrared spectrum of the rotator phase measured by Reid.[159] The simulated autocorrelation function decays, as in the liquid, faster than the measured cross-correlation function, although the shift in the time at which these

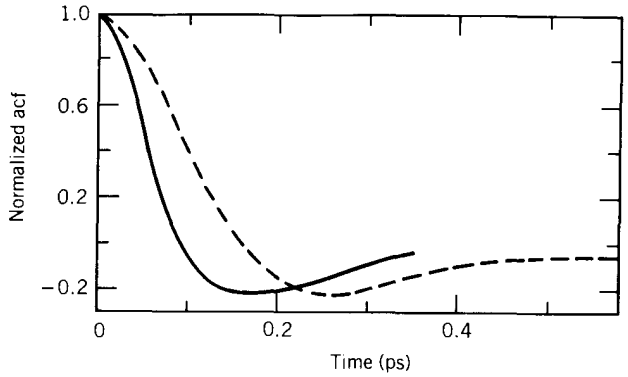

Figure 25. Comparison of far-infrared spectrum and computer simulation in the rotator phase. ----, $\langle \dot{\mathbf{e}}_C(t)\cdot\dot{\mathbf{e}}_C(0)\rangle\langle\dot{\mathbf{e}}_C^2(0)\rangle$, rotator phase at 228 K, computer simulation; — , Fourier transform of the far-infrared spectrum. [Reproduced by permission from M. W. Evans et al., *J. Chem. Soc., Faraday II*, **79**, 767 (1983).]

functions intersect the abscissa is the same in both experimental and theoretical cases: about 50%.

We conclude this section by emphasizing that the experimental techniques themselves do not provide us with a consistent view of the orientational dynamics of molecules of C_{3v} symmetry. A series of liquids have been considered, and it is established that we do obtain a more consistent view with use of the simulation data now becoming available. This is particularly so if we choose our molecules carefully. For example, in choosing *t*-butyl chloride, we were aware that the atom–atom and charge–charge parameters that were to be used in the simulation produce the correct enthalpy of transition for more than one phase change in *t*-butyl chloride. The thermodynamicist obviously has a major role to play in any future progress in this field. Methods like the ones we are now using to gain insights into the interaction of rotation with translation may be developed to gain similar insights into the interaction of other modes of motion with each other.

In general we must conclude that the results of the present literature search, and of the many years of experimentation and theoretical analysis that have enabled such a search, leave many of the questions raised in Section I unanswered for molecules of C_{3v} symmetry. Experimental spectra are not easily reduced to functions that may be compared with theory. Oversimplistic theories are used in the data-reduction processes, and the same theories are then used to interpret the "reduced" profiles. A concerted experimental effect, using in conjunction the technique of computer simulation and better reduction processes, is required if significant inroads into the molecular dynamics of such "simple" liquids are to be made.

VII. DICHLOROMETHANE

We now proceed to molecules of lower symmetry, in particular CH_2Cl_2. Acetone (C_{2v} symmetry) and ethyl chloride (C_1 symmetry) are considered in subsequent sections.

Dichloromethane is mechanically a near-prolate symmetrical top. Hence, there are infrared active vibrations with transition moment vectors parallel to any one of the axes of inertia. Spectroscopic studies on this molecule have already been reviewed.[162-164] It is relevant here to recall some pertinent facts.

There are nine infrared active vibrations in dichloromethane with transition moment vectors parallel to any one of the axes of inertia. By evaluating the bandshapes of different vibrational modes we should, in principle, be able to discern whether the motion is anisotropic and reflects the asymmetry of the moments of inertia, as in the gas phase, or if dipole–dipole interactions in the condensed state distort this rotational motion.

About 70 papers have been published on infrared studies of CH_2Cl_2 alone.[162] It has been made clear[165] for CH_2Cl_2 that it is not possible to factor the relevant autocorrelation functions into a vibrational autocorrelation function and a rotational autocorrelation function. However, this factorization has been done *a priori* in many papers and therefore the conclusions in these papers *are not* meaningful.

Generally, in choosing a set of axes for a molecule of arbitrary geometry, the principal axes of the rotational diffusion tensor are not related to those of the inertia tensor. However, the C_{2v} symmetry of CH_2Cl_2 ensures that these directions coincide and the molecule is consequently a favorable molecule for study. Inertial or molecular-shape considerations would predict symmetrical top behavior, but the complex nature of the intermolecular interactions arising from the effects of the dipole moment along the *b*-axis may invalidate such simple arguments. However, infrared evidence suggests that the angular motion is indeed axially symmetric.

Since the transition moment vector studied in the infrared is always parallel to only one of the inertial axes of the molecules, the rotational motion of each axis is studied by choosing an appropriate vibrational band. Figure 26 shows the motions of inertial axes *a*, *b*, and *c*. The correlation functions decay more slowly for motion around the larger axis of inertia. The rotational motion in the liquid is anisotropically about the same as the motion of freely rotating molecules, so that it appears that the forces that tend to twist the axis containing the dipole moment are not markedly different from those acting on the other two axes.

Brier and Perry[164] emphasize that the infrared and NMR data provide almost diametrically conflicting pictures of the anisotropy of the motion. In comparing these experimental results, care must be taken. Correlation times

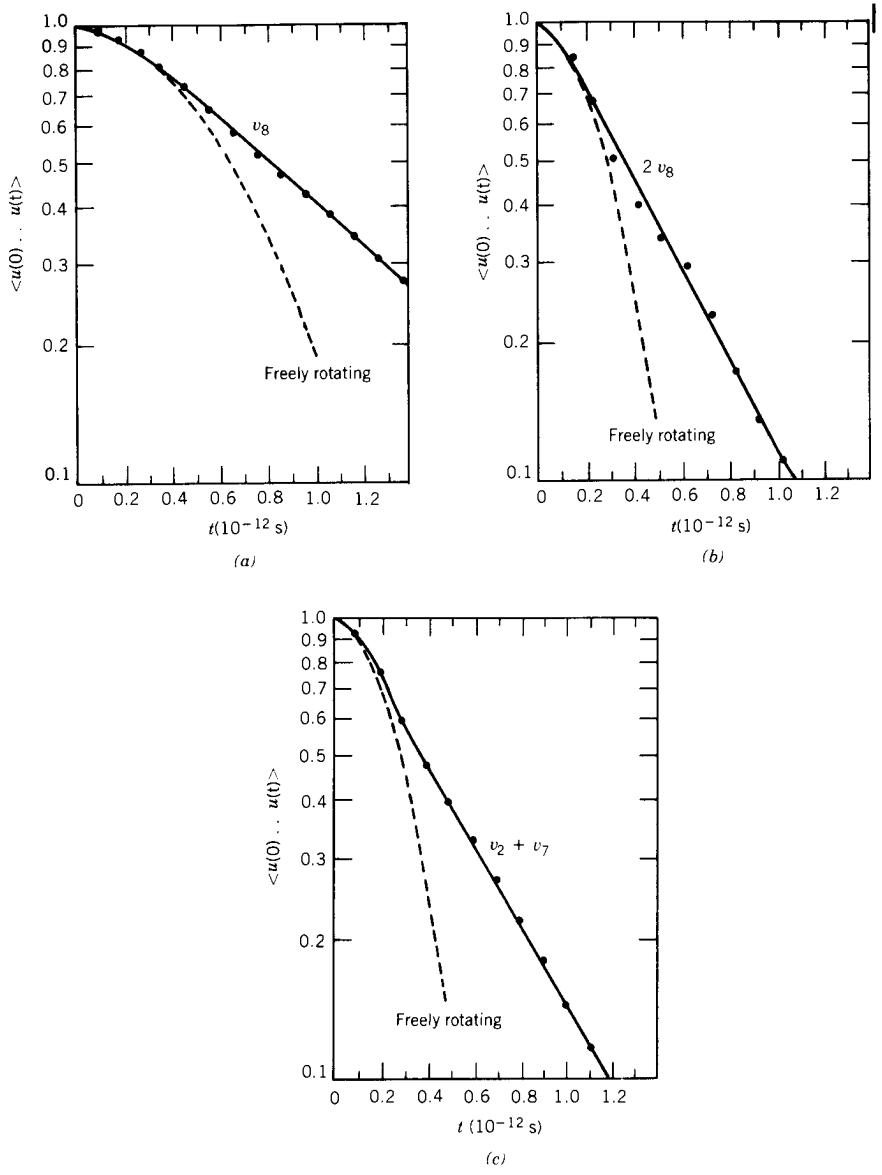

Figure 26. Correlation functions of the motions of inertial axes *A*, *B*, and *C* of the freely rotating and liquid-phase CH_2Cl_2 molecules. (*a*) Rotational motion of axis *A* (symmetry species B_2). (*b*) Rotational motion of axis *B* (symmetry species *A*). (*c*) Rotational motion of axis *C* (symmetry species B_1).

from the nuclear resonance experiment are calculated using a rotational diffusion model, so experimental spin–lattice relaxation times of the equivalent protons of CH_2Cl_2, extrapolated to zero proton concentration, can be equated with the rotational spin–lattice relaxation time of a *single* CH_2Cl_2 molecule in the liquid by means of *a simple expression*. For CH_2Cl_2 in CD_2Cl_2 solution, the relaxation time estimated in this way is 0.5 ps. The infrared experiment gives a correlation time of 1.1 ps. A discrepancy is evident, because if the rotational process is indeed Debye-like, the latter should be 3 times the former, which is clearly not the case.

For CH_2Cl_2 it is possible to look at the movements of the carbon, hydrogen, and chlorine atoms separately and to evaluate the anisotropy of the reorientational motion with NMR spectroscopy. The studies that are available typify the problems associated with intertechnique comparisons, which are more acute for CH_2Cl_2 than for the molecules of C_{3v} symmetry considered earlier.

O'Reilly et al.[166] measured the intramolecular ^1H, ^2H, and ^{35}Cl relaxation rates over a range of temperature. For orientation of the C—H vector, O'Reilly reports a correlation time of 0.64 ps, which compares well with Rothschild's[167] measurement of 0.66 ps for CH_2Cl_2 at various dilutions in CD_2Cl_2. Unfortunately, Rothschild's measurement was carried out at a temperature 11 K higher. Adjusting the two to the same temperature reveals a considerable discrepancy. In addition, we have to correct the two sets of correlation times to the same concentration, which increases the discrepancy further. It becomes clear that experimentalists should make more effort to collect their results at the same state points to aid such intercomparison.

In another investigation of the proton τ_1, Heatley[168] made measurements on ^{13}C satellites. His experiment gave $\tau_2(H) = 0.48 \pm 0.06$ ps at 308 K or 0.53 ps at 300 K. This value for $\tau_2(H)$ was a key result in Brier and Perry's discussion. If Heatley's measurements are analyzed using a zero contribution from spin–rotation relaxation ($1/\tau_1(S\text{–}R) = 0$), the correlation time $\tau_2(H)$ for the H—H vector is found to be 0.66 ps at 310 K, 0.73 ps at 300 K, in perfect agreement with the adjusted values of both O'Reilly and Rothschild.

On analyzing his value for $\tau_2(H)$ in terms of the small-step rotational diffusion model for a *symmetric top* (CH_2Cl_2 is in fact an inertial asymmetric top), Heatley observed that stochastic models for large angular steps are generally experimentally *indistinguishable* from small-step theory unless the angular steps are larger than 30°. In contrast to this analysis, O'Reilly et al. tried to interpret their NMR data in terms of models involving the idea that significant rotational motion occurs during the period in which a molecule is excited to an "interstitial site" in the "liquid lattice" by "hard" collisions. They assumed that during this time the anisotropy of the reorientational motion was determined entirely by the inertial properties of the molecule.

The model predicts a $\tau_2(^{13}C)/\tau_2(D)$ ratio for the C—H/C—D vector in CH_2Cl_2 and CD_2Cl_2 of 0.87, which compares favorably with the value of 0.88 ± 0.14 estimated experimentally. However, within experimental uncertainty, the measured ratio also agrees with the predictions of stochastic models for which the correlation times are independent of inertial changes produced bydeuteration.

Brier and Perry considered the anisotropy implied by the NMR results. Heatley's value of $\tau_2(H) = 0.53$ ps does not support the infrared result of axial symmetry, because $\tau_2(H\text{—}H) \neq \tau_2(C\text{—}H)$. Using a formula given by Woessner,[169] they found that no single set of values for the three adjustable parameters in the model would produce the NMR results (viz. $\tau_2(H\text{—}H) = 0.53$, $\tau_2(C\text{—}H) = 0.75$, and $\tau(C\text{—}Cl) = 1.2$ ps) simultaneously. The value for $\tau_2(H\text{—}H)$ is incompatible with the value of $\tau_2(C\text{—}H)$ in this model. Also, if the three variables of the model were fitted to experimental data, the "best fit" values of the $\ell = 2$ NMR data predicted an anisotropy completely different from that implied by the infrared data and the $\ell = 1$ NMR data. If these best-fit data are compared with available neutron-scattering results, they turn out to have only the most approximate validity. Brier and Perry analyzed four different dynamical models with the neutron-scattering data. They assumed that rotational and translational motions are decoupled. For the translational motions they considered only the Egelstaff–Schofield (E–S) modification of the simple diffusion model. Though this, in contrast to the simple Fick's law, gives the correct short-time behavior ($\approx t^2$), it predicts a velocity autocorrelation function that monotonically decreases to zero. This is *not* in accord with molecular-dynamics results, which show that the correlation function has a negative overshoot.

For rotational motion Brier and Perry considered four models. The first two were empirical, allowing for axial symmetry about the *a*-axis. No detailed physical interpretation of the reorientational dynamics or even an estimate of the degree of anisotropy of the motion can be obtained from such an empirical approach. They also considered the M and J diffusion models. The agreement for both was poor. Changing the one adjustable parameter of the models did little to improve the situation: It altered the magnitude but not the position of maximum absorption. Brier and Perry increased the anisotropy of the motion many times in an attempt to improve the agreement with experiment. However, the agreement was only slightly improved. This does not mean that neutron-scattering data are insensitive to the anisotropy of the motion. Rather, it indicates how insensitive the models used are to the anisotropy of the motion. Indeed, we have found similar results using our own 0 THz spectroscopy.[170]

Thus, from a literature search we conclude that the lack of any coordination in the research has resulted in a situation in which we are unable to state,

with any degree of certainty, the anisotropy of the molecular motion of CH_2Cl_2. There have been no spectroscopic studies on the liquid under applied external pressure. There appears to be a strong interaction of rotation with vibration that affects infrared and Raman studies to unknown degrees. Baranov[171] has established the predominant role of dipole–dipole interaction in his Raman study, and Nestor and Lippincott[172] have considered the effect of the internal field by comparing of gas- and liquid-phase spectra. They conclude that the cross section for each Raman band is greater for molecules in the liquid than in the gas because of strong internal-field effects. These effects should also distort Rayleigh and 0 THz band profiles.

We can see how changing this field affects the far-infrared spectrum dramatically by extending the spectroscopic work to supercooled and vitreous solutions. For example, if we study a glassy solution of CH_2Cl_2 in decalin, the low-frequency part of the loss curve exhibits a peak that shifts upward by about two decades with a 4 K increase in temperature and at the glass-to-liquid transition temperature moves very quickly out of the audiofrequency range toward the microwave. The far-infrared peak in the loss curve is displaced by 30 cm^{-1} to 90 cm^{-1} in the glass, as compared with 60 cm^{-1} in the liquid solution at room temperature, indicating that the molecular-dynamical evolution in CH_2Cl_2 in the glassy state starts on the picosecond time scale and evolves gradually into a process occurring on immensely longer time scales (seconds and much longer). The whole process should, in principle, be described by the orientational correlation function of the resultant dipole in the sample. This would require a molecular-dynamics simulation (on present-day computers) lasting approximately 10^9 years!

Brier and Perry conclude that "despite the numerous studies on CH_2Cl_2, no clear picture of the reorientational dynamics has yet emerged, even of a semi-quantitative nature." If we consider our own 0 THz studies,[162] a similar picture emerges. In particular, currently popular models of the liquid state give *poor* representations of the measured quantities. The far-infrared profile provides, even at ambient temperature and pressure, a highly discriminating test for all models, and has revealed the deficiencies of the currently popular molecular models, including Debye's, the extended diffusion models, models derived from the Kubo–Mori formalism, and even the models with more realistic physical interpretations—the itinerant oscillator and its various extensions. In addition to these theoretical problems (quoting Brier and Perry again) "there are limitations and assumptions involved in both the measurement and subsequent analysis of the data itself... and the available data may not be sufficiently varied and accurate to make a critical test of any model of the liquid dynamics."

Let us consider inferences from a molecular-dynamics simulation of this liquid. The molecular dynamics has been simulated with two model representations of the intermolecular potential. These consist of 3×3 and 5×5 atom–atom simulations with and without fractional charges at atomic sites. These empirical forms for the potential energy of two interacting CH_2Cl_2 molecules are used in the absence of a more acceptable quantitative expression. In the 3×3 representation the CH_2 group is taken as a moiety and is developed from an algorithm of Singer et al.[173] The core atom–atom interaction is Lennard-Jones in type, with the following parameters:

$$\sigma(\mathrm{Cl—Cl}) = 3.35\ \text{Å}$$
$$\sigma(\mathrm{CH_2—CH_2}) = 3.96\ \text{Å}$$
$$\varepsilon/k(\mathrm{Cl—Cl}) = 173.5\ \mathrm{K}$$
$$\varepsilon/k(\mathrm{CH_2—CH_2}) = 70.5\ \mathrm{K}$$

The $Cl—CH_2$ interaction is evaluated using the equations

$$\sigma(\mathrm{Cl—CH_2}) = \tfrac{1}{2}(\sigma(\mathrm{Cl—Cl}) + \sigma(\mathrm{CH_2—CH_2}))$$
$$\frac{\varepsilon}{k}(\mathrm{Cl—CH_2}) = \left(\frac{\varepsilon}{k}(\mathrm{Cl—Cl})\frac{\varepsilon}{k}(\mathrm{CH_2—CH_2})\right)^{1/2}$$

Partial charges are added to reproduce the total dipole of 1.6 D, so that the charge in the Cl unit is $-0.151|e|$ and that on the CH_2 units is $+0.302|e|$. The full potential (atom–atom + charges) was tested by McDonald[174] at 287 K (a molar volume of 62.92 $cm^3\ mol^{-1}$), and gave a mean potential energy of -6.2 kcal mol^{-1}, which compares with a measured value‡ of -6.2 to -6.3 kcal mol^{-1} estimated from experimental ΔH values of 6.69–6.83 kcal mol^{-1}. Approximately 0.5 kcal mol^{-1} has been allowed for the $\Delta(PV)$ term. From this indication it seems that the main features of the force field are correct. There are *no free parameters* in this 3×3 model.

The 5×5 simulation algorithm, originally written by Singer et al.,[173] has been modified by Ferrario and Evans[175] to include a charge–charge interaction and a force-cutoff criterion based on molecule center of mass-to-center of mass distance (cutoff radius = 11.28 Å). The Lennard-Jones parameters are:

$$\sigma(\mathrm{H—H}) = 2.75\ \text{Å}$$
$$\sigma(\mathrm{Cl—Cl}) = 3.35\ \text{Å}$$
$$\sigma(\mathrm{C—C}) = 3.2\ \text{Å}$$
$$\varepsilon/k(\mathrm{H—H}) = 13.4\ \mathrm{K}$$
$$\varepsilon/k(\mathrm{Cl—Cl}) = 175.0\ \mathrm{K}$$
$$\varepsilon/k(\mathrm{C—C}) = 51.0\ \mathrm{K}$$

‡For energy of vaporization see "selected values of chemical thermodynamic properties," 1961, p. 588. At 760 mm Hg, 313 K $\Delta H = 6.69$ kcal mol^{-1}; $\Delta S = 21.4$ cal $(mole\ K)^{-1}$.

TABLE VI
Experimental and Simulated Correlation times for Dichloromethane[a]

Technique	Vector	Correlation Time (ps)	
^{1}H (intra)	H—H ($\parallel$ to $\mathbf{e}_C$)	0.53 ± 0.06	
^{2}D (quadrupole)	C—D	0.80 ± 0.10	
^{13}C—H (dipolar)	C—H	0.70 ± 0.07	P_2
^{35}Cl (quadrupole relaxation)	C—Cl (approx. $\parallel \mathbf{e}_B$)	1.20 ± 1.10	
Computer simulation	$\mathbf{e}_A$	0.50	
Computer simulation	$\mathbf{e}_B$	0.9	
Computer simulation	$\mathbf{e}_C$	0.51	
Neutron scattering	Center of mass to H	0.56	
Dielectric	$\mathbf{e}_A$	1.45	
relaxation	$\mathbf{e}_A$	0.5	
Infrared (Rothschild)	$\mathbf{e}_B$	1.1	P_1
Infrared	$\mathbf{e}_A$	1.1	
(van Konynenberg and Steele)[15]	$\mathbf{e}_A$	1.2	
Computer simulation	$\mathbf{e}_B$	3.8	
Computer simulation	$\mathbf{e}_C$	1.21	
Rayleigh scattering (van Konynenberg and Steele)	$\mathbf{e}_A$	1.85	P_2

[a] Compiled by M. W. Evans, and reported in *J. Mol. Liq.*, **23**, 113 (1982). Reproduced by permission. See this paper for original data sources.

with fractional charges of $0.098|e|$ on H, $-0.109|e|$ on Cl, and $0.022|e|$ on C. The former were chosen to optimize the thermodynamic conditions and the latter from a molecular-orbital calculation by del Re (see ref. 176). Again there are no free parameters to be varied.

The 5×5 and 3×3 algorithms produce data that are directly comparable because the thermodynamic conditions are the same (293 K, 1 bar, $V_m = 64.0$ cm^3 mol^{-1}). Any difference in the resulting dynamical functions may therefore be attributed only to the difference in the pairwise-additive force fields used. Simulated and experimental correlation times are compared in Table VI.

We will consider briefly the results of the structural functions before considering the dynamics. Unlike chloroform (Section II), no diffraction results with which to compare the simulated distribution functions are available for CH_2Cl_2. However, it is of interest to compare the simulated distribution functions for the 5×5 algorithm with and without charges. Any differences

will reflect the sensitivity of the pdf structure to electrodynamic parts of the pair potential. If the pair distribution is structured, this implies that the liquid has a fair degree of residual ordering—local order. Based on the pair distribution function describing the H–H atom–atom positions (Fig. 27), it is by no means certain that the structure may be attributed solely to repulsive parts of the intermolecular potential (as in RISM theory) because the addition of charges clearly inhibits the first peak at about 2.8 Å while enhancing the second.

For the dynamics, experimental results are available with which to make comparisons. We are also now able to establish which of the two models (the 3×3 or 5×5) best approximates the true intermolecular potential. For example, far-infrared spectra are most discriminating. The simulated and experimental results are compared in Fig. 28. The 5×5 is obviously the most realistic potential, since the 3×3 produces a result that both is too sharp and peaks at too low a frequency. The profile in fact resembles very closely the result we anticipate for the extended diffusion models, which are unable to shift the far-infrared profile from the free rotor maximum. The 5×5, though better, produces a profile still displaced some 30–40 cm^{-1} from the measured spectrum for the neat liquid. Either the potential is still an oversimplification or other factors (induced absorption, cross correlations, etc.) contribute significantly to the far-infrared profile. Whichever of these is the case, Fig. 28 shows just how discriminating a test 0 THz spectra provide for any model of the liquid state.

We referred above to contributions from cross correlation (i.e., the mutual dependence of the motion of one molecule on that of its immediate neighbors). Such correlations are anticipated to be removed (gradually) on dilution—providing the solvent is noninteracting. Certainly, if CH_2Cl_2 is dissolved in CCl_4 or decalin, the far-infrared peak frequency shifts gradually to a lower frequency. It is interesting that the simulated spectrum for a 10% solution of CH_2Cl_2 in CCl_4 reproduces well the measured spectrum (Fig. 28*b*). It is debatable whether such a comparison is meaningful, because the simulation involves a neat solution of the liquid in which the "probe" molecule is surrounded by similar and not solvent molecules. Also, at a concentration of 10% CH_2Cl_2 in CCl_4 the far-infrared spectrum is still in the process of shifting to lower frequencies. The plot of $\bar{\nu}_{max}$ versus concentration (Fig. 29) shows a linear dependence in the concentration range from neat solution to 10%, the shift continuing below 10%. It may even emerge that the shift *does not* remain linear below 10%, as for CH_3CN (Section IV), if and when the necessary experimentation is done. So the simulated function, though agreeing well with the spectrum for a 10% solution, must in fact peak at higher frequencies than does the measured spectrum of, say, a 1% solution.

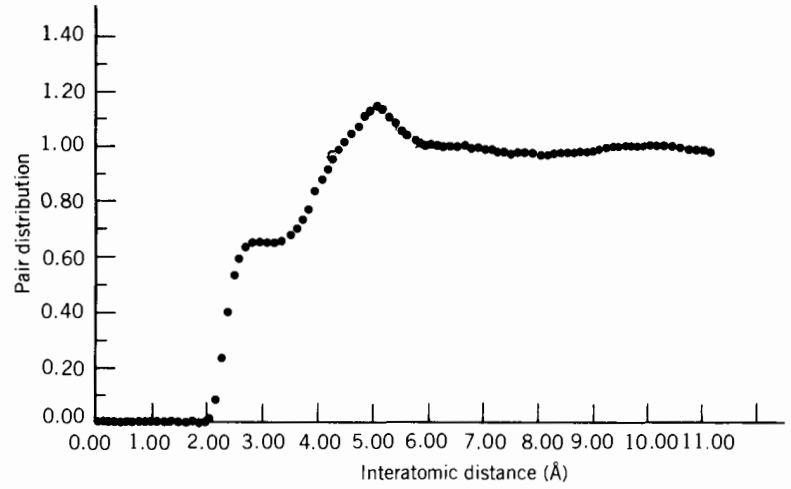

(a)

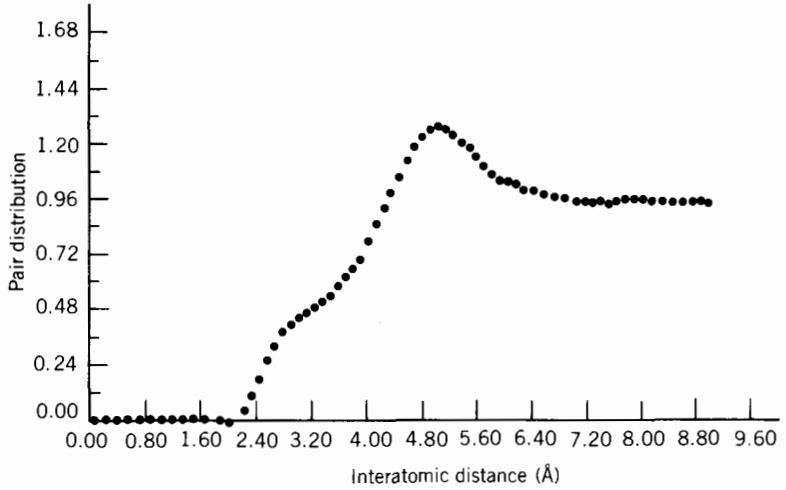

(b)

Figure 27. (*a*) Hydrogen-to-hydrogen atom–atom pair distribution function extracted as a mean over the equilibrium run. 5×5 potential, no charges, 293 K, 1 bar. (*b*) Same as *a*, but with charges included. [Reproduced by permission from M. W. Evans and M. Ferrario, *Adv. Mol. Rel. Int. Proc.*, **24**, 75 (1982).]

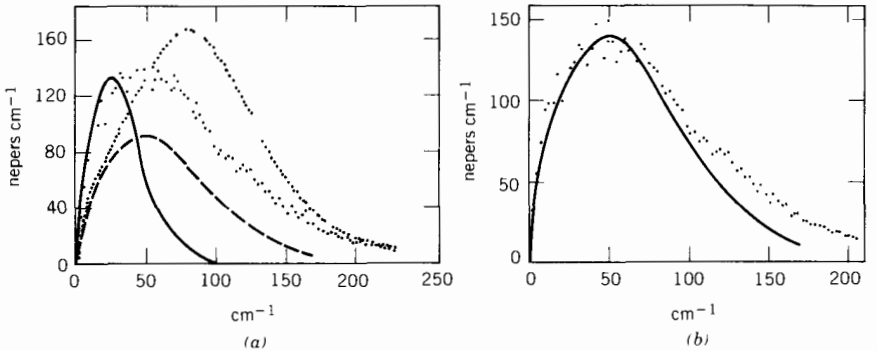

Figure 28. (*a*) Comparison of molecular-dynamics simulation and far-infrared spectra of CH_2Cl_2 and solution in CCl_4. O, —O—, □, measured data, G. J. Evans and M. W. Evans; ●, computer simulation, 5×5 potential, no charges; —, computer simulation, 3×3 potential, no charges; ---, 10% solution in CCl_4, experimental. (*b*) —, Scaled-up spectrum of CH_2Cl_2 in CCl_4; · · · · ·, simulation of same. [Reproduced by permission from M. W. Evans and M. Ferrario, *Adv. Mol. Rel. Int. Proc.*, **24**, 75 (1982).]

The discrepancy is not easily explained. However, we may at least conclude that since the 5×5 is a better representation than the 3×3 simulation, the *hydrogen atoms play an important part in the dynamics of* CH_2Cl_2. This is a surprising result and emphasizes to the exponents of molecular and hydrodynamic theories the need to represent the shape of the molecules carefully in their modeling procedures and also to account for the smallest atoms

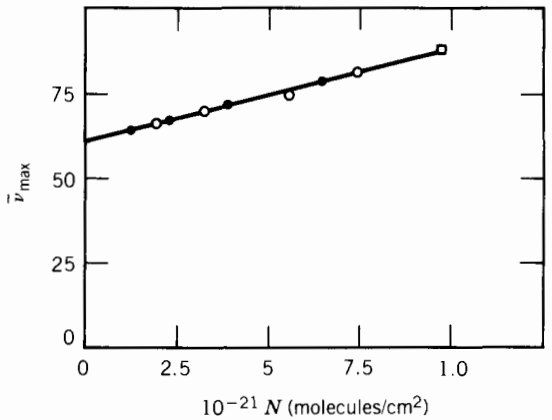

Figure 29. Variation of peak frequency $\bar{\nu}_{max}$ with concentration for CH_2Cl_2 in CCl_4 (○) and decalin (●). [Reproduced by permission from M. W. Evans and M. Ferrario, *Adv. Mol. Rel. Int. Proc.*, **24**, 75 (1982).]

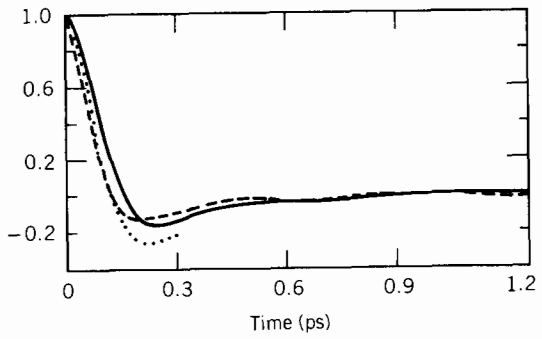

Figure 30. Rotational velocity autocorrelation functions (of $\dot{\mathbf{e}}_A(t)$): — , 3×3 potential, no charges; ---, 5×5 potential, no charges; · · · · ·, for 10% (volume/volume) CH_2Cl_2 in CCl_4. [Reproduced by permission from M. W. Evans and M. Ferrario, *Adv. Mol. Rel. Int. Proc.*, **24**, 75 (1982).]

of the molecule. The extensive use of spheres, needles, and the like to represent molecules, and the complete neglect of molecules (as in the hydrodynamic theories), are obvious oversimplifications.

It is also revealing to compare actual correlation functions. Those of $\langle \mathbf{e}_A(t) \cdot \mathbf{e}_A(0) \rangle$, for example, are shown in Fig. 30. The experimental curve is in fact deeper and slightly more oscillatory than both the 3×3 and 5×5 simulated functions. We emphasize that it is difficult to Fourier transform from time to frequency domains because of the observable long-time tails (Fig. 31). The angular momentum autocorrelation function has a small but long positive tail, and the rotational velocity autocorrelation function a correspondingly long negative tail.

When charges are incorporated into the algorithms, the effect on the equilibrium time correlation functions is not pronounced but is nevertheless significant. This indicates that the dynamics of the liquid are only approximately describable in terms of Lennard-Jones parameters. A full description requires the inclusion of electrodynamic terms. The inclusion of charge–charge interaction modifies the P_1 and P_2 correlation functions. The far-infrared spectrum, for example, is shifted to higher frequency. Consequently, the P_1 and P_2 correlation times are increased; in particular, the microwave and NMR relaxation times are increased by the long-range terms of this nature, often to a significant degree. Figures 32 and 33 show the effect of including charges using the 3×3 potential—the algorithm is still not capable of reproducing the observed spectra. The effect of adding charges to the 5×5 simulation is illustrated in Figs. 34–36. The far-infrared spectrum is shifted slightly to higher frequencies (Fig. 37), but is still below the measured spectrum, which peaks at $> 80\ cm^{-1}$.

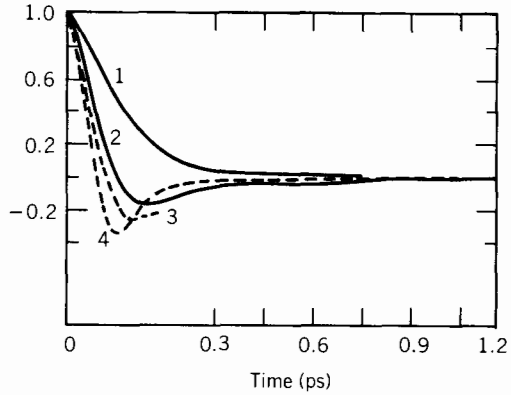

Figure 31. Comparison of (1) angular momentum autocorrelation function with (2) the autocorrelation function of $\dot{\mathbf{e}}_A(t)$ and (3) and (4) the rotational velocity autocorrelation functions from data for CH_2Cl_2 in solution and in the pure liquid state, respectively. Normalized to 1 at $t = 0.3$ × 3 potential, no charges. [Reproduced by permission from M. W. Evans and M. Ferrario, *Adv. Mol. Rel. Int. Proc.*, **24**, 75 (1982).]

It is interesting to observe how the effect of rototranslational interaction changes as we move from molecules of C_{3v} symmetry to those of lower symmetry. Up to nine elements of the mixed autocorrelation function matrices (discussed elsewhere in this volume) are observable, depending on the molecular symmetry. As we have already emphasized, it is a truism that the outcome of every experiment on liquid-state molecular motion is the observation of rototranslation in a time-averaged form. Even though it is an orientational function that we may measure how these functions evolve in a system in which rotation and translation motions interact to varying degrees.

For CH_2Cl_2, of the nine cross elements already referred to, only two exist by symmetry in the molecule-frame autocorrelation function of the *linear*

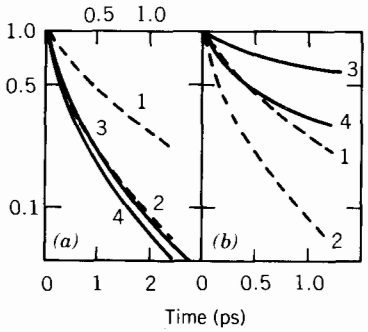

Figure 32. (*a*) 1 and 2, P_1 and P_2 autocorrelation functions 3×3 potential including charges (upper abscissa); 3 and 4, P_1 and P_2 autocorrelation functions of $\mathbf{e}_A$, 3×3 potential, no charges (lower abscissa). Both at 293 K, 1 bar. (*b*) 1 and 2, as for *a*; 3 and 4, 3×3 potential including charges at 177 K, 1 bar. [Reproduced by permission from M. W. Evans and M. Ferrario, *Adv. Mol. Rel. Int. Proc.*, **24**, 75 (1982).]

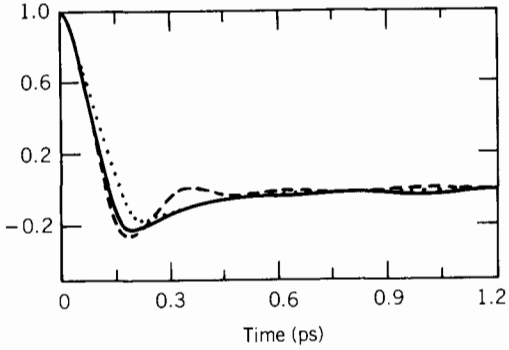

Figure 33. Rotational velocity autocorrelation functions of $\dot{\mathbf{e}}_A(t)$: — , 3×3, including rges, at 293 K, 1 bar; ----, 3×3, including charges, at 177 K, 1 bar; · · · · ·, 3×3, no charges, 293 K, 1 bar. [Reproduced by permission from M. W. Evans and M. Ferrario, *Adv. Mol. . Int. Proc.*, **24**, 75 (1982).]

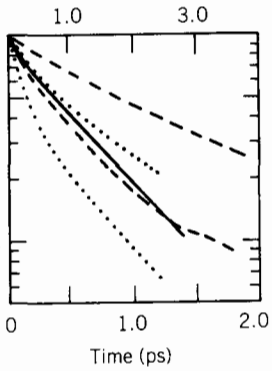

Figure 34. — , P_1 autocorrelation function of $\mathbf{e}_A$, 5 ×5 no charges, 293 K, 1 bar (upper abscissa); ---, P_1 and P_2 autocorrelation functions of $\mathbf{e}_A$, 5×5, including charges, 293 K, 1 bar (lower abscissa); · · · · ·, P_1 and P_2 autocorrelation functions of $\mathbf{e}_A$, 3×3, including charges, 293 K, 1 bar (lower abscissa). [Reproduced by permission from M. W. Evans and M. Ferrario, *Adv. Mol. Rel. Int. Proc.*, **24**, 75 (1982).]

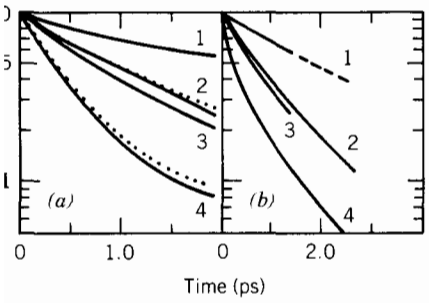

Figure 35. (*a*) Anisotropy of rotational diffusion: 5×5 potential, including charges, 293 K, 1 bar. 1, P_1 autocorrelation function of $\mathbf{e}_B$: 2, P_1 autocorrelation function of $\mathbf{e}_A$ and (●) of $\mathbf{e}_C$; 3, P_2 autocorrelation function of $\mathbf{e}_B$; 4, P_2 autocorrelation function of $\mathbf{e}_B$ and (●) of $\mathbf{e}_C$. (*b*) As for *a*, but no charges. Note that P_1 and P_2 of $\mathbf{e}_C$ are not shown for clarity, as they are similar to P_1 and P_2 of $\mathbf{e}_A$. [Reproduced by permission from M. W. Evans and M. Ferrario, *Adv. Mol. Rel. Int. Proc.*, **24**, 75 (1982).]

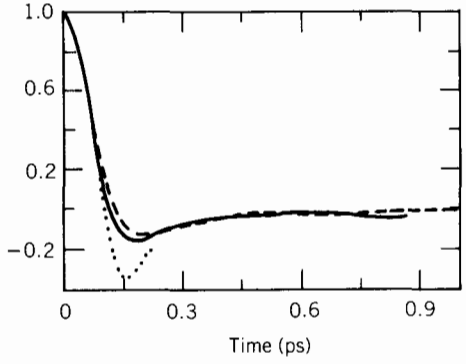

Figure 36. Rotational velocity autocorrelation functions (of $\mathbf{e}_A(t)$): ---, 5×5, no charges, 293 K, 1 bar; — , 5×5, with charges, 293 K, 1 bar; · · · ·, computed from far-infrared data on pure liquid CH_2Cl_2. [Reproduced by permission from M. W. Evans and M. Ferrario, *Adv. Mol. Rel. Int. Proc.*, **24**, 75 (1982).]

center of mass momentum **p** with the resultant molecular *angular* momentum **J** at the instant t in time. The mixed laboratory-frame autocorrelation function $\langle \mathbf{p}(0)\cdot\mathbf{J}(t)\rangle_{\text{lab.}}$ vanishes for all t in an *isotropic* molecular liquid because the parity of **p** to time reversal is opposite in sign to that of **J**. We wish to emphasize that these cross interactions and their extent of influence on the molecular dynamics are not in any sense critically dependent on the

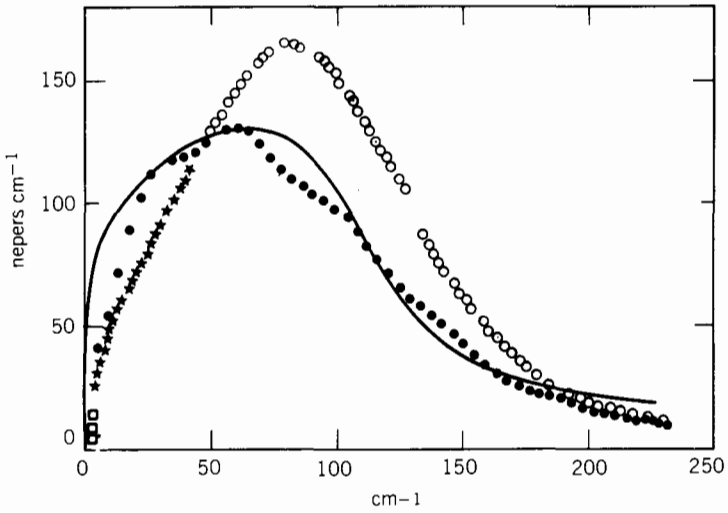

Figure 37. Far-infrared spectrum of dichloromethane from 5×5 simulation with charges. ●, simulation; □, —O—, O, experimental (neat solution); — , experimental (10% solution in CCl_4). [Reproduced by permission from M. W. Evans and M. Ferrario, *Adv. Mol. Rel. Int. Proc.*, **24**, 75 (1982).]

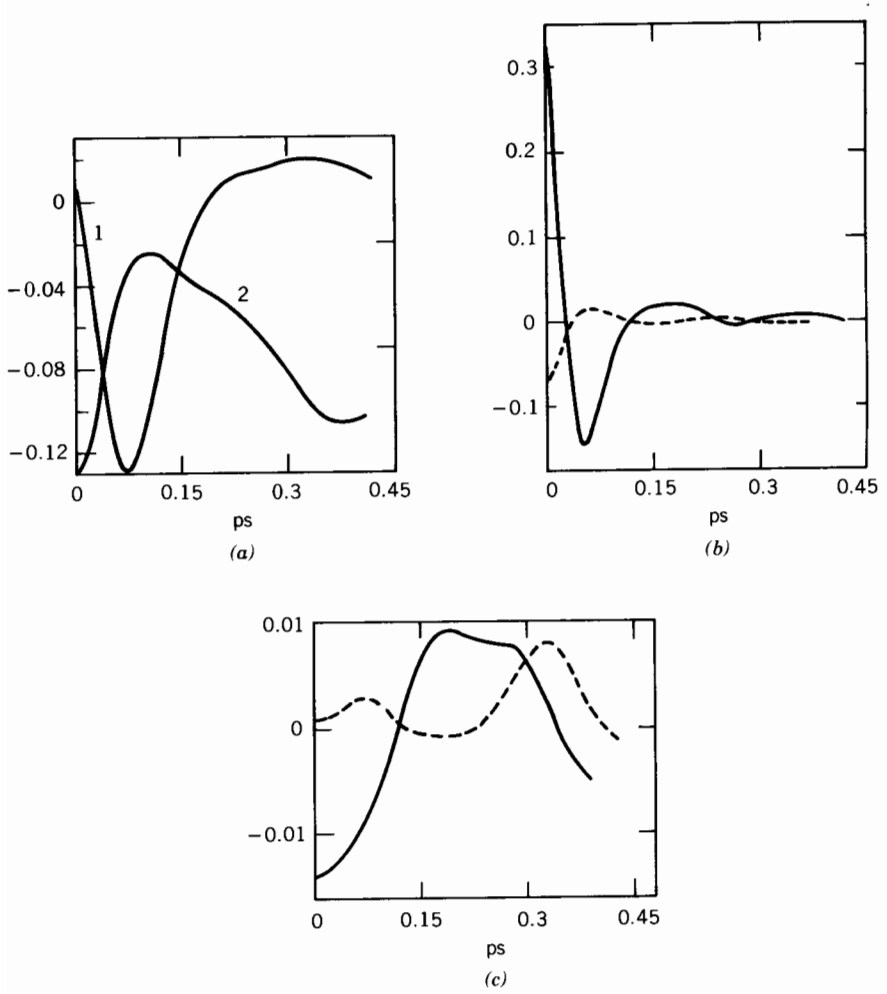

Figure 38. (*a*) The nonvanishing elements of the molecule-frame correlation matrix $\langle \mathbf{p}(0)\mathbf{J}^T(t)\rangle_{\text{mol}}$. 1, $[\langle p_1(0)J_2(t)\rangle + \langle p_1(t)J_2(0)\rangle]_{\text{mol}}/2\langle p_1^2\rangle^{1/2}\langle J_2^2\rangle^{1/2}$ (left-hand scale); 2, $[\langle p_2(0)J_1(t)\rangle + \langle p_2(t)J_1(0)\rangle]_{\text{mol}}/2\langle p_2^2\rangle^{1/2}\langle J_1^2\rangle^{1/2}$ (right-hand scale). (*b*) —, (1,2) element of the molecule-frame force–torque mixed autocorrelation function, normalized as in *a*; ---, (2,1) element. (*c*) Illustration of the noise level in *a* and *b*. —, (3,2) element of the linear–angular momentum correlation matrix; ---, (2,2) element. Both of these autocorrelation functions should vanish by symmetry. [Reproduced by permission from M. W. Evans and M. Ferrario, *Adv. Mol. Rel. Int. Proc.*, **24**, 75 (1982).]

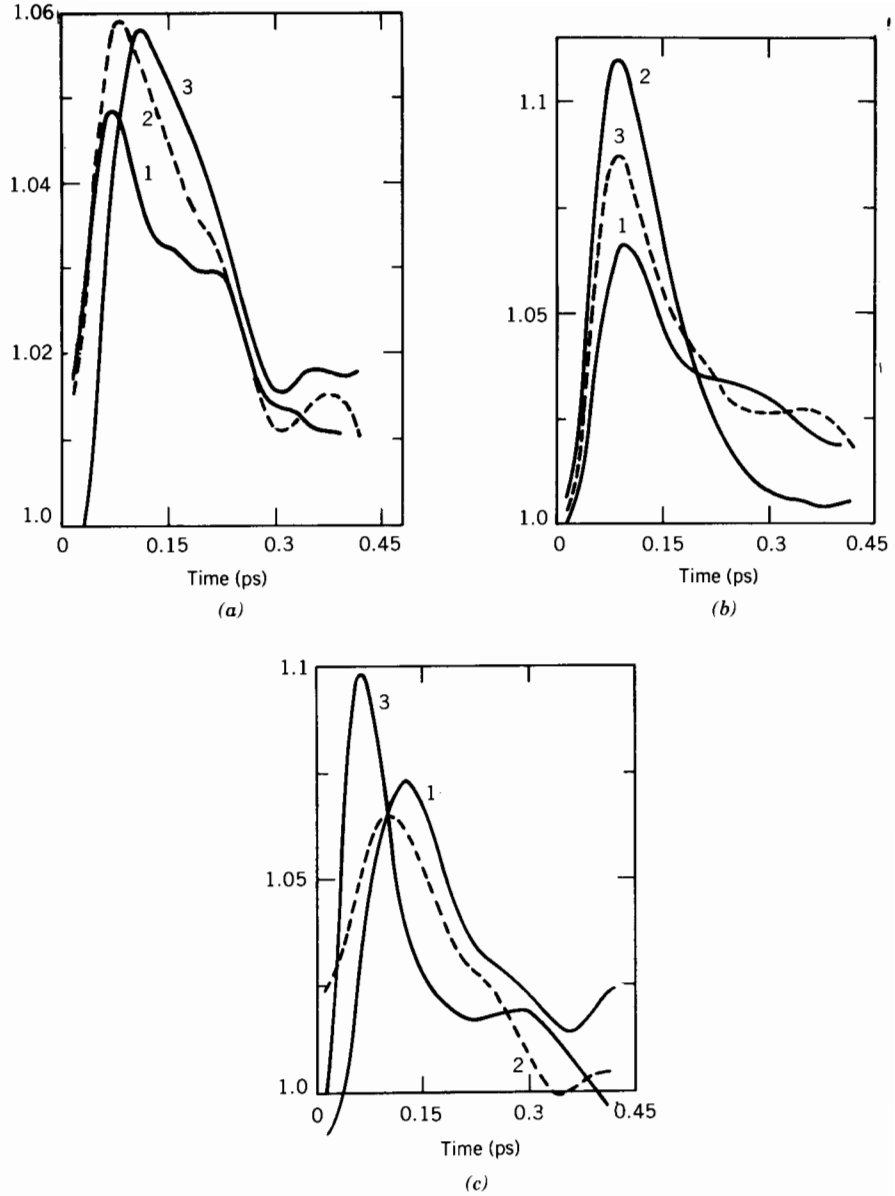

Figure 39. Second-moment autocorrelation functions of linear–angular momentum. These are invariant to frame transformation and *do not* vanish in the laboratory frame. (*a*) 1, $[\langle p_3^2(0)J_2^2(t)\rangle + \langle p_3^2(t)J_2^2(0)\rangle]/[2\langle p_3^2\rangle\langle J_2^2\rangle]$; 2, (2,2) element; 3, (2,3) element. (*b*) 1, (2,1) element; 2, (1,3) element; 3, (3,1) element. (*c*) 1, (1,1) element; 2, (3,3) element; 3, (1,2) element. [Reproduced by permission from M. W. Evans and M. Ferrario, *Adv. Mol. Rel. Int. Proc.*, **24**, 75 (1982).]

simulation model, so long as that model has elements of realism (i.e., reflects the known C_{2v} symmetry in some sense).

Figure 38 shows that the (2,1) and (1,2) elements of the cross matrix *are not* symmetric for either the linear–angular momentum or force–torque mixed autocorrelation functions ("auto" because they refer to the rotation and translation of the *same* molecule).

The second-moment autocorrelation functions $\langle p^2(0)J^2(t)\rangle$ and $\langle F^2(0)T_q^2(t)\rangle$ are invariant to frame transformation and may be observed in the laboratory frame. All elements (i, j) exist. These functions are illustrated in Figs. 39 and 40 and provide a detailed description of molecular rototranslation. Obviously the rototranslation coupling perturbation in CH_2Cl_2, one of the most extensively studied molecules of C_{2v} symmetry, is pronounced.

Rototranslational equations have no known analytical solutions. The phenomenological theories, as developed by Debye and his contemporaries and extended by many others in ensuing years, consider rotational motion of (in the case of Debye) spherical entities. Rototranslation leads to a morass of supermatrices with too many adjustable coefficients to be useful.

The influence of rototranslation is not straightforwardly related to the molecular symmetry because the sizes of the atoms making up a molecule are also significant. It appears that a full understanding of liquid-state dynamics requires starting at the level of the atoms or even of the constituents of the atoms themselves.

VIII. ACETONE [M. W. EVANS AND G. J. EVANS, *J. CHEM. SOC., FARADAY II*, 79, 153 (1983).]

Many of the spectroscopic techniques available molecular motion by bandshape transformation have been applied to liquid acetone. Koga et al.[177] used infrared bandshape analysis to study the anisotropy of rotational diffusion through three correlation times, τ_A, τ_B, and τ_C, defined about the three inertial axes A, B, and C. In nondipolar solvents, the ratio $\tau_A : \tau_B : \tau_C$ does not vary much from solvent to solvent. Reorientation about the B-axis is more restricted. In dipolar solvents the correlation times are longer, especially τ_B. The Favro[178] model of rotational diffusion produces the result $\tau_A : \tau_B : \tau_C = 1.02 : 1.00 : 0.88$, in contrast to the observed (except in CS_2) $1.3 : 1 : 1.1$. Using van der Waals radii the excluded volumes about each axis are $V_A = 55.1$ Å^3, $V_B = 44.4$ Å^3, and $V_C = 48.5$ Å^3, which does not explain the order of the three correlation times. Koga et al. observe that only motions about the A- and C-axes are restricted by dipole–dipole interactions.

The paper of Dill et al.[179] on the Rayleigh scattered bandshape of liquid acetone under hydrostatic pressure is one of the most interesting in the literature on any isotropic liquid. These authors have provided angular-position

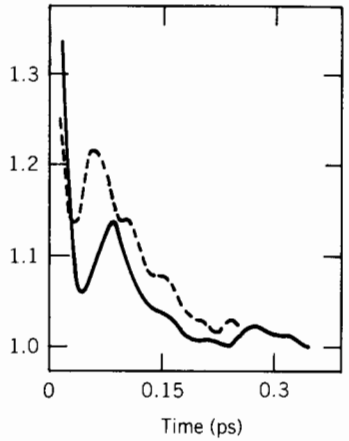

Figure 40. Two elements of the mixed force–torque molecule-frame autocorrelation function matrix: —, (1,1) element; ----, (2,2) element. [Reproduced by permission from M. W. Evans and M. Ferrario, *Adv. Mol. Rel. Int. Proc.*, **24**, 75 (1982).]

correlation functions and angular-velocity correlation functions for liquid acetone at 1 bar, 293 K. Dill et al. compare their light-scattering data with the NMR relaxation results on liquid acetone of Jonas and Bull,[180] who estimated a translational correlation time $\langle\tau_t\rangle_{NMR}$ a rotational correlation time $\langle\tau_2\rangle_{NMR}$, and their density dependence. The NMR data in acetone show that $\langle\tau_t\rangle_{NMR}$ has the same density dependence as the viscosity, η, but that $\langle\tau_2\rangle_{NMR}$ and the Rayleigh-scattering correlation time are much less density dependent than $\langle\tau_t\rangle_{NMR}$. To a good approximation $\langle\tau_2\rangle_{NMR} = \langle\tau_2\rangle_{\text{light scattering}}$. This can be interpreted in two ways: Either two components of the diffusion tensor are equal, or the light-scattering correlation time is related to a mixture of the same two.

Schindler et al.[181] have reported a Raman study of pressure effects in liquid acetone. The Raman bandshape of the symmetric C=0 stretch at 1710 cm^{-1} was measured up to 4 kbar over a wide range of temperature. They conclude that intermolecular dipole–dipole coupling is responsible for unusual effects as the hydrostatic pressure is increased. The frequencies of the polarized (VV) and depolarized (VH) bands in acetone differ by several wavenumbers. These authors point out that hydrodynamic theories usually consider repulsive forces as the main source of line broadening, but in reality the increase or decrease of half-width (and frequency) with pressure depends on the relative importance of attractive and repulsive intermolecular forces that influence a specific vibration. Schindler et al. expected that repulsive forces play a minor role in acetone compared with the attractive forces. However, their interpretation was based on the *simple* Kubo stochastic bandshape theory containing one parameter τ_m, defined as the modulation time. Oxtoby et al.[182] have equated this parameter to the duration of a colli-

sion; Döge[183] and Wang,[184] to the rotational correlation time; and Lynden-Bell,[185] to the correlation time governing translational diffusion. Schindler et al. defined it as the correlation time for frequency fluctuations in their calculations.

Perrot et al.[186] have studied liquid acetone using depolarized Rayleigh scattering. The function $\omega^2 I(\omega)$ (the second moment) peaks at 64.5 cm^{-1}, with a half-width of 92 cm^{-1}. This may be compared with the far-infrared spectrum for a 10% (volume/volume) in decalin solution of Reid and Evans,[187] in which the peak absorption is at 52 cm^{-1}. The integrated absorption intensity (A) of the $\alpha(\omega)$ in the far infrared is linearly dependent on the number density (N) of acetone solute molecules in nondipolar solvents such as decalin. This seems to imply the absence or insignificance of induced effects, but to confirm this the dilution studies should be extended to well below 10% (see the review by Vij and Hufnagel in this volume).

Electrooptic techniques have been used to study acetone. Burnham and Gierke[188] have used results from the optical Kerr effect, Cotton–Mouton effect, and light scattering to obtain orientational pair correlation functions from the theory of Laudanyi and Keyes.[189] They also estimated orientational pair correlation parameters for liquid acetone. The values range from 0.5 (Kerr effect) to 1.4 (anisotropic Rayleigh scattering), which values yield contradictory implications concerning the local structure.

A contradiction is observed in dielectric studies. At 293 K the relaxation time of pure liquid acetone is 3.1 ± 0.1 ps, which decreases to 2.5 ± 0.3 ps at 317 K. In 0.19 (mole fraction) CCl_4 solution, the relaxation time decreases slightly to 2.9 ± 0.3 ps at 293 K. The effect of dilution is small, which agrees with far-infrared observation. However, in dilute CCl_4 the three correlation times calculated by Koga et al.[177] are $\tau_A = 1.29$ ps, $\tau_B = 1.01$ ps, and $\tau_C = 1.11$ ps. These contrast with the dielectric relaxation time of acetone in CCl_4 of 2.9 ± 0.3 ps.

Jonas and Bull[180] have calculated a reorientational spin–spin NMR correlation for acetone of 0.75 ps at 290 K, 1 bar, which increases to 1 ps at 296 K, 2 kbar. The translational correlation times under the same conditions are 4.8 and 11.0 ps, respectively, showing that these times are more dependent on density. In deriving these times, Jonas and Bull again made use of rotational diffusion theory with the assumption of isotropic diffusion. This theory implies that the mean first-rank correlation time should be 3 times the mean second-rank correlation time. Comparing the dielectric relaxation time in the same liquid (3.1 ± 0.1 ps) with the NMR spin–spin time (0.75 ps) shows this to be approximately the case. However, such a comparison is not meaningful, because the measurements of Koga et al. and Dill et al. clearly show that the theory of rotational diffusion does not explain the molecular-dynamical properties in liquid acetone.

We may also compare depolarized Rayleigh correlation times with Raman and NMR correlation times. Dill et al.[179] report that the Rayleigh and NMR correlation times for pure liquid acetone are the same at 1 bar and 2 kbar. This result contrasts markedly with that of the equivalent "first rank" procedure, for which we have seen already that the dielectric relaxation time is 4 times the infrared correlation time at 293 K and 1 bar in dilute CCl_4 solution. The Raman correlation times of Schindler et al.[181] are 0.27 ps for pure liquid acetone at 1 bar and 298 K, and 0.55 ps at 2 kbar and 298 K. These are considerably shorter than those from spin–spin NMR and depolarized Rayleigh scattering and seem to have little significance in terms of rotational dynamics, except that they are considerably more dependent on density. We have already commented on the interpretation of the correlation times measured by Schindler et al. It seems certain that they cannot be translational in origin, because the NMR results yield translational correlation times of 4.8 ps at 296 K and 1 bar and 11 ps at 2 kbar. These are an order of magnitude longer than the corresponding Raman correlation times of Schindler et al., but interestingly, have a similar density dependence. They are too short to be purely rotational in origin.

There is inconsistency in the literature on acetone, as indeed there has been for all the liquids we have considered in this review. No overall viewpoint concerning the molecular dynamics of liquid acetone is obtained from the many studies reported. In such circumstances a computer simulation study must contribute to our understanding of the liquid-state dynamics; it will certainly again clarify, for example, the anisotropy of the rotational diffusion. In this respect, the picosecond laser-induced inhomogeneous broadening of Raman bands reported by George et al.[190] has clearly shown that rotovibrational diffusion in liquid acetone is anisotropic.

In the simulation the interaction between $(CH_3)_2CO$ molecules is modeled with a 4×4 Lennard-Jones atom–atom "core" with point charges localized at each site. The CH_3 group is taken as an entity (an oversimplification —see Section VII for CH_2Cl_2, which revealed the significance of the hydrogen atoms in determining the molecular dynamics) and the complete set of parameters is as follows:

$$\sigma(CH_3—CH_3) = 3.92 \text{ Å}$$
$$\sigma(C—C) = 3.00 \text{ Å}$$
$$\sigma(O—O) = 2.80 \text{ Å}$$
$$\varepsilon/k(CH_3—CH_3) = 72.0 \text{ K}$$
$$\varepsilon/k(C—C) = 50 \text{ K}$$
$$\varepsilon/k(O—O) = 58.4 \text{ K}$$

The cross terms were evaluated by Lorentz–Berthelot combining rules. The $-CH_2$ parameters were taken from a paper by Bellemans et al.[191] on the molecular-dynamics simulation of *n*-alkanes, the O—O parameters from molecular crystal data, and the C–C parameters from our previous work on CH_2Cl_2, $CHCl_3$, and $CHBr_3$. We adhere to our method of using literature values without adjustment so that future comparisons with more precise algorithms may be made.

We represent electrostatic interactions with point charges taken from a calculation by Wellington and Khouwaiter.[192] These are $q_{CH_3} = -0.032|e|$, $q_C = 0.566|e|$, and $q_O = -0.502|e|$. The three principal moments of inertia used in the computer-simulation program were calculated from structural data. These are $I_A = 71.2 \times 10^{-40}$ g cm^2, $I_B = 83.0 \times 10^{-40}$ g cm^2, and $I_C = 154.2 \times 10^{-40}$ g cm^2. The dipole axis in this notation is that of I_B and the dipole unit vector is $\mathbf{e}_B$.

TABLE VII
Experimental and Simulated Correlation Times for Acetone[a]

Technique	Experimental correlation time (ps)	Simulated autocorrelation time (ps)[b] (293 K, 1 bar)
Dielectric relaxation		
(i) pure acetone	(i) 3.1 ± 0.1	$\tau_{1A} = 3.2$, $\tau_{1B} = 2.2$, $\tau_{1C} = 2.2$
(ii) 20% (mole fraction in CCl_4	(ii) 2.9 ± 0.3	
Infrared bandshapes in dilute solution	$\tau_{1A} = 1.29$, $\tau_{1B} = 1.01$, $\tau_{1C} = 1.11$	$\tau_{1A} = 3.2$, $\tau_{1B} = 3.3$, $\tau_{1C} = 2.2$
Spin–spin NMR, rotational correlation time	0.75	$\tau_{2A} = 0.75$, $\tau_{2B} = 0.6$, $\tau_{2C} = 0.6$
NMR translational	4.80	$\tau_t \approx 1.0$
Raman, C=O stretch	0.27	$\tau_{2B} = 0.6$
Rayleigh scattering	0.75	$\tau_{2A} = 0.75$, $\tau_{2B} = 0.6$, $\tau_{2C} = 0.6$
	Frequency maximum/cm^{-1}	
Far-infrared power absorption		
(i) pure acetone (this work)	(i) 57	
(ii) 10% acetone in decalin	(ii) 52	
Rayleigh scattering	64.5	

[a] Compiled by M. W. Evans and reported in *J. Chem. Soc., Faraday II*, **79**, 153 (1983); reproduced by permission. See this paper for original data sources.

[b] The dipole unit vector is $\mathbf{e}_B$.

Computed and experimental correlation times are compared in Table VII. The simulated infrared rotational correlation time τ_B is 2.2 ps, which is compared with the infrared and dielectric relaxation measurements in the table. Note that the dielectric relaxation time is a weighted mean of the three simulated correlation times about the three principal moment-of-inertia axes. The experimentally measured dielectric relaxation time is longer than the simulated times. This conforms with the pattern that emerged in our discussions of other liquids in the preceding sections.

The anisotropy of the rotational diffusion in acetone from infrared bandshape analysis suggested a ratio $\tau_A : \tau_B : \tau_C$ of 1.3 : 1 : 1.1, which compares

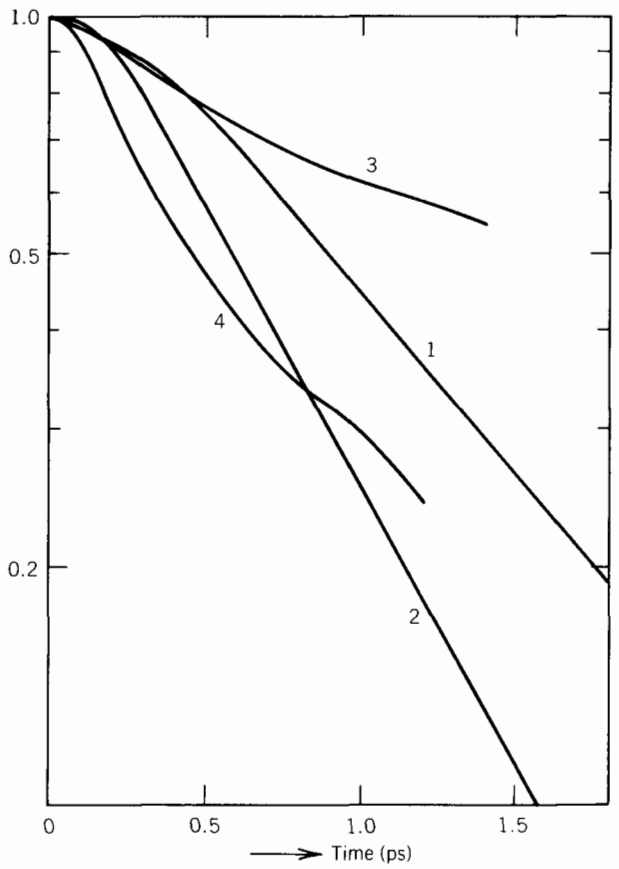

Figure 41. First-rank orientational autocorrelation functions $P_1(\mathbf{e}_B)$. 1, Acetone in acetonitrile, infrared bandshape analysis; 2, as for 1, but in *n*-hexane; 3, computer simulation; 4, as for 3, but second-rank orientational autocorrelation function $P_2(\mathbf{e}_B)$. [Reproduced by permission from M. W. Evans et al., *J. Chem. Soc., Faraday II*, **79**, 153 (1983).]

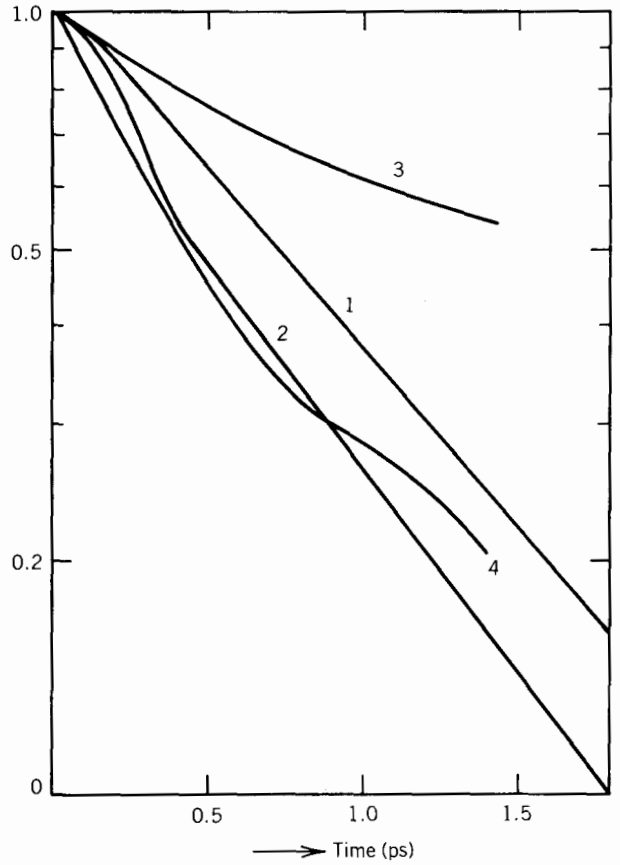

Figure 42. As for Fig. 41, but for the unit vector $\mathbf{e}_C$. 1, infrared bandshape analysis, acetone in CCl_4; 2, as for 1, but in cyclohexane; 3, computer simulation; 4, second-rank orientational autocorrelation function $P_2(\mathbf{e}_C)$. [Reproduced by permission from M. W. Evans et al., *J. Chem. Soc., Faraday II*, **79**, 153 (1983).]

favorably with that of 1.5 : 1 : 1 from the simulation. Figure 41 compares the simulated dipole autocorrelation function $\langle \mathbf{e}_B(t) \cdot \mathbf{e}_B(0) \rangle$ with the results of Koga et al.[177] in acetonitrile and *n*-hexane, which exhibited the extremes of molecular motion for the solvents they considered. The simulated result decays more slowly than either of the experimental functions. We also show the P_2 function $\frac{1}{2}\langle 3\mathbf{e}_B(t) \cdot \mathbf{e}_B(0)^2 - 1) \rangle$ for comparison. Figure 42 is the same as Fig. 41 except that it is for the $\mathbf{e}_C$ vector autocorrelation function. The experimental results refer to carbon tetrachloride and cyclohexane, and again results for other solvents fall between these two extremes. The simulated function also decays more slowly for this vector.

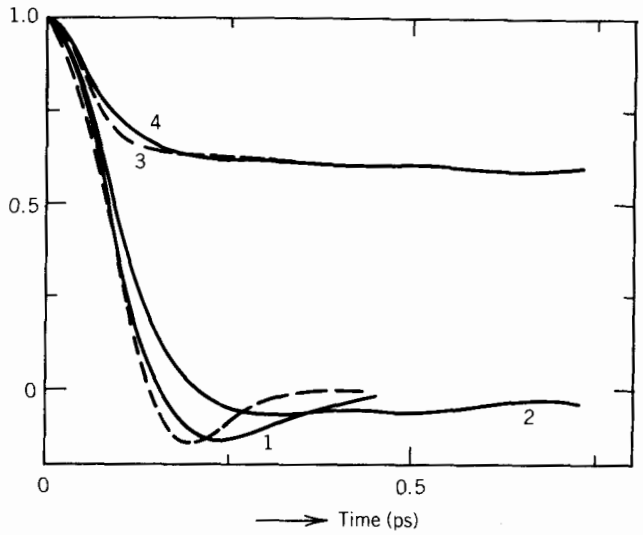

Figure 43. ---, Angular-velocity correlation function from depolarized Rayleigh scattering; 1, simulated angular-velocity autocorrelation function; 2, simulated angular-momentum autocorrelation function; 3, simulated second-moment angular-velocity autocorrelation function, $\langle \boldsymbol{\omega}(t) \cdot \boldsymbol{\omega}(t) \boldsymbol{\omega}(0) \cdot \boldsymbol{\omega}(0) \rangle / \langle \omega^4(0) \rangle$; 4, simulated second-moment angular-momentum autocorrelation function, $\langle \mathbf{J}(t) \cdot \mathbf{J}(t) \mathbf{J}(0) \cdot \mathbf{J}(0) \rangle / \langle J^4(0) \rangle$. [Reproduced by permission from M. W. Evans et al., *J. Chem. Soc., Faraday II*, **79**, 153 (1983).]

In Fig. 43 we compare the simulated function with the angular-velocity correlation function from the depolarized Rayleigh wing of acetone as measured by Dill et al.[179] Note that the angular-velocity and angular-momentum autocorrelation functions *do not* have the same time dependence in an asymmetric top. Up to 0.1 ps the experimental and simulated functions decay similarly; thereafter the experimental function decays faster than the simulated one. The simulated second-moment autocorrelation functions, also shown in the figure, are transiently non-Gaussian, but go to the correct Gaussian limit of ca. 0.6.

In Fig. 44 we compare simulated results with the Fourier transforms of the far-infrared spectra of pure liquid acetone and acetone in 10% (volume/volume) decalin. The experimental functions decay more quickly. The shapes of the functions show the characteristic long negative tails. However, the far-infrared bandshapes and simulated bandshapes are similar when scaled, so that contributions such as induced absorption and internal-field effects, if they do exist, appear to have time dependences similar to that of the pure rotational functions.

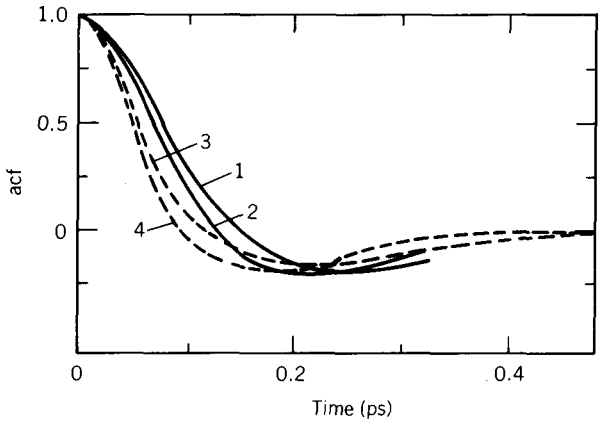

Figure 44. 1, Computer-simulated rotational-velocity autocorrelation function of the dipole unit vector, $\langle \dot{\mathbf{e}}_B(t)\cdot\dot{\mathbf{e}}_B(0)\rangle/\langle \dot{e}_B^2(0)\rangle$; 2, same as 1, but $\langle \dot{\mathbf{e}}_C(t)\cdot\dot{\mathbf{e}}_C(0)\rangle/\langle \dot{e}_C^2(0)\rangle$; 3, Fourier transform of the far-infrared power coefficient of a 10% solution of acetone in decalin; 4, Fourier transform of the far-infrared band of pure liquid acetone. [Reproduced by permission from M. W. Evans et al., *J. Chem. Soc., Faraday II*, **79**, 153 (1983).]

There are other inconsistencies in the table. The most serious is represented by the translational correlation time from NMR spectroscopy by Jonas and Bull,[180] 4.80 ps. The simulated laboratory-frame velocity autocorrelation function is not exponential, as this function is assumed to be by Jonas and Bull. We also observed this in $CHBr_3$ (Section V), for which the NMR correlation time measured by Sandhu was far longer than the computer-simulated center-of-mass velocity correlation time. This may be due to definition. In the extreme narrowing limit, the translational NMR correlation time is sometimes quoted in the literature as τ_t, defined as

$$\tau_t = \frac{ma}{12kT\tau_v}$$

where m is the molecular mass and a the radius. Using $a = 2.0$ Å and our simulated τ_v of ca. 0.08 ps, we obtain $\tau_t = 1.0$ ps, which is still significantly shorter than that measured. We should remember that the center-of-mass velocity autocorrelation function is oscillatory, with a long negative tail and positive longer time tail decaying as $t^{-3/2}$. The NMR data-reduction process, however, assumes a Stokes's law behavior, implying that the autocorrelation function is an exponential with, of course, a finite correlation time.

Another inconsistency is that the Raman C=O stretch band, after data reduction, produces a correlation time of 0.27 ps, which compares with a simulated τ_B value of 0.6 ps and a spin–spin NMR rotational correlation

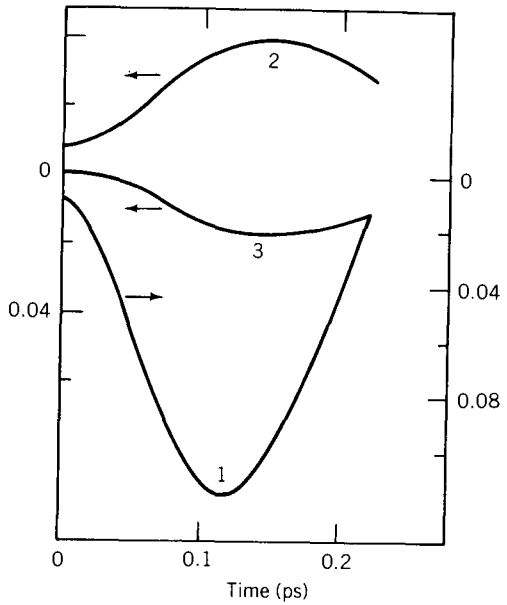

Figure 45. Elements of the rototranslational matrix: 1, $[\langle v_C(0)J_A(t)\rangle + \langle v_C(t)J_A(0)\rangle]/(\langle v_C^2\rangle^{1/2}\langle J_A^2\rangle^{1/2})$; 2, as for 1, but (A,C) element; 3, as for 1, but (B,A) element. All other elements vanish for all t. [Reproduced by permission from M. W. Evans et al., *J. Chem. Soc., Faraday II*, **79**, 153 (1983).]

time of 0.75 ps. The Raman correlation time is already too short because of the data-reduction process. It is more realistic to take the correlation time as the inverse half-width of the band, carefully decoupling rotational and vibrational effects (though this is by no means a trivial matter).

If we use our simulation to give details of the interaction of rotation with translation for this molecule of C_{2v} symmetry, the (1,2), (2,1), and (3,1) elements are nonvanishing (Fig. 45). Our moving frame is defined as that of the principal moments of inertia, so that $(1,2) \equiv (A,C)$, $(2,1) \equiv (C,A)$, and $(3,1) \equiv (B,A)$. We remark that the elements are not symmetric with respect to each other (e.g., $(A,C) \neq (C,A)$, $(B,A) \neq (A,B)$). In the simulations discussed earlier for the molecules of C_{3v} symmetry, the (A,C) and (C,A) elements were symmetric.

The existence of a phase change in $CHBr_3$ (liquid to rotator-phase solid) was dependent on the fact that the (A,B) and (B,A) elements were very small (i.e., that rotation was almost wholly decoupled from translation). In acetonitrile, which is also of C_{3v} symmetry, the same normalized elements were an order of magnitude larger, peaking at ± 0.21 in amplitude. In acetone and CH_2Cl_2, the (C,A) elements peak at -0.11 and -0.12, respectively. CH_3CN, CH_2Cl_2, and acetone, of course, do not form rotator phases be-

e of this pronounced coupling. In the next section, we consider a mole-
of yet lower symmetry in which the rotation–translation interaction is
ı increased significantly.

IX. ETHYL CHLORIDE

thyl chloride [M. W. Evans, *J. Chem. Soc., Faraday II*, **79**, 719 (1983)]
example of a low-symmetry (asymmetric) top with a dipole moment that
not lie on an axis of the principal-moment-of-inertia frame. At 1 bar
iquid boils at 285 K. For either or both of these reasons, the liquid has
been investigated in any depth for details of its molecular dynamics.
lowever, ethyl chloride is a favorable molecule for study because the sec-
virial coefficient of gaseous ethyl chloride is known, suggesting that there
tle or no association or dimerization. The existence of this coefficient can
plicate spectral profiles considerably, as we have seen. In ethyl chloride
molecular interactions are probably dominated by Lennard–Jones-type
ılsion and dispersion, and not by strong electrodynamic and polarizabil-
ffects. It is interesting that unlike molecules of C_{3v} symmetry, which *may*
ı rotator phases, the liquids of molecules of lower symmetry can often
itrified, and the liquid supercooled. That is, translational motions may
tinue when rotational motion is considerably hindered. We recall that in
rotator phase the reverse is true—translational freedom is constrained
molecules are often confined to solid lattice sites), yet rotational free-
ı remains. In molecules of C_{3v} symmetry the rotation–translation cou-
g is small. Our computer simulation will indicate the importance of this
raction as a prerequisite for the formation of a glass phase.
When glassy C_2H_5Cl is heated, an endothermic process begins at a tem-
ature T_v at which the glass softens. The glass is transformed into a super-
led liquid by the appearance of free volume (holes). At a temperature T_r
supercooled liquid recrystallizes. It would be interesting to try to follow
of this in a computer simulation—to see just how this complex liquid- to
d-state phase transition is controlled by features of the molecular dy-
nics. We consider, in other sections of this volume, the significant role of
T coupling in determining details of the melting process in optically ac-
liquids. This coupling may cause individual enantiomers to remain liquid
ı temperature at which an equimolar racemic mixture is a solid, or vice
sa. It appears to depend on the nature of the *intra* cross-rototranslation
trix and the signs of individual elements of this matrix. This phenome-
ı illustrates how mathematical laws may account for features of real
sical systems in one of the most subtle ways the authors have encoun-
d. Certainly it seems to be established that the melting process is con-
lled almost entirely by the molecular symmetry properties and sizes of the

atoms of the molecule, which in turn determine the molecular dynamics of the condensed phase itself.

If for the present we return to ethyl chloride, X-ray powder spectra indicate that there is no crystallization below T_r. Infrared spectra prove that in the glassy and supercooled-liquid states the same rotational isomers coexist as may be observed in the liquid state above the melting point—only the *trans* isomer exists. NMR spectra show that between T_v and T_r a dynamic reorientation of the different segments of the hydrocarbon chain occurs that ceases in the crystal. The existence of an intense dielectric absorption between T_v and T_r confirms the reorientation of the polar group CH_2X, which reorientation is related to the appearance of "holes" in the lattice.

The total electric polarization of C_2H_5Cl has been measured in the gaseous state by Barnes et al.[193] at various temperatures, and the density and complex permittivity have been measured over the liquid range by McMullen et al.[194] The density ranges from 0.9214 g cm^{-3} at 273 K to 1.1281 g cm^{-3} in the supercooled liquid at 118.3 K. In the solid at 112.9 K the density increases to 1.139 g cm^{-3}. The dielectric loss above 203 K is small up to 8 MHz, but at lower temperatures the loss process begins to appear at the highest frequencies and increases with decreasing temperature until freezing.

Neutron-scattering spectroscopy has been used[195] to observe the C–C–Cl deformation and CH_3 torsional modes of ethyl chloride in the liquid and solid states, and the torsional frequency of the methyl group internal rotation, which is assigned at 278 cm^{-1}.

The potential between two ethyl chloride molecules is represented in the simulation by a 5×5 site–site model of atom–atom Lennard-Jones interactions with partial charges localized on the atom sites. The partial charges were obtained from a paper by Mark and Sutton,[196] who estimated a dipole of 1.86 D from values of $q_{CH_3} = 0.0465$, $q_C = -0.0502$, $q_H = 0.0808$, and $q_{Cl} = -0.157$ in units of $|e|$. These values compare with the previous set derived by del Re using a linear combination of atomic orbitals: $q_{CH_3} = 0.040$, $q_C = 0.001$, $q_H = 0.068$, and $q_{Cl} = -0.177$. The Lennard-Jones parameters are

$$\varepsilon/k(\text{Cl—Cl}) = 127.9\ \text{K}$$
$$\sigma(\text{Cl—Cl}) = 3.6\ \text{Å}$$
$$\varepsilon/k(\text{C—C}) = 35.8\ \text{K}$$
$$\sigma(\text{C—C}) = 3.4\ \text{Å}$$
$$\varepsilon/k(\text{CH}_3\text{—CH}_3) = 158.6\ \text{K}$$
$$\sigma(\text{CH}_3\text{—CH}_3) = 4.0\ \text{Å}$$
$$\varepsilon/k(\text{H—H}) = 10.0\ \text{K}$$
$$\sigma(\text{H—H}) = 2.8\ \text{Å}$$

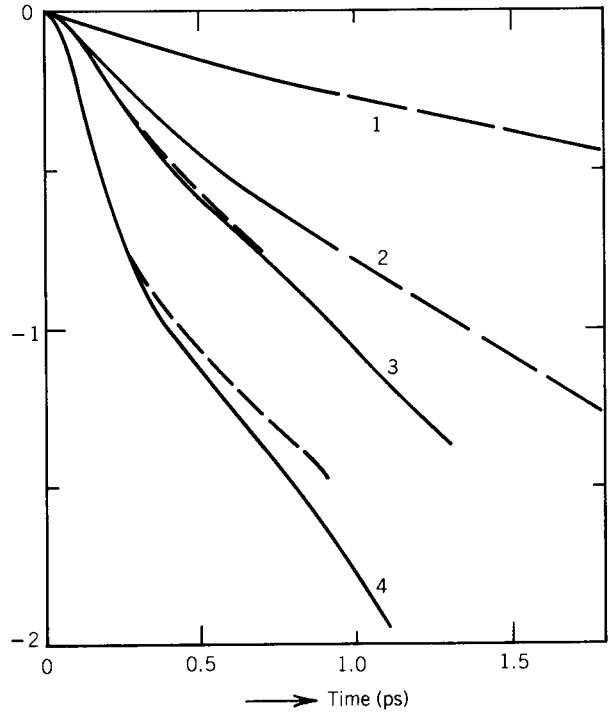

Figure 46. Orientational autocorrelation functions at 293 K; first- (P_1) and second- (P_2) rank Legendre polynomials. 1, $P_1(\mathbf{e}_3)$; 2, $P_2(\mathbf{e}_3)$; 3, $P_1(\mathbf{e}_1)$ (---, $P_1(\mathbf{e}_2)$); 4, $P_2(\mathbf{e}_1)$ (---, $P_2(\mathbf{e}_2)$). [Reproduced by permission from M. W. Evans, *J. Chem. Soc., Faraday II*, **79**, 719 (1983).]

Simulations were carried out at room temperature and, by simulating sudden drops in the temperature, also in the supercooled or vitreous states. The room-temperature liquid was simulated at 293 K, d (density) = 0.8978 g cm^{-3}; the supercooled liquid at 118 K, d = 1.1281 g cm^{-3}. The liquid boils at 285 K, 1 bar, so that the simulated liquid state at 293 K is under slightly more than an atmosphere of its vapor pressure.

The only available literature relaxation time for liquid ethyl chloride is the NMR spin–spin time of Miller and Gordon.[197] The derived second-rank orientational correlation time is 0.7 ± 0.1 ps. It is not clear to which vector this refers; consequently there are no acceptable data available with which to compare our simulated results.

The first- (P_1) and second- (P_2) rank orientational autocorrelation functions of the three unit vectors $\mathbf{e}_1$, $\mathbf{e}_2$, and $\mathbf{e}_3$ are illustrated in Fig. 46. These unit vectors are in the three axes of the principal moment-of-inertia frame. There is a simple relationship between the unit vector $\mathbf{u} = \boldsymbol{\mu}/|\boldsymbol{\mu}|$ (the dipole

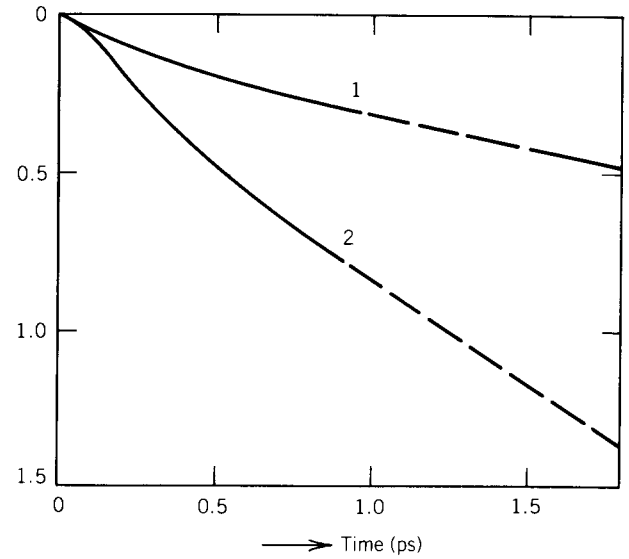

Figure 47. As for Fig. 46. 1, $P_1(\mathbf{u})$; 2, $P_2(\mathbf{u})$, where $\mathbf{u}$ is the dipole unit vector. [Reproduced by permission from M. W. Evans, *J. Chem. Soc., Faraday II*, **79**, 719 (1983).]

unit vector) and $\mathbf{e}_1$ and $\mathbf{e}_3$. This takes the form

$$\mathbf{u} = x\mathbf{e}_1 + y\mathbf{e}_3$$

where x and y are numbers, if we assume that $\mathbf{u}$ lies in the C—Cl bond. So it is straightforward to compute the first- and second-rank orientational autocorrelation functions of $\mathbf{u}$ (Fig. 47). Neglecting cross correlations and other contributions, the Fourier transform of $P_1(\mathbf{u})$ is a measure of the dielectric loss spectrum, and that of $\langle \dot{\mathbf{u}}(t) \cdot \dot{\mathbf{u}}(0) \rangle / \langle \dot{\mathbf{u}}(0) \cdot \dot{\mathbf{u}}(0) \rangle$ is the far-infrared spectrum. $P_2(\mathbf{u})$ can be obtained from the Raman spectrum or from the depolarized Rayleigh spectrum. All simulated functions are now available for comparison with future experimental results.

Simulation results show that the anisotropy of the rotational diffusion in the moment-of-inertia frame is very large—a result that NMR spectroscopy should be able to reproduce. The "tumbling" of the ethyl chloride molecule (reorientation of the $\mathbf{e}_3$ axis) is slower than its spinning (reorientation of either the $\mathbf{e}_1$ or $\mathbf{e}_2$ axes). The spinning motion is "inertia dominated"; that is, the P_1 and P_2 autocorrelation functions of $\mathbf{e}_1$ or $\mathbf{e}_2$ are not exponential initially, but become so after about 0.7 ps. The $P_1(\mathbf{e}_3)$ and $P_2(\mathbf{e}_3)$ functions, on the other hand, become exponential after the autocorrelation function has dropped only to about 80% of its initial value. The motion of $\mathbf{u}$, and conse-

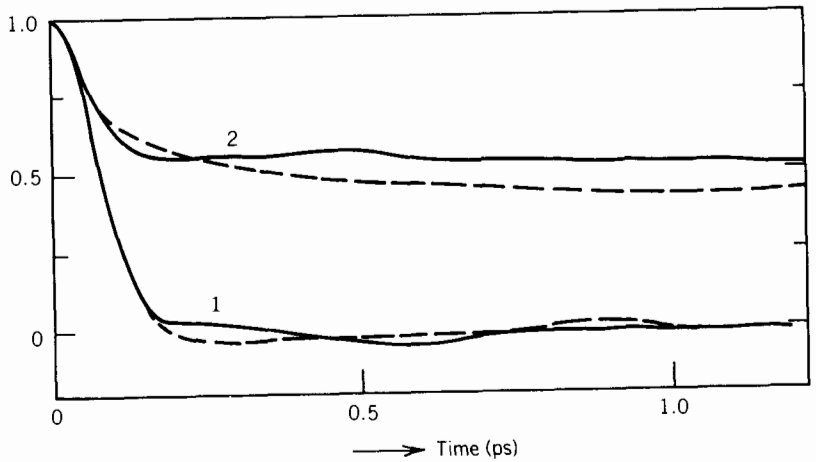

Figure 48. —, Angular-velocity autocorrelation function at 293 K, $\langle \boldsymbol{\omega}(t)\cdot\boldsymbol{\omega}(0)\rangle/\langle\omega^2\rangle$: 1, $(\boldsymbol{\omega}(t)\cdot\boldsymbol{\omega}(t)\boldsymbol{\omega}(0)\cdot\boldsymbol{\omega}(0))/\langle\omega^4\rangle$; 2, $\langle\boldsymbol{\omega}(t)\cdot\boldsymbol{\omega}(0)\rangle/\langle\omega^2\rangle$. ---, Angular-momentum autocorrelation function: 1 and 2 as above. [Reproduced by permission from M. W. Evans, *J. Chem. Soc., Faraday II*, **79**, 719 (1983).]

quently the experimentally measured functions, reflects a combination of tumbling and spinning in ethyl chloride, as is the case for most asymmetric tops of C_{2v} symmetry.

The angular-velocity and angular-momentum autocorrelation functions (Fig. 48) do not decay in the same way, as is true for molecules of any symmetry lower than T_d. In Fig. 48 the second-moment autocorrelation functions are also shown. These decay to a constant level depending on the nature of the equilibrium statistics. They attain a Gaussian limit as $t \to \infty$, but are transiently non-Gaussian. The same is true for the linear center-of-mass velocity autocorrelation function and its second moment. Both linear- and angular-velocity autocorrelation functions have the characteristic long negative tail at intermediate time, as discussed in the last section for acetone.

It is interesting to observe that rotation–translation interaction is larger in this molecular liquid than in any other liquid we have simulated. There are four finite elements of the autocorrelation matrix $\langle \mathbf{v}(t)\mathbf{J}^T(0)\rangle$ for $t > 0$. They are illustrated in Fig. 49. The (1,2) and (2,1) elements are mirror images and greater in intensity than the (3,2) and (2,3) elements. The significance of the rotation–translation interaction may be attributed to the fact that the relatively heavy Cl atom is so close to the center of mass. It is not possible for the molecule to rotate without simultaneously translating a good deal, and vice versa.

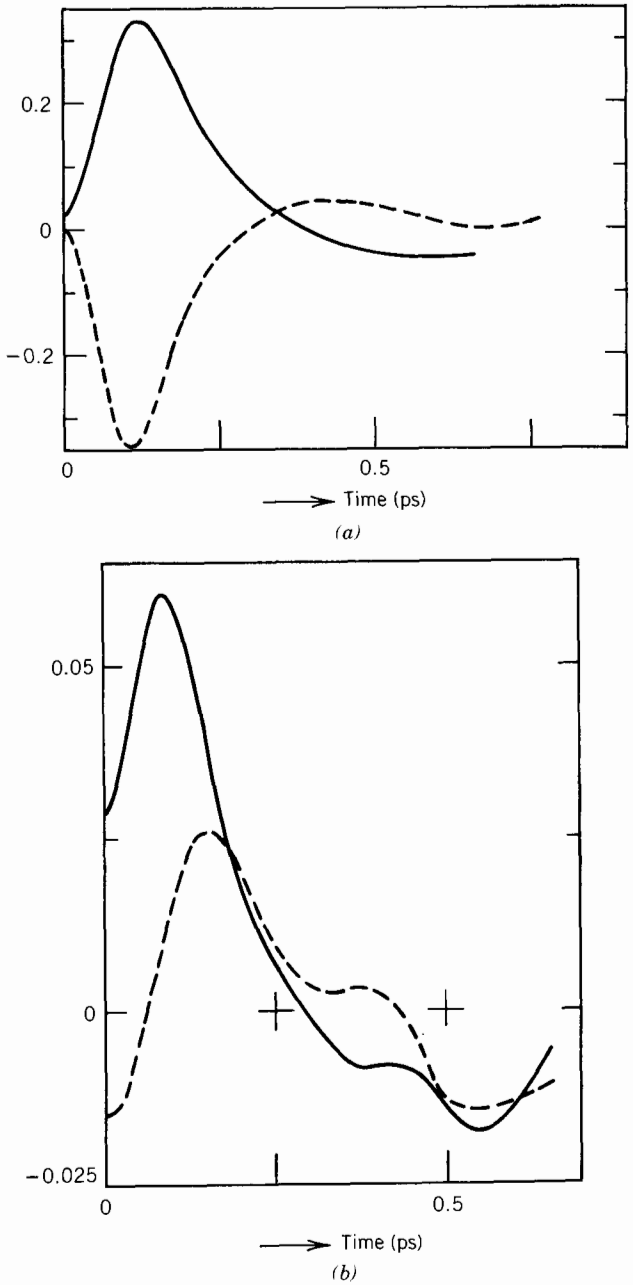

Figure 49. (*a*) —, (1,2) element of the rotating-frame matrix $\langle \mathbf{v}(t)\mathbf{J}^T(0)\rangle$ at 293 K, normalized as $\langle v_1(t)J_2(t)\rangle/(\langle v_1^2\rangle^{1/2}\langle J_2^2\rangle^{1/2}$; ---, (2,1) element. (*b*) As for *a*. —, (2,3) element; ---, (3,2) element. Note that the latter is very much smaller than the (1,2) or (2,1) elements. [Reproduced by permission from M. W. Evans, *J. Chem. Soc., Faraday II*, **79**, 719 (1983).]

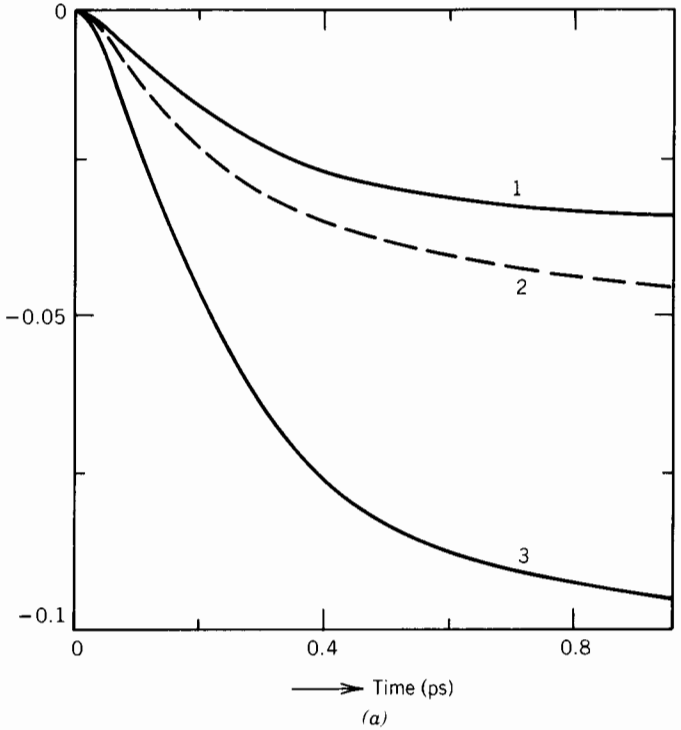

Figure 50. Orientational autocorrelation functions for supercooled ethyl chloride at 118 K, plotted as log (correlation function) versus time; $\mathbf{u}$ = dipole unit vector. (*a*) 1, $P_1(\mathbf{e}_3)$; 2, $P_1(\mathbf{u})$; 3, $P_2(\mathbf{e}_3)$. Note that the slope at long times (> 1.0 ps) is almost parallel to the time axis. (*b*) 1, $P_1(\mathbf{e}_2) = P_1(\mathbf{e}_1)$ (on this scale); 2, $P_2(\mathbf{e}_2) = P_2(\mathbf{e}_1)$. [Reproduced by permission from M. W. Evans, *J. Chem. Soc., Faraday II*, **79**, 719 (1983).]

Results in the supercooled states are shown in Figs. 50 and 51. The P_1 and P_2 orientational autocorrelation functions of $\mathbf{e}_1$, $\mathbf{e}_2$, $\mathbf{e}_3$, and $\mathbf{u}$ are *not* exponential in the interval up to 1 ps, and for $t > 1$ ps they tail on this scale parallel to the time axis. This implies that the correlation times are effectively infinite (on the picosecond time scale of the abscissa), or in other words, that the dynamical process originating in the picosecond time scale evolves into one that spans a complete time scale covering many decades of frequency. Note how this contrasts with the rotator-phase systems, in which rotation–translation interaction was almost absent. Rotation–translation coupling becomes exceedingly large in the glassy state (Fig. 51). Such interactions are undoubtedly effective in setting up long-lived vortices in the supercooled-liquid state—the interactions become coherent on a macroscopic scale. The function $\langle \dot{\mathbf{u}}(t) \cdot \dot{\mathbf{u}}(0) \rangle / \langle \dot{u}^2 \rangle$, when Fourier transformed, provides

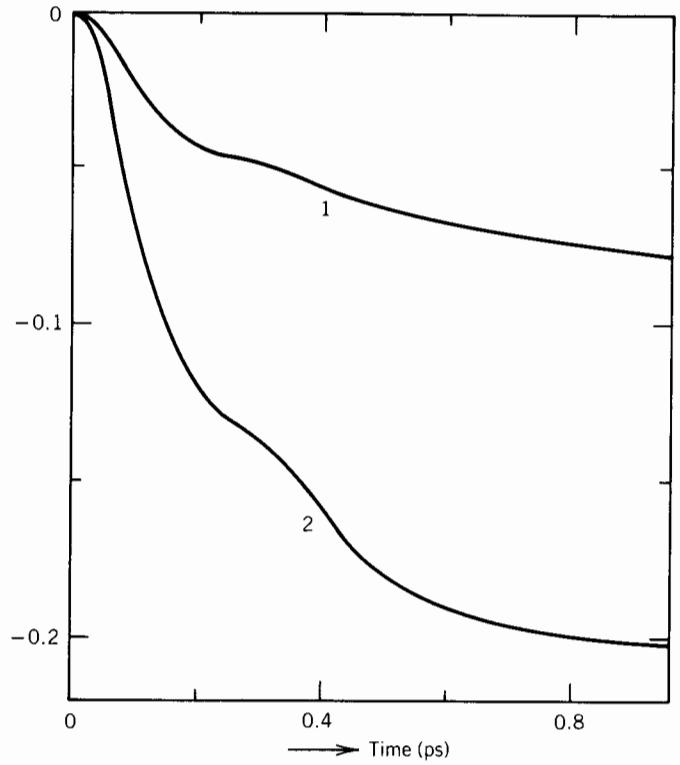

Figure 50. (*Continued*)

the far-infrared spectrum. It intersects the time axis (Fig. 52*b*) earlier than in the liquid (Fig. 52*a*) at room temperature, which means that the far-infrared spectrum is shifted to higher frequencies and considerably sharpened in the supercooled liquid. This is precisely what is observed experimentally (see ref. 162, Chapter 7) for a variety of dipolar solutes in supercooled decalin, which seems to corroborate the (α, β, γ) hypothesis of Evans and Reid.[198] This states that far-infrared process is the high-frequency (γ) adjunct of a multidecade relaxation representing the evolution of the molecular dynamics from picosecond time scales to time scales effectively on the order of years (recall the slow flow of common window glass).

So it is established that these molecules of low symmetry cannot possibly rotate without simultaneously displacing their *own* centers of mass. It should also be noted that the molecule must simultaneously displace neighboring molecules. These are the rotation–translation coupling effects observed by Ewing et al. (1966) in a series of experiments. The existence of rotation–

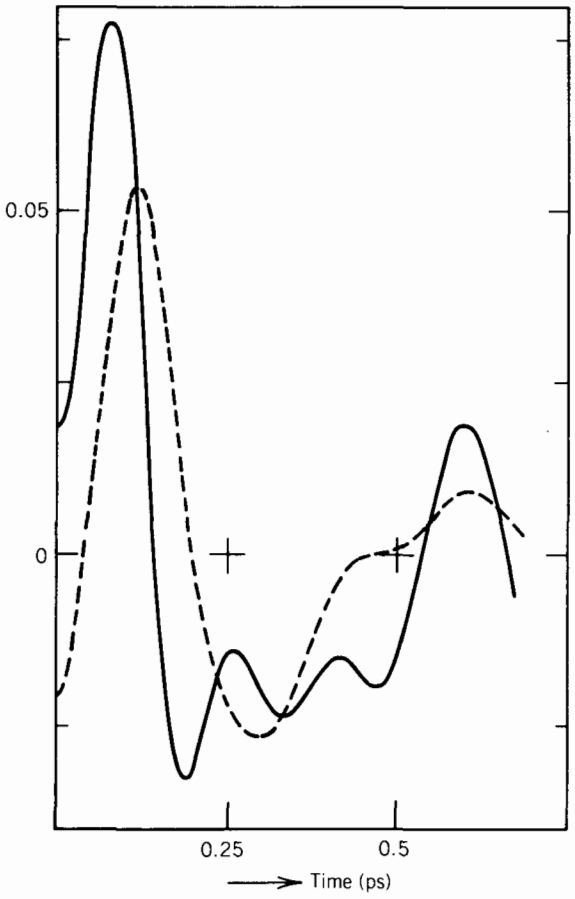

(a)

Figure 51. Elements of the rotating-frame matrix $\langle \mathbf{v}(t)\mathbf{J}^T(0)\rangle$ at 118 K, supercooled liquid, showing very strong rotation–translation coupling. (*a*) ---, (1,2) element; — , (2,1) element. (*b*) ---, (3,2) element; — , (2,3) element. [Reproduced by permission from M. W. Evans, *J. Chem. Soc., Faraday II*, **79**, 719 (1983).]

translation interaction seems to explain many properties of the liquid state, ranging from the existence of rotator-phase states to the formation of vitreous or glassy states. As we consider elsewhere in this volume, it also explains other basic phenomena, relating to optically active systems of yet lower symmetry. For example, it explains for the first time *in terms of the molecular dynamics* why the melting point of a racemic mixture of lactic acid is 18°C, yet that of the pure R and S enantiomers is 53°C. In addition, we may

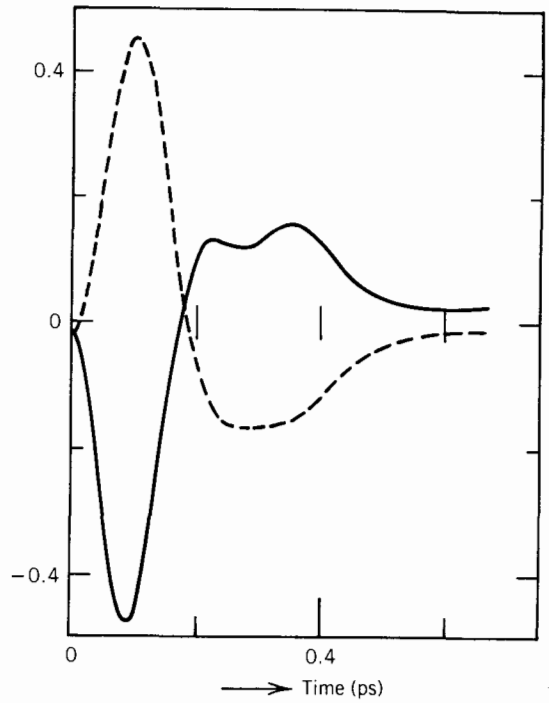

(*b*)

Figure 51. (*Continued*)

now try to explain why the solubilities of some optically active species in common solvents (e.g., *n*-hexane) are 9 times larger for the racemic mixture than the enantiomers.

We should note at this stage that the boiling point is not significantly affected by this rotation–translation interaction, but that the liquid–solid transition (i.e., the melting point) may be greatly affected.

X. CONCLUSION

As we have seen, computer simulation can be used to clarify and even to provide new insights into certain aspects of the molecular dynamics of the condensed state of matter. As computing power grows, so too the sizes of the molecules and the ensembles that may be studied will grow, intermolecular potentials will be improved (the Lennard-Jones interactions currently used in computer simulations are already orders of magnitude more realistic than those implied by the most advanced analytical theories), and other de-

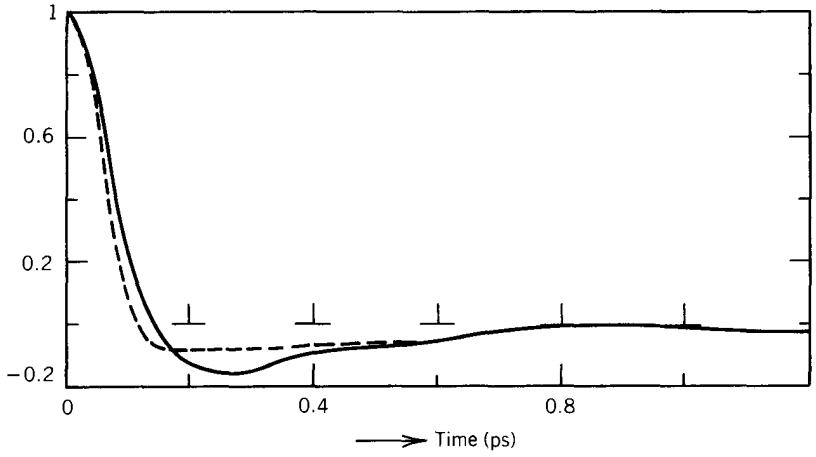

(a)

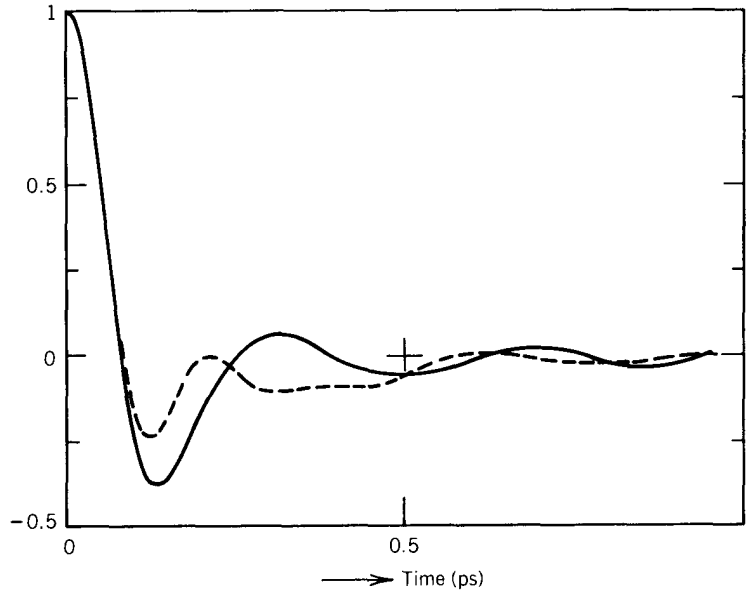

(b)

Figure 52. (*a*) Rotational velocity autocorrelation functions at 293 K: —, $\langle \dot{\mathbf{e}}_1(t)\cdot\dot{\mathbf{e}}_1(0)\rangle/\langle \dot{e}_1^2\rangle$; ---, $\langle \dot{\mathbf{u}}(t)\cdot\dot{\mathbf{u}}(0)\rangle/\langle \dot{u}^2\rangle$. (*b*) Rotational velocity autocorrelation functions at 118 K; ---, $\langle \dot{\mathbf{e}}_3(t)\cdot\dot{\mathbf{e}}_3(0)\rangle/\langle \dot{e}_3^2\rangle$; —, $\langle \dot{\mathbf{e}}_2(t)\cdot\dot{\mathbf{e}}_2(0)\rangle/\langle \dot{e}_2^2\rangle$. (*c*) Same as *b*, only for: ---, $\langle \dot{\mathbf{u}}(t)\cdot\dot{\mathbf{u}}(0)\rangle/\langle \dot{u}^2\rangle$; —, $\langle \dot{\mathbf{e}}_1(t)\cdot\dot{\mathbf{e}}_1(0)\rangle/\langle \dot{e}_1^2\rangle$. [Reproduced by permission from M. W. Evans, *J. Chem. Soc., Faraday II*, **79**, 719 (1983).]

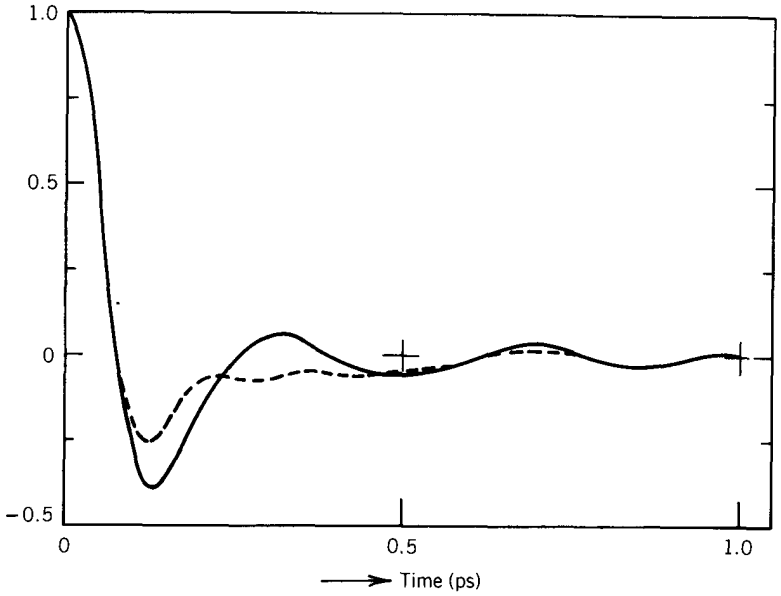

(c)

Figure 52. (*Continued*)

tails of the simulations that are presently questioned (e.g., the assumption of pair additivity) will be better understood. At this stage the foundations are being laid. Already it is apparent that we have not had the foresight to envisage many of the subtleties of the liquid state, and particularly the role of molecular shape and the constituent atoms in determining condensed-state properties. Molecular theories for liquid-state dynamics are oversimplified and restricted and have tended to lead us into great morasses of mathematical complexity without solving or shedding new light on the problems at hand. Hydrodynamic theories, by definition (they aim to explain liquid-state behavior in terms of macroscopic data), do not consider the detailed molecular structure of the medium, let alone the structure of the molecules.

Computer simulation of the molecular dynamics by-passes many of the problems that plague these analytical theories because the postulates are comparatively few. Gordon[199] once said that "it becomes impractical to follow the dynamics at long times because of the complexity of the molecular trajectories," and so analytical theories have evolved dependent on the methods of statistical mechanics, in which the number of dynamical variables was reduced from Avogadro's order of magnitude (the real number involved) to only a few. Modern-day simulations are doing just what was con-

sidered impossible then, and follow the complete time evolution of the molecular trajectories. In so doing they change the very basis of our subject. We believe we have entered an exciting new era of liquid-state molecular dynamics.

Acknowledgments

The SERC is thanked for two Advanced Fellowships and the University of Wales for University Fellowships at Bangor and Swansea to M. W. E. after contract termination at Aberystwyth.

References

1. G. W. F. Pardoe, Ph.D. Thesis, University of Wales, Aberystwyth, 1969.
2. G. J. Evans, Ph.D. Thesis, University of Wales, Aberystwyth, 1977.
3. G. J. Evans and M. W. Evans, *J. Mol. Liq.*, **26**, 63 (1983); M. W. Evans, *Phys. Rev. Lett.*, **50**, 371 (1983); G. J. Evans and M. W. Evans, *Chem. Phys. Lett.*, **96**, 416 (1983).
4. G. Ewing, *Acc. Chem. Res.*, **2(6)**, 168 (1966).
5. B. J. Berne and R. Pecora, *Dynamic Light Scattering*, Wiley, New York, 1975.
6. R. M. Lynden-Bell, *Mol. Phys.*, **33(4)**, 907 (1977).
7. G. J. Evans, *J. Chem. Soc., Faraday II*, **79**, 547 (1983).
8. M. W. Evans, *Adv. Mol. Rel. Int. Proc.*, **24**, 123 (1982).
9. H. Bertagnolli, D. O. Leicht, and M. D. Zeidler, *Mol. Phys.*, **35**, 199 (1978).
10. C. Brodbeck, I. Rossi, N. van Thanh, and A. Ruoff, *Mol. Phys.*, **32**, 71 (1976).
11. J. Soussen-Jacob, E. Devril, and J. Vincent-Geisse, *Mol. Phys.*, **28**, 935 (1974).
12. A. Gerschel, I. Darmon, and C. Brot, *Mol. Phys.*, **23**, 317 (1972).
13. A. Gerschel and C. Brot, *Mol. Phys.*, **20**, 279 (1971).
14. J. Schroeder, V. H. Schiemann, and J. Jonas, *Mol. Phys.*, **34**, 1501 (1977).
15. P. van Konynenberg and W. A. Steele, *J. Chem. Phys.*, **56**, 4776 (1972).
16. J. Schroeder and J. Jonas, *Chem. Phys.*, **34**, 11 (1978).
17. P. A. Lund, O. Faurskov-Nielsen, and E. Praestgaard, *Chem. Phys.*, **28**, 167 (1978).
18. S. Claesson and D. R. Jones, *Chem. Scripta*, **9**, 103 (1976).
19. G. R. Alms, D. R. Bauer, J. I. Brauman, and R. Pecora, *J. Chem. Phys.*, **59**, 5310 (1973).
20. K. Kamagawa, *Bull. Chem. Soc. Jpn.*, **51**, 3475 (1978).
21. M. W. Evans, G. J. Evans, W. T. Coffey, and P. Grigolini, *Molecular Dynamics*, Wiley, New York, 1982.
22. G. J. Evans, *Spectrochim. Acta*, **33A**, 699 (1977).
23. G. J. Evans and M. W. Evans, *Chem. Phys. Lett.*, **45**, 454 (1977).
24. T. Suzuki, Y. K. Tsutsui, and T. Fujiyama, *Bull. Chem. Soc. Jpn.*, **53**, 1931 (1980).
25. W. G. Rothschild, G. J. Rosasco, and R. C. Livingston, *J. Chem. Phys.*, **62**, 1253 (1975).
26. A. Moradi-Araghi and M. Schwartz, *J. Chem. Phys.*, **68**, 5548 (1978).
27. J. S. Rowlinson, *Trans. Faraday Soc.*, **45**, 974 (1949).
28. K. Tanabe and J. Higashi, *Chem. Phys. Lett.*, **71**, 46 (1980).
29. A. Laubereau, G. Wochner, and W. Kaiser, *Chem. Phys.*, **28**, 363 (1978); A. Laubereau, *C. R. Int. Conf. Sp. Raman 7th*, p. 450, (1980).

30. A. Moradi-Araghi and M. Schwartz, *J. Chem. Phys.*, **71**, 166 (1979).
31. P. C. M. van Woerkom, J. de Bleisser, M. de Zwart, P. M. J. Burgers, and J. C. Leyte, *Ber. Bunsenges. Phys. Chem.*, **78**, 1303 (1974).
32. R. K. Wertheimer, *Mol. Phys.*, **36**, 1631 (1978); *ibid.*, **35**, 257 (1978).
33. G. Doege, T. Bien, and M. Possiel, *Ber. Bunsenges. Phys. Chem.*, **85**, 1074 (1981).
34. C. W. Carlson and P. J. Flory, *J. Chem. Soc., Faraday Trans. II*, **73**, 1729 (1977).
35. J. A. Bucaro and T. A. Litovitz, *J. Chem. Phys.*, **54**, 3846 (1971); *ibid.*, **55**, 3585 (1971).
36. J. H. K. Ho and G. C. Tabisz, *Can. J. Phys.*, **51**, 2025 (1973).
37. A. K. Burnham, G. Alms, and W. H. Flygare, *J. Chem. Phys.*, **62**, 3289 (1975).
38. M. W. Evans, G. J. Evans, and B. Janik, *Spectrochim. Acta*, **38A**, 423 (1982).
39. Y. Leroy, E. Constant, C. Abbar, and P. Desplanques, *Adv. Mol. Rel. Proc.*, **1**, 273 (1967).
40. P. Hindle, S. Walker, and J. Warren, *J. Chem. Phys.*, **62**, 3230 (1975).
41. C. J. Reid and M. W. Evans, *J. Chem. Soc., Faraday II*, **76**, 286 (1980).
42. G. Bossis, These d'Etat, Université de Nice, Nice, 1981.
43. B. Quentrec and P. Bezot, *Mol. Phys.*, **27**, 879 (1974).
44. V. I. Gaiduk and Y. P. Kalmykov, *J. Chem. Soc., Faraday II*, **77**, 929 (1981).
45. F. Hermans and E. Kestemont, *Chem. Phys. Lett.*, **55**, 305 (1978).
46. S. Forsen, H. Gustavsson, B. Lindman, and N. O. Persson, *J. Mag. Res.*, **23**, 515 (1976).
47. R. R. Shoup and T. C. Farrar, *J. Mag. Res.*, **7**, 48 (1972).
48. W. T. Huntress, *J. Phys. Chem.*, **73**, 103 (1969).
49. M. Ohuchi, T. Fujito, and M. Imanari, *J. Mag. Res.*, **35**, 415 (1979).
50. Dinesh and M. T. Rogers, *Chem. Phys. Lett.*, **12**, 352 (1971).
51. T. C. Farrar, S. J. Druck, R. R. Shoup, and E. D. Becker, *J. Am. Chem. Soc.*, **94**, 699 (1972).
52. J. C. Duplan, A. Briguet, and J. Delmar, *J. Chem. Phys.*, **59**, 6269 (1973).
53. P. P. Ho and R. R. Alfano, *Phys. Rev.*, **20**, 2170 (1979).
54. M. T. Ratzch, E. Rickelt, and H. Rosner, *Z. Phys. Chem.*, **256**, 349 (1975).
55. M. S. Beevers and G. Khanarian, *Aust. J. Chem.*, **32**, 263 (1979); *ibid.*, **33**, 2585 (1980).
56. A. Proutière and J. G. Baudet, *Ann. Univ. Abidjan, Ser. C*, **11**, 13 (1975).
57. M. P. Bogaard, A. D. Buckingham, and G. L. D. Ritchie, *Mol. Phys.*, **18**, 575 (1970).
58. G. J. Evans, *J. Chem. Soc., Faraday II*, **79**, 547 (1983).
59. K. Takagi, P. K. Choi, and K. Negishi, *J. Chem. Phys.*, **74**, 1424 (1981).
60. D. Samios, T. Dorfmuller, and A. Asembaum, *Chem. Phys.*, **65**, 305 (1982).
61. A. Yoshihara, A. Anderson, R. A. Aziz, and C. C. Lim, *Chem. Phys.*, **61**, 1 (1981).
62. K. Altenburg, *Z. Phys. Chem.*, **250**, 399 (1972).
63. R. Vallauri and M. Zoppi, *Lett. Nuovo Cimento So. Ital. Fis.*, **9**, 447 (1974).
64. C. A. Chatzidimitriou-Dreismann and E. Lippert, *Ber. Bunsenges. Phys. Chem.*, **84**, 775 (1980); *ibid.*, *Croatica Chimica Acta*, in press.
65. H. S. Goldberg and P. S. Persham, *J. Chem. Phys.*, **58**, 3816 (1973).
66. J. Hyde-Campbell, J. F. Fisher, and J. Jonas, *J. Chem. Phys.*, **61**, 346 (1974).
67. G. Döge and A. Schaeffer, *Ber. Bunsenges. Phys. Chem.*, **77(a)**, 682 (1973).

68. R. Arndt and J. Yarwood, *Chem. Phys. Lett.*, **45**, 155 (1977).
69. C. K. Cheung, D. R. Jones, and C. H. Wang, *J. Chem. Phys.*, **64**, 3567 (1976).
70. R. B. Wright, M. Schwartz, and C. H. Wang, *J. Chem. Phys.*, **58**, 5125 (1973).
71. G. D. Patterson and J. Griffiths, *J. Chem. Phys.*, **63**, 2406 (1975).
72. J. F. Dill, T. A. Litovitz, and J. A. Bucaro, *J. Chem. Phys.*, **62**, 3839 (1975).
73. M. Constant and M. Fauquembergue, *C. R. Seances Acad. Sci.*, **272**, 31293 (1971).
74. E. N. Shermatov and A. K. Atakhodzhaev, *Theor. Spektrosk.*, 29–30 (1977).
75. A. Laubereau and W. Kaiser, *NATO Adv. Study Inst.-Ser.*, **B37**, 329 (1977).
76. Z. Gburski and W. Szczepanski, *Mol. Phys.*, **40**, 649 (1980).
77. D. W. Oxtoby, D. Levesque, and J. J. Weiss, *J. Chem. Phys.*, **68**, 5528 (1978).
78. K. T. Gillen, M. Schwartz, and J. H. Noggle, *Mol. Phys.*, **20**, 199 (1971).
79. G. Döge, R. Arndt, and A. Khuen, *Chem. Phys.*, **21**, 53 (1977).
80. N. Trisdale and M. Schwartz, *Chem. Phys. Lett.*, **68**, 461 (1979).
81. G. Döge, *Z. Naturforsch.*, **28A**, 919 (1973).
82. P. C. M. van Woerkom, J. de Bleyser, M. de Zwart, and J. C. Leyte, *Chem. Phys.*, **4**, 236 (1974).
83. S. F. Fisher and A. Laubereau, *Chem. Phys. Lett.*, **35**, 6 (1975).
84. J. H. Hildebrand, *Faraday Disc.*, **66** (1978).
85. M. L. Bansal, S. K. Debard, and A. P. Roy, *Chem. Phys. Lett.*, **83**, 83 (1981).
86. W. A. Steele, *Adv. Chem. Phys.*, **34** (1976).
87. C. M. Roland and W. A. Steele, *J. Chem. Phys.*, **73**, 5924 (1980).
88. J. R. Maple, R. S. Wilson, and J. T. Knudtson, *J. Chem. Phys.*, **73**, 3346 (1980).
89. J. P. Riehl and D. J. Diestler, *J. Chem. Phys.*, **64**, 2593 (1976).
90. O. F. Nielsen, D. H. Christensen, P. A. Lund, and E. Praestgaard, *Proc. Int. Conf. Raman Spect.*, **2**, 208 (1978).
91. M. Schwartz, *Chem. Phys. Lett.*, **73**, 127 (1980).
92. J. E. Griffiths, *J. Chem. Phys.*, **59**, 751 (1973).
93. F. Heatley, *J. Chem. Soc., Faraday II*, **70**, 148 (1970).
94. C. O. Fischer, *Ber. Bunsenges. Phys. Chem.*, **75**, 361 (1971).
95. J. A. Janik, J. M. Janik, A. Bajorek, K. Parlinski, and M. Sudnik-Hoynkiewicz, *Physica*, **35**, 4 (1967).
96. E. K. Eliel, N. L. Allinger, S. J. Angyal, and G. A. Morrison, *Conformational Analysis*, Wiley, New York, 1965.
97. G. Bossis, B. Quentrec, and C. Brot, *Mol. Phys.*, **39**, 123 (1980).
98. E. Kluk, T. W. Zerda, and J. Zerda, *Acta Phys. Polonica*, **56A**, 121 (1979).
99. G. Ciccotti, J. P. Ryckaert, and A. Bellemans, *Mol. Phys.*, **44**, 979 (1981).
00. H. Bertagnolli, D. O. Leicht, and M. D. Zeidler, *Mol. Phys.*, **35**, 199 (1978).
01. G. J. Evans, *J. Chem. Soc. Faraday II*, **79**, 547 (1983).
02. M. W. Evans, *J. Mol. Liq.*, **25**, 149 (1983).
03. T. Bien, M. Possiel, G. Döge, J. Yarwood, and K. Arnold, *Chem. Phys.*, **56**, 203 (1981).
04. T. E. Bull, *Chem. Phys. Lett.*, **73**, 127 (1980).
05. M. Schwartz, *Chem. Phys. Lett.*, **73**, 127 (1980).

106. C. Breulliard-Alliot and J. Soussen-Jacob, *Mol. Phys.*, **28**, 903 (1974).
107. B. Tiffon, B. Ancian, and J. E. Dubois, *J. Chem. Phys.*, **74**, 6981 (1981).
108. S. L. Whittenberg and C. H. Wang, *J. Chem. Phys.*, **66**, 5138, (1977).
109. J. T. Hynes, R. Kapral, and M. Weinberg, *J. Chem. Phys.*, **69**, 2725 (1978).
110. G. Patterson and J. E. Griffiths, *J. Chem. Phys.*, **63**, 2406 (1975).
111. H. Versmold, *Ber. Bunsenges. Ges. Phys. Chem.*, **82**, 451 (1978).
112. E. Knozinger, D. Leutloff, and R. Wiltenbeck, *J. Mol. Struct.*, **60**, 115 (1980).
113. G. Fini and P. Mirone, *Spectrochim. Acta*, **32A**, 439 (1976).
114. A. M. Amorim da Costa, M. A. Norman, and J. H. R. Clarke, *Mol. Phys.*, **29**, 191 (1975).
115. J. Yarwood, P. L. James, G. Döge, and R. Arndt, *Disc. Faraday Soc.*, **66**, 252 (1972).
116. J. Yarwood, R. Arndt, and C. Döge, *Chem. Phys.*, **25**, 387 (1977).
117. F. Heatley, *J. Chem. Soc., Faraday II*, **70**, 148 (1974).
118. J. R. Lyerla, D. M. Grant, and C. H. Wang, *J. Chem. Phys.*, **55**, 4670 (1971).
119. T. K. Leipert, J. H. Noggle, and K. T. Gillen, *J. Mag. Res.*, **13**, 158 (1974).
120. G. D. Stucky, D. A. Matthews, J. Hedman, M. Klasson, and C. Nordling, *J. Am. Chem. Soc.*, **94**, 8009 (1972).
121. J. A. Pople and K. Beveridge, *J. Am. Chem. Soc.*, **92**, 5298 (1970).
122. J. Yarwood, R. Ackroyd, K. E. Arnold, G. Döge, and R. Arndt, *Chem. Phys. Lett.*, **77**, 239 (1981).
123. J. K. Eloranta and P. K. Kadaba, *Mat. Sci. Eng.*, **8(4)**, 203 (1971).
124. E. Krishnaji and A. Mansigh, *J. Chem. Phys.*, **41**, 827 (1964).
125. W. G. Rothschild, *J. Chem. Phys.*, **57**, 991 (1972).
126. A. K. Burnham and T. D. Gierke, *J. Chem. Phys.*, **73**, 4822 (1980).
127. M. S. Beevers and D. A. Elliott, *Mol. Cryst. Liq. Cryst.*, **26**, 411 (1979).
128. A. Kratochwill, *Ber. Bunsenges. Ges. Phys. Chem.*, **82**, 783 (1978).
129. C. S. Hsu and D. Chandler, *Mol. Phys.*, **36**, 215 (1978).
130. E. Lippert, W. Schroer, H. Mahnke, and H. Michel, in *International Conference on Hydrogen Bonding*, H. J. Bernstein, ed., Ottowa, 1972, p. 22.
131. G. J. Evans, *Chem. Phys. Lett.*, in press (1983).
132. R. J. Jakobsen and J. W. Brasch, *J. Am. Chem. Soc.*, **86**, 3571 (1964).
133. B. J. Bulkin, *Helv. Chim. Acta*, **52**, 1348 (1969).
134. A. M. Saum, *J. Polym. Sci.*, **42**, 57 (1960).
135. R. Lobo, J. E. Robinson and S. Rodriguez, *J. Chem. Phys.*, **59**, 5992 (1973).
136. G. Ascarelli, *Chem. Phys. Lett.*, **39**, 23 (1976).
137. M. W. Evans and G. J. Evans, *J. Chem. Soc.*, Faraday II, **76**, 767 (1982).
138. C. Brodbeck, I. Rossi, N. van Thanh, and A. Ruoff, *Mol. Phys.*, **32**, 71 (1976).
139. A. E. Boldeskal, S. S. Esman, and V. E. Pogornelov, *Opt. Spectrosc.*, **37**, 521 (1974).
140. E. K. Eliel, N. L. Allinger, S. J. Angyal, and G. A. Morrison, *Conformational Analysis*, Wiley, New York, 1965.
141. R. Del Re, *J. Chem. Soc.*, **43**, (1958).
142. J. O. Hirschfelder, *J. Chem. Phys.*, **8**, 431 (1940).
143. H. S. Sandhu, *J. Mag. Reson.*, **34**, 141 (1979).

144. J. Soussen-Jacob, E. Devvil, and J. Vincent-Geisse, *Mol. Phys.*, **28**, 935 (1974).
145. V. K. Agarwal, A. K. Sharma, and A. Mansingh, *Chem. Phys. Lett.*, **68**, 151 (1979).
146. G. D. Patterson and J. E. Griffiths, *J. Chem. Phys.*, **63**, 2406 (1975).
147. V. K. Agarwal, G. J. Evans, and M. W. Evans, *J. Chem. Soc., Faraday II*, **79**, 137 (1983).
148. B. Lassier and C. Brot, *J. Chim. Phys.*, **65**, 1723 (1968).
149. K. E. Larson and T. Mansson, *J. Chem. Phys.*, **67**, 4995 (1977).
150. P. S. Goyal, W. Navrocik, S. Urban, J. Dornosiawski, and I. Nathaniel, *Proc. Nucl. Phys., Solid State Phys. Symp.*, **16C**, 193 (1973); *ibid., Acta Phys. Polonica*, **A46 141**, 399 (1974).
151. A. A. Boguslavskii, R. S. Lotfullin, and G. K. Senun, *Phys. Stat. Solidi*, **66(2)**, K95 (1974).
152. F. Koeksal, *J. Chem. Soc., Faraday II*, **76**, 55P (1980).
153. M. Constant and R. Fauquembergue, *J. Chem. Phys.*, **72**, 2459 (1980).
154. C. W. Carlson and P. J. Flory, *J. Chem. Soc., Faraday II*, **73**, 1505 (1977).
155. K. Czarniecka, J. M. Janik, and J. A. Janik, *Acta Phys. Polonica*, **55A**, 421 (1979).
156. C. J. Reid and M. W. Evans, *Mol. Phys.*, **40**, 1357 (1980).
157. R. Haffmans and I. W. Larkin, *J. Chem. Soc., Faraday II*, **68**, 1729 (1972).
158. I. W. Larkin, *J. Chem. Soc., Faraday II*, **69**, 1379 (1973).
159. C. J. Reid, Thesis, University of Wales, 1979.
160. M. W. Evans, *J. Mol. Liq.*, **27**, 11, 19 (1983).
161. G. Bossis, These d'Etat, Université de Nice, Nice, 1981.
162. M. W. Evans, G. J. Evans, W. T. Coffey, and P. Grigolini, *Molecular Dynamics*, Wiley-Interscience, New York, 1982, Chaps. 6 and 12.
163. M. W. Evans and J. Yarwood, *Adv. Mol. Rel. Int. Proc.* **21**, 2 (1981).
164. P. N. Brier and A. Perry, *Adv. Mol. Rel. Int. Proc.*, **13**, 46 (1978).
165. P. C. M. van Woerkom, J. de Bleyser, M. de Zwart, P. M. Burgers, and J. C. Leyte, *Ber. Bunsenges. Phys. Chem.*, **78**, 1303 (1979).
166. D. E. O'Reilly, E. M. Peterson, and E. L. Yasaites, *J. Chem. Phys.*, **57**, 890 (1972).
167. W. G. Rothschild, *J. Chem. Phys.*, **53**, 990, 3265 (1970).
168. F. Heatley, *J. Chem. Soc., Faraday II*, **70**, 148 (1974).
169. D. E. Woessner, J. Chem. Phys., **37**, 647 (1962).
170. M. W. Evans and G. J. Evans, *J. Chim. Phys. (Paris)*, **72**, 522 (1978).
171. V. F. Baranov, *Vopt. Mol. Specktrosk.*, **89**, (1974).
172. J. R. Nestor and E. R. Lippincott, *J. Raman Spectrosc.*, **1(3)**, 305 (1973).
173. K. Singer, J. V. L. Singer, and A. J. Taylor, *Mol. Phys.*, **37**, 1239 (1979).
174. I. R. McDonald, personal communication.
175. M. Ferrario and M. W. Evans, *Adv. Mol. Rel. Int. Proc.*, **24**, 139 (1982).
176. P. S. Y. Cheung, *Mol. Phys.*, **3**, 519 (1977).
177. K. Koga, Y. Kamazawa, and H. Shimizu, *J. Mol. Spectrosc.*, **47**, 107 (1973).
178. L. D. Favro, *Phys. Rev.*, **53**, 119 (1960).
179. J. F. Dill, T. A. Litovitz, and J. A. Bucaro, *J. Chem. Phys.*, **62**, 3839 (1975).
180. J. Jonas and T. E. Bull, *J. Chem. Phys.*, **52**, 4553 (1972).
181. W. Schindler, P. T. Sharko, and J. Jonas, *J. Chem. Phys.*, **76**, 3493 (1982).
182. D. W. Oxtoby, D. Levesque, and J. J. Weis, *J. Chem. Phys.*, **68**, 5528 (1978).
183. C. Döge, *Z. Naturforsch. A*, **28**, 919 (1973).

184. C. H. Wang, *Mol. Phys.*, **33**, 207 (1977).
185. R. M. Lynden-Bell, *Mol. Phys.*, **33**, 907 (1977).
186. M. Perrot, M. H. Brooker, and J. Lascombe, *J. Chem. Phys.*, **74**, 2787 (1981).
187. C. J. Reid and M. W. Evans, *Mol. Phys.*, **40**, 1357 (1980).
188. A. K. Burnham and T. D. Gierke, *J. Chem. Phys.*, **73**, 4822 (1980).
189. B. M. Laudanyi and T. Keyes, *Mol. Phys.*, **37**, 1413 (1979).
190. S. M. George, H. Auweter, and C. B. Harris, *J. Chem. Phys.*, **73**, 5573 (1976).
191. A. Bellemans, G. Ciccotti, and J-P. Ryckaert, *Mol. Phys.*, **44**, 979 (1981).
192. C. A. Wellington and S. H. Khouwaiter, *Tetrahedron*, **34**, 2183 (1978).
193. A. N. M. Barnes, D. J. Turner, and L. E. Sutton, *Trans. Faraday Soc.*, **67**, 2902 (1971).
194. T. McMullen, E. D. Crozier, and R. McIntosh, *Can. J. Chem.*, **46**, 2945 (1968).
195. K. A. Strong, R. M. Brugger, and R. J. Pugmire, *J. Chem. Phys.*, **52**, 2277 (1970).
196. J. E. Mark and C. Sutton, *J. Am. Chem. Soc.*, **94**, 1083 (1972).
197. C. M. Miller and S. L. Gordon, *J. Chem. Phys.*, **53**, 3531 (1970).
198. M. W. Evans and C. J. Reid, *J. Chem. Phys.*, **76**, 2576 (1982).
199. R. G. Gordon, *J. Chem. Phys.*, **45**, 1649 (1966).